IMPROVING RUNNING PERFORMANCE AND MONITORING INJURY RISK WITH WEARABLE DEVICES

by

RYAN SKYLER ALCANTARA

B.Sc., Seattle Pacific University, 2011

M.Sc., University of Colorado Boulder, 2019

A thesis submitted to the Faculty of the Graduate School of the

University of Colorado in partial fulfillment

of the requirement for the degree of

Doctor of Philosophy

Integrative Physiology

2021

Committee Members:

Alena Grabowski[1], Ph.D. (Faculty Mentor, Chair)
Rodger Kram[1] Ph.D.
Allison Anderson[2], Ph.D.
Brent Edwards[3], Ph.D.
Michael Hahn[4], Ph.D.

[1]Department of Integrative Physiology, University of Colorado Boulder
[2]Smead Department of Aerospace Engineering Sciences, University of Colorado Boulder
[3]Faculty of Kinesiology, University of Calgary
[4]Department of Human Physiology, University of Oregon

Alcantara, Ryan Skyler (Ph.D., Integrative Physiology)
Improving Running Performance and Monitoring Injury Risk with Wearable Devices
Thesis directed by Associate Professor Alena M. Grabowski

Aim 1 of my dissertation was to determine the effects of running-specific prosthesis (RSP) mass on the running economy of long distance runners with a transtibial (below-knee) amputation. To accomplish this, runners with a transtibial amputation ran with 100 g or 300 g added to their RSP while I measured metabolic power. I found that metabolic power increased by 0.9% for every 100 g added to the RSP, suggesting that decreases in RSP mass would reduce metabolic power and likely improve long distance running performance.

Aim 2 of my dissertation was to identify the biomechanical limitations of sprinting on the flat curves of regulation 200 m and 400 m tracks. To accomplish this, athletes performed a series of maximum effort sprints on a straightaway and curves while I measured lower body kinematics, kinetics, and ground reaction forces. I found that the inside and outside leg have distinct biomechanical functions during curve sprinting and the orientation of the hips, knees, and ankles affect force production and maximum velocity. These findings highlight opportunities for athletes to improve their sprinting performance.

Aim 3 of my dissertation was to monitor a runner's injury risk with wearable devices. To accomplish this, I first developed a statistical model that uses data from an accelerometer clipped on the back of an athlete's running shorts to accurately predict biomechanical variables associated with the magnitude and duration of external forces applied to the body during level ground running. Next, I developed a neural network capable of predicting a runner's ground reaction forces across a range of speeds and slopes in near-real time. This approach was up to 2x more accurate than

current state-of-the-art methods. These findings represent a substantial step towards using wearable technology to accurately monitor a runner's injury risk and provide biomechanical feedback during an outdoor run.

Overall, my dissertation identified physiological factors that limit long distance running performance and biomechanical factors that limit sprinting performance, and developed methods to accurately monitor a runner's injury risk with wearable devices.

Acknowledgements

This thesis is dedicated to Maggie Peterson, without whom the research described in the following pages would have been impossible. Mags, thanks for your love and support through the highs and lows.

I would like to acknowledge all the mentors, friends, and family that provided guidance, perspective, and support throughout my academic career thus far. I am grateful for my undergraduate mentor, Cara Wall-Scheffler, for introducing me to the scientific method, fostering a love for research, and leading this first-generation college student through the maze of academia. Thank you, Alena Grabowski, for your patience and guidance throughout my graduate studies. I am grateful for your support over the last four years. Thank you, Rodger Kram, for welcoming me into your academic family and providing invaluable wisdom as I evolved as a person and scientist. I would also like to thank past and present members of the Applied Biomechanics Lab, Locomotion Laboratory, Neuromechanics Laboratory, and Neurophysiology of Movement Laboratory for their friendship and the conversations had on runs, over beers, and in the mountains. Your impact on my life during graduate school cannot be overstated. Lastly, I feel compelled to acknowledge the global pandemic that has affected many lives over the past year and recognize that this was a particularly challenging time to complete a Ph.D. Thank you to everyone who made quarantine enjoyable.

Contents

Figures

Tables

0 Introduction

Improving a runner's performance depends on the unique biomechanical and physiological requirements of the race (e.g. 10 km cross country race vs. 400 m track sprint). For example, long distance running performance can be improved by improving running economy, which is the rate of metabolic energy expended at a given velocity (Hoogkamer et al., 2016). Improvements in running economy, and thus improvements in running performance, have been achieved most notably through novel footwear designs (Hoogkamer et al., 2018) and reductions in footwear mass (Hoogkamer et al., 2016). Previous research suggests that for every 100 g added to both shoes, metabolic power increases by ~1% (Frederick et al., 1984). However, similar to shoes, running specific prosthesis (RSP) mass likely affects running economy in runners with a transtibial (below-knee) amputation. The first goal of my dissertation was to determine how mass added to an RSP and to the biological foot affected running economy and thus performance in long distance runners with unilateral transtibial amputation. In Chapter 1, I determined the effect of RSP and lower leg mass on metabolic power during running. This study was published in the *European Journal of Applied Physiology*.

In contrast to long distance running, improvements in sprinting performance can be achieved by increasing force production and maximum sprinting velocity (Weyand et al., 2000). For track and field events like the 200 m and 400 m sprint, more than half the race is run on a curve (Meinel, 2008) and maximum velocity is slower on a curve than a straightaway (Churchill et al., 2015). However, the underlying biomechanical mechanisms responsible for this decrease in maximum velocity are not completely understood. An improved understanding of the limitations to curve sprinting may provide opportunities to improve sprinting performance. The second goal of my dissertation was to identify biomechanical factors that limit sprinting performance on flat

track curves. In Chapter 2, I quantified the distinct biomechanical function of the inside and outside leg during curve sprinting and thus identified the underlying mechanisms that affect curve sprinting performance. This manuscript is in preparation for submission to the *Journal of Sports Sciences* in the coming months. Together, Chapters 1 and 2 highlight opportunities for long distance runners and sprinters to understand physiological and biomechanical factors that affect their performance.

A runner's performance can be indirectly improved by reducing the occurrence of injuries that result in lost training or competition opportunities. Long distance runners are particularly susceptible to stress fractures, an overuse injury that typically occurs in the bones of the feet, legs, or pelvis and requires month for full recovery (Matheson et al., 1987). The repetitive nature of running lends itself to overuse injuries, as ground reaction forces (GRFs) of 2 – 3x body weight (BW) and muscle forces of 6 – 10x BW are exerted on the bones with each step (Scott & Winter, 1990). Measurement of GRFs has led to the identification of biomechanical risk factors for overuse injuries (Davis et al., 2016) but has historically been restricted to a laboratory environment. Alternatively, wireless wearable devices like accelerometers can be used to measure biomechanical variables outside the laboratory and monitor changes in a runner's injury risk over the course of a run, or even months of running (Kiernan et al., 2018).

Advances in machine learning algorithms have facilitated the use of wearable devices to predict a variety of biomechanical variables not directly measured by the device. For example, accelerometers have been used to predict GRFs and joint moments (torque) during running (Johnson et al., 2021). Although a promising strategy for measuring a runner's biomechanics outside the laboratory, the accuracy of these methods must be improved if they are to be used to detect changes in biomechanical risk factors. The third goal of my dissertation was to improve the

accuracy of statistical models and machine learning algorithms that use accelerometer data to predict a runner's discrete and continuous motion and forces outside the laboratory setting. In Chapter 3, I developed statistical models that use data from a single accelerometer to predict biomechanical variables associated with the magnitude and duration of GRFs applied to the body during level ground running. This study is currently in press in *PeerJ*. In Chapter 4, I developed a neural network capable of predicting ground reaction forces across a range of running speeds and uphill/downhill slopes in near-real time. This study will be submitted to *PeerJ* in the coming weeks. Together, Chapters 3 and 4 present strategies for coaches, clinicians, and researchers to accurately monitor a runner's injury risk with wearable devices.

In summary, Chapter 1 determined the effects of RSP mass on running economy and biomechanics for long distance runners with a transtibial amputation. Chapter 2 identified biomechanical limitations and the distinct functions of the inside and outside leg during maximum velocity curve sprinting. Chapters 3 and 4 present novel applications of statistical models and machine learning algorithms to predict GRFs from accelerometer data during running.

0.1 References

Churchill, S. M., Salo, A. I. T., & Trewartha, G. (2015). The effect of the bend on technique and performance during maximal effort sprinting. *Sports Biomechanics*, *14*(1), 106–121. https://doi.org/10.1080/14763141.2015.1024717

Davis, I. S., Bowser, B. J., & Mullineaux, D. R. (2016). Greater vertical impact loading in female runners with medically diagnosed injuries: a prospective investigation. *British Journal of Sports Medicine*, *50*(14), 887–892. https://doi.org/10.1136/bjsports-2015-094579

Frederick, E. C., Daniels, J. T., & Hayes, J. W. (1984). The effect of shoe weight on the aerobic demands of running. In N. Bachl, L. Prokop, & R. Suckert (Eds.), *Current Topics in Sports Medicine, Proceedings of the World Congress of Sports Medicine* (pp. 616–625). Urban and Schwarzenberg.

Hoogkamer, W., Kipp, S., Frank, J. H., Farina, E. M., Luo, G., & Kram, R. (2018). A Comparison of the Energetic Cost of Running in Marathon Racing Shoes. *Sports Medicine (Auckland, N.Z.)*, *48*(4), 1009–1019. https://doi.org/10.1007/s40279-017-0811-2

Hoogkamer, W., Kipp, S., Spiering, B. A., & Kram, R. (2016). Altered Running Economy Directly Translates to Altered Distance-Running Performance. *Medicine and Science in Sports and Exercise*, *48*(11), 2175–2180. https://doi.org/10.1249/MSS.0000000000001012

Johnson, W. R., Mian, A., Robinson, M. A., Verheul, J., Lloyd, D. G., & Alderson, J. (2021). Multidimensional ground reaction forces and moments from wearable sensor accelerations via deep learning. *IEEE Transactions on Biomedical Engineering*, *68*(1), 289–297. https://doi.org/10.1109/TBME.2020.3006158

Kiernan, D., Hawkins, D. A., Manoukian, M. A. C., McKallip, M., Oelsner, L., Caskey, C. F., & Coolbaugh, C. L. (2018). Accelerometer-based prediction of running injury in National Collegiate Athletic Association track athletes. *Journal of Biomechanics*, *73*, 201–209. https://doi.org/10.1016/j.jbiomech.2018.04.001

Matheson, G. O., Clement, D. B., McKenzie, D. C., Taunton, J. E., Lloyd-Smith, D. R., & MacIntyre, J. G. (1987). Stress fractures in athletes. A study of 320 cases. *The American Journal of Sports Medicine*, *15*(1), 46–58. https://doi.org/10.1177/036354658701500107

Meinel, K. (2008). *IAAF track and field facilities manual IAAF requirements for planning, constructing, equipping and maintaining* (D. Wilson, R. Bryborn, A. Guy, D. Katz, K. Meinel, J. Salcedo, & K. Wauhkonen, Eds.; 2008th ed.). Editions EGC.

Scott, S. H., & Winter, D. A. (1990). Internal forces at chronic running injury sites. *Medicine & Science in Sports & Exercise*, *22*(3), 357–369.

Weyand, P. G., Sternlight, D. B., Bellizzi, M. J., & Wright, S. (2000). Faster top running speeds are achieved with greater ground forces not more rapid leg movements. *Journal of Applied Physiology*, *89*(5), 1991–1999. https://doi.org/10.1152/jappl.2000.89.5.1991

1 Added lower limb mass does not affect biomechanical asymmetry but increases metabolic power in runners with a unilateral transtibial amputation

We determined the metabolic and biomechanical effects of adding mass to the running-specific prosthesis (RSP) and biological foot of individuals with a unilateral transtibial amputation (TTA) during running. 10 individuals (8 males, 2 females) with a TTA ran on a force-measuring treadmill at 2.5 m/s with 100 g and 300 g added to their RSP alone or to their RSP and biological foot while we measured their metabolic rates and calculated peak vertical ground reaction force (vGRF), stance-average vGRF, and step time symmetry indices. For every 100 g added to the RSP alone, metabolic power increased by 0.86% ($p = 0.007$) and for every 100 g added to the RSP and biological foot, metabolic power increased by 1.74% ($p < 0.001$) during running. Adding mass had no effect on peak vGRF ($p = 0.102$), stance-average vGRF ($p = 0.675$), or step time ($p = 0.413$) symmetry indices. We also found that the swing time of the affected leg was shorter than the unaffected leg across conditions ($p < 0.007$). Adding mass to the lower limbs of runners with a TTA increased metabolic power by more than what has been reported for those without an amputation. We found no effect of added mass on biomechanical asymmetry, but the affected leg had consistently shorter swing times than the unaffected leg. This suggests that individuals with a TTA maintain asymmetries despite changes in RSP mass and that lightweight prostheses could improve performance by minimizing metabolic power without affecting asymmetry.

1.1 Introduction

Metabolic power and oxygen consumption increases 1% for every 100 g added to each foot/ankle of runners without amputations across speeds ranging from 3.35 to 4.88 m/s (Frederick et al. 1984; Franz et al. 2012; Hoogkamer et al. 2016; Divert et al. 2008; Fuller et al. 2015; Martin 1985; Jones et al. 1984; Claremont and Hall 1988; Myers and Steudel 1985) and increased metabolic power worsens 3000 m running performance (Hoogkamer et al. 2016). While the directional changes between metabolic power and distance running performance are likely the same for individuals with and without a transtibial amputation (TTA), the effects of added lower limb mass on metabolic power for individuals with a TTA is unknown.

Most individuals with a TTA run using a running-specific prosthesis (RSP), which is a passive-elastic carbon fiber device that lacks an ankle joint and is attached to a carbon fiber socket that surrounds the residual limb. The effect of increased lower limb mass on metabolic power has been investigated in runners without a TTA (Modica and Kram 2005; Moed and Kram 2005), but the use of an RSP in individuals with a TTA likely influences the effect of lower limb mass on metabolic power. Because an RSP has approximately half the mass of a biological foot and shank (Brüggemann et al. 2008; De Leva 1996), adding mass to the RSP and biological foot of an individual with a TTA would result in a relatively larger increase in the mass of their affected leg compared to their unaffected leg. Thus, adding mass to the RSP may increase metabolic power by a greater amount in individuals with a TTA compared to values reported in individuals without a TTA.

The structural and functional differences between the biological foot and ankle and RSP of an individual with a TTA result in asymmetric running biomechanics (Beck and Grabowski 2017; Baum et al. 2016; Arellano et al. 2015; McGowan et al. 2012). For example, previous studies

found that when individuals with unilateral TTAs used a recommended RSP configuration, their affected leg generated 9% lower stance-average vertical ground reaction forces compared to their unaffected leg across a wide range of running speeds (3m/s—top speed) (Grabowski et al. 2009; Baum et al. 2016). In individuals with and without a TTA, asymmetric running biomechanics have been identified as risk factors for injury (Lloyd et al. 2010; Daly et al. 2016) and increase metabolic cost (Beck et al. 2017). However, adding mass to the RSP of individuals with a TTA may not affect the biomechanics of the affected leg. For example, Grabowski et al. (2009) found that adding 100 and 300 g to the RSP of sprinters with a TTA had no effect on leg swing time, stance-average vGRF, or maximum speed (Grabowski et al. 2009).

When a prosthetist prescribes an RSP to an individual with a TTA, they typically adjust prosthesis height, stiffness, and alignment to reduce kinematic asymmetries such as step frequency between legs (Innovations 2014). However, prosthetists are not often equipped to detect and minimize asymmetries in variables such as peak or stance-average vertical ground reaction force (vGRF), which have been associated with reductions in metabolic cost during running (Beck et al. 2017). Decreases in peak and stance-average vGRF asymmetry have been achieved by changing RSP model and height (Beck et al. 2017), but adding relatively small (≤ 300 g) amounts of mass to the RSP could increase the affected leg peak and stance-average vGRF (Clark et al. 2017), decrease asymmetry, and potentially lower metabolic power during running. Determining how RSP mass affects metabolic cost during running may therefore inform RSP design and rehabilitation strategies seeking to reduce running injury prevalence and improve running performance in individuals with a TTA.

We investigated the metabolic and biomechanical effects of adding mass to the RSP alone or to the RSP and biological foot of individuals with a TTA during running. We hypothesized that

adding mass to the RSP alone would decrease peak vGRF, stance-average vGRF, and step time asymmetry. Decreased biomechanical asymmetry in individuals with a TTA could potentially decrease metabolic cost (Beck et al. 2017), but adding mass to the RSP alone may increase metabolic power due to the additional metabolic energy required to support the increased body weight and to swing a heavier leg. Thus, we hypothesized that adding mass to the RSP alone would have no effect on metabolic power due to the offsetting effects of symmetry and biomechanical changes that increase metabolic power when running with added mass. We also hypothesized that mass added to the RSP and biological foot would have no effect on peak vGRF, stance-average vGRF, or step time asymmetry, and would increase metabolic power during running.

1.2 Methods

1.2.1 Participants

Ten individuals (8 males, 2 females; mean ± SD: mass 70.3 ± 8.3 kg, height 1.76 ± 0.09 m, age 38 ± 5 years) with a TTA participated. All participants had at least 1 year of experience using an RSP and reported running at least 3 days per week over the 6 months prior to data collection. The protocol was approved by the University of Colorado Boulder Institutional Review Board and all participants provided informed consent prior to participation.

1.2.2 Experimental Protocol

Each participant ran on a force-measuring treadmill (1000 Hz; Treadmetrix, Park City, UT, USA) while we measured their rates of oxygen consumption and carbon dioxide production via indirect calorimetry (ParvoMedics TrueOne 2400, Sandy, UT, USA). Participants were instructed to refrain from eating food or drinking anything but water for the 2 h leading up to data collection. Following a 5-min warm-up on the treadmill, participants ran at 2.5 m/s for 5 min under 5

conditions in a random order: no added mass, 100 g added to the RSP alone, 300 g added to the RSP alone, 100 g added to the RSP and biological foot (200 g total), and 300 g added to the RSP and biological foot (600 g total). Participants were given at least 5 min rest between conditions. During each trial we monitored respiratory exchange ratios and ensured that participants maintained primarily aerobic metabolism, indicated by a respiratory exchange ratio < 1.0. We added 100 g and 300 g to allow for comparison with prior work (Grabowski et al. 2009; Franz et al. 2012; Hoogkamer et al. 2016). We adhered the center of 100 g (10 cm × 5 cm × 2 cm) and 300 g (10 cm × 10 cm × 3 cm) 10 cm from the distal end of the RSP or shoe (**Figure 1.1**).

1.2.3 Analysis

We averaged rates of oxygen consumption and carbon dioxide production over the last 2 min of each trial, calculated gross metabolic power (Brockway 1987), and normalized metabolic power to each participant's body mass including their RSP and running clothes, but excluding the 100 g or 300 g added mass. At most, the added mass constituted ∼1% of a runner's body mass, and prior studies have not included this in the normalization of metabolic power (Hoogkamer et al. 2016; Myers and Steudel 1985; Franz et al. 2012). We measured ground reaction forces for 30 s during the final minute of each condition. We used a custom MATLAB script (Mathworks, Natick, MA, USA) to filter vGRF data using a zero-lag 4th-order low-pass Butterworth filter with a 30 Hz cut-off and used ten steps from each leg for analyses (Alcantara 2019). Step time was

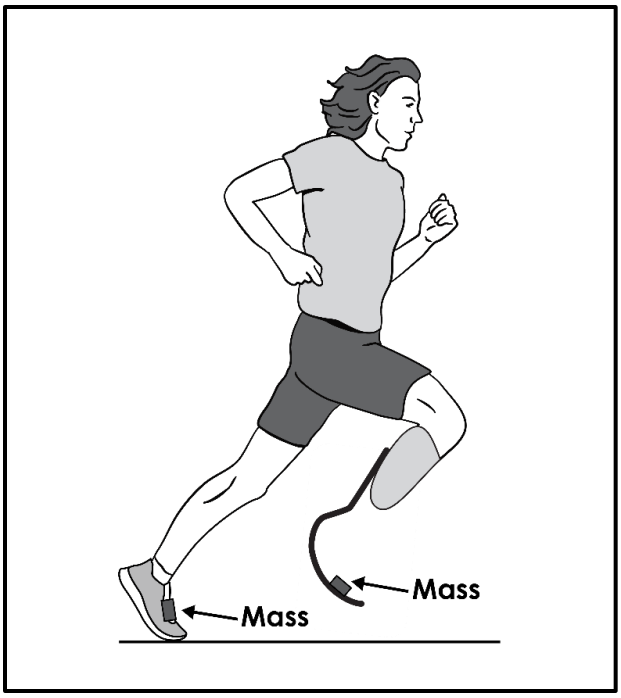

Figure 1.1 The center of the added mass was adhered 10 cm from the distal end of the shoe on the unaffected leg and of the RSP on the affected leg.

calculated as the time between a limb's initial contact with the ground and the initial contact of the contralateral limb. We defined stance phase as the period when the runner's vGRF exceeded a 20 N threshold. Stance-average vGRF was normalized to body weight and calculated as the mean vGRF during ground contact for each of the respective leg's ten steps. We used the absolute value of the symmetry index (SI) to determine peak vGRF, stance-average vGRF, and step time asymmetry between the affected and unaffected leg (Herzog et al. 1989). Symmetry Index is represented as a percentage (Eq. 1.1) where complete symmetry between the affected and unaffected leg is 0%:

$$SI = \left| \frac{Unaffected - Affected}{0.5 * (Unaffected - Affected)} \right| * 100 \quad (1.1)$$

We constructed linear mixed-effects models ($\alpha = 0.05$) to determine the effect of added mass on gross metabolic power, peak vGRF SI, stance-average vGRF SI, and step time SI during running. In each model, condition was considered a fixed effect and participant was considered a random effect. All models were verified for normality of residuals and homogeneity of variance

using the Shapiro–Wilk test ($\alpha = 0.05$). Non-statistically significant model coefficients were removed from the model on the basis that the coefficient was not significantly different than 0. Unstandardized model coefficients (B) are reported alongside the p value or within the model equation. Model coefficients represent the change in a dependent variable per unit change in an independent variable. This approach allows us to predict the change in gross metabolic power per 100 g added to the RSP, for example. We analyzed data in R (version 3.5.1) (R Core Team 2019) using custom scripts and packages (Pinheiro et al. 2018; Wickham 2016). We performed an a priori power analysis (Faul et al. 2007) based on prior results (Franz et al. 2012; Grabowski et al. 2009) to determine the appropriate number of participants to include in this study. Ten participants were needed to achieve a power of 0.9 and determine potential changes in metabolic power and limb symmetry due to mass added to the lower limbs during running.

We also performed a post hoc analysis to determine if adding mass to the lower limb affects leg swing time in individuals with a TTA. We calculated leg swing time as the duration between the end of the stance phase and the start of the subsequent stance phase. We constructed a linear mixed effects model ($\alpha = 0.05$) and considered condition a fixed effect and participant a random effect.

1.3 Results

The mean (± standard error) metabolic power of running at 2.5 m/s with no added mass was 11.97 ± 0.35 W/kg. For every 100 g added to the RSP alone, gross metabolic power increased 0.86 ± 0.25% ($p = 0.007$; **Figure 1.2**). When mass was added to the RSP and biological foot, the

effect approximately doubled as gross metabolic power increased by 1.74 ± 0.25% per 100 g added to each limb ($p < 0.001$; **Figure 1.2**).

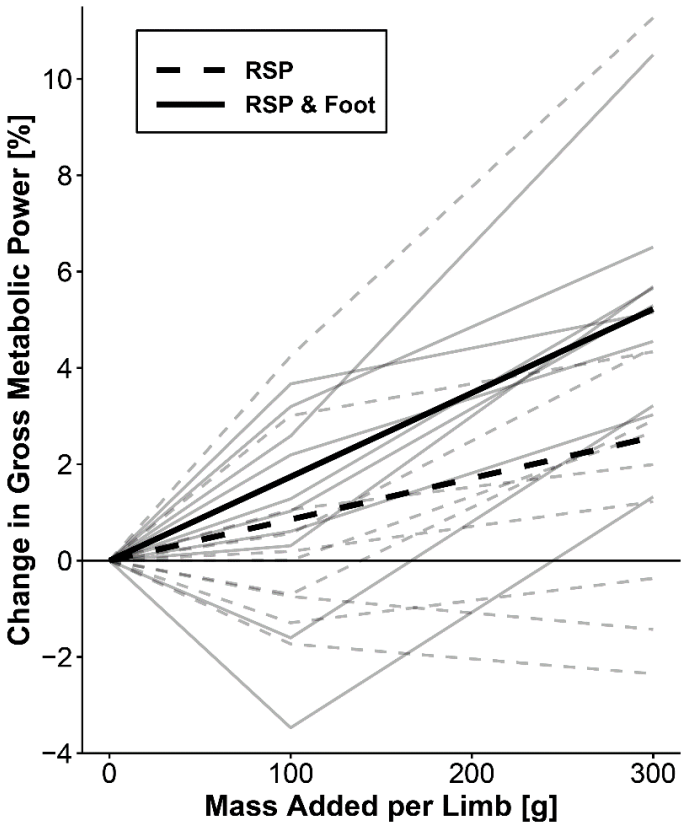

Figure 1.2 Percentage change in gross metabolic power for running at 2.5 m/s without added mass and with added mass of 100 and 300 g. Mass added to both the RSP alone resulted in a 0.86% increase in metabolic power (W/kg) per 100 g ($p = 0.007$; Metabolic Power [W/kg] = 11.947 + 0.001 × mass [g]). Mass added to the biological foot and RSP resulted in a 1.74% increase in metabolic power per 100 g added to each foot ($p < 0.001$; Metabolic Power [W/kg] = 11.924 + 0.002 × mass [g]). Thin lines represent participant-specific data, where the dashed lines indicate mass added to the RSP alone and the solid lines indicate mass added to RSP and biological foot. Thick black lines represent model overall predictions across conditions.

When running with no added mass, participants had a mean (± SE) stance-average vGRF SI of 7.39 ± 2.03%, peak vGRF SI of 13.95 ± 2.63%, and step time SI of 5.77 ± 1.58%. There was no significant change in symmetry indices regardless of the amount of mass added (100 or 300 g) or limb(s) mass was added to (RSP alone or RSP and biological foot). There were no differences in stance-average vGRF SI, peak vGRF SI, or step time SI between mass added to the RSP alone or mass added to the RSP and biological foot ($p = 0.389$, $p = 0.442$, and $p = 0.579$, respectively). Further, there were no effects of added mass on stance-average vGRF SI ($p = 0.675$), peak vGRF SI ($p = 0.102$), or step time SI ($p = 0.413$; **Table 1.1**).

When running with no additional mass, participants had a mean (± SE) leg swing time of 459 ± 16 ms for the affected leg and 468 ± 18 ms for the unaffected leg. This difference between leg swing times was statistically significant and persisted across added mass conditions. When we added mass to the RSP and biological foot, unaffected leg swing time was 10 ± 3 ms greater than affected leg swing time ($p = 0.007$), but there was no effect of added mass on leg swing time ($p = 0.228$). When we added mass to the RSP alone, unaffected leg swing time was 10 ± 3 ms greater than affected leg swing time ($p = 0.005$) and for every 100 g added to the RSP alone, swing time for both legs increased by 5 ± 1 ms ($p = 0.001$; **Figure 1.3**).

Table 1.1 Mean (± SE) symmetry Index (SI) for stance-average vertical ground reaction force (vGRF), peak vGRF, and step time across all conditions. There were no significant differences ($p > 0.05$) between adding mass to the running specific prosthesis (*RSP*) alone or adding mass to the RSP and biological foot (*both*). There were no significant changes in stance-average vGRF SI, peak vGRF, SI, or step time SI across added mass conditions ($p > 0.05$).

		Mass Added per Limb		
Symmetry Index (SI)	Location	0 g	100 g	300 g
Stance-Average vGRF SI	RSP	7.39 ± 2.03%	8.35 ± 1.95%	7.59 ± 2.06%
	Both		7.54 ± 2.16%	7.68 ± 2.01%
Peak vGRF SI	RSP	13.95 ± 2.63%	14.01 ± 3.03%	12.33 ± 2.82%
	Both		13.40 ± 2.79%	13.91 ± 2.43%
Step Time SI	RSP	5.77 ± 1.58%	5.75 ± 1.36%	5.23 ± 1.29%
	Both		5.66 ± 1.55%	5.77 ± 1.48%

1.4 Discussion

We reject our first and second hypotheses that mass added to the RSP alone would decrease peak vGRF asymmetry, stance-average vGRF, and step time asymmetry and have no effect on metabolic power during running. Although adding mass to the RSP alone reduced the mass discrepancy between the affected and unaffected leg, adding 100–300 g to the RSP had no effect on biomechanical asymmetry but increased metabolic power by 0.86% per 100 g added. This

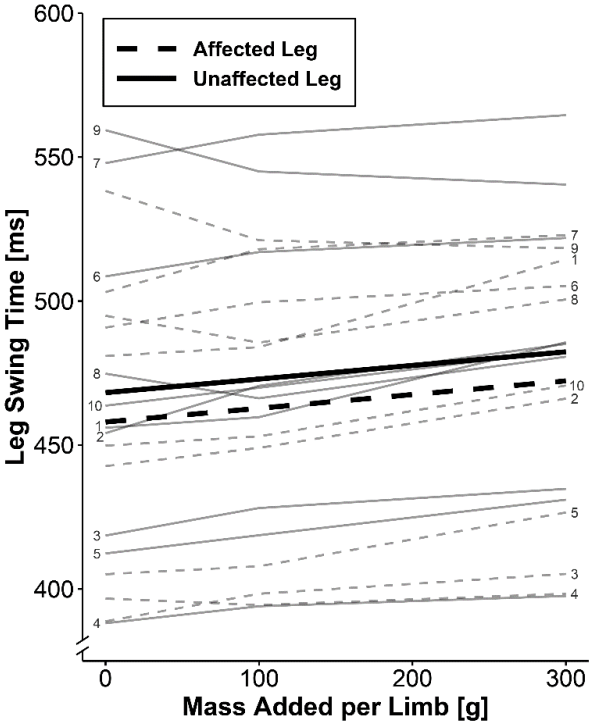

Figure 1.3 Swing time of the affected leg and unaffected leg for running at 2.5 m/s without added mass and with added mass of 100 and 300 g to the RSP alone. Across the added mass conditions, unaffected leg swing time was greater than affected leg swing time ($p = 0.005$), and swing time of both legs increased by 5 ms per 100 g ($p = 0.001$; Swing time [ms] = 458.01 + 0.0475 × mass [g] + 10.148 × leg [Affected: 0, Unaffected: 1]). Thin lines represent participant-specific data, where the dashed lines indicate the affected leg, and the solid lines indicate the unaffected leg. Participant number for unaffected leg swing time is on the left vertical axis and participant number for affected leg swing time is on the right vertical axis. Thick black lines represent model overall predictions across conditions.

finding highlights a potential area for RSP development, as a lighter RSP may decrease metabolic power while having no effect on biomechanical asymmetry. If a long-distance runner with a TTA was able to decrease their metabolic power using a lighter RSP, they may be able to improve their running performance due to the association between decreased metabolic power and improved long distance running performance in individuals without a TTA (Hoogkamer et al. 2016). Although adding mass to the RSP alone increased metabolic power in the present study, Beck et al. (2017) found that an optimal combination of RSP model, stiffness, and height increased peak vGRF symmetry and decreased metabolic cost of transport during running at 2.5–3.0 m/s (Beck et al. 2017). Our data suggest that RSP mass does not affect these measures of symmetry, as participants maintained asymmetric peak vGRF, stance-average vGRF, step time, and leg swing time despite running with up to 300 g added to their RSP. While RSP mass had no effect on biomechanical asymmetry, we found that increasing RSP mass increased metabolic power during running.

Adding mass to the RSP and biological foot had no effect on peak vGRF, stance-average vGRF, or step time asymmetry, but increased metabolic power by 1.74% per 100 g added to each limb (RSP and biological foot), which is greater than the reported ~1% increase in metabolic power per 100 g added to each foot or ankle in runners without a TTA (Frederick et al. 1984; Franz et al. 2012; Hoogkamer et al. 2016; Fuller et al. 2015; Martin 1985; Jones et al. 1984; Claremont and Hall 1988; Myers and Steudel 1985). We failed to reject our third and fourth hypotheses that mass added to the RSP and biological foot would have no effect on biomechanical asymmetry and that runners with a TTA would experience an increase in metabolic power when mass is added to the RSP and biological foot. Further, our data suggest that individuals with a transtibial amputation may be more metabolically sensitive to mass added to their RSP and biological foot compared to individuals without an amputation, potentially resulting in even slower long distance running performances (Hoogkamer et al. 2016).

The location of mass added to a runner's body has a differential effect on metabolic cost during running. Teunissen et al. (2007) found that when adding mass around the waist, every 10% increase in body mass (~6 kg) increased net metabolic power by ~13% to run at 3.0 m/s. The greater metabolic cost to run was primarily attributed to the increased force generation required to support body weight (Farley and McMahon 1992; Taylor et al. 1980). We extrapolated these findings to determine the effect of adding 600 g to the waist, which is ~1% of the average participant body mass and found that every 1% increase in body weight around the waist would increase net metabolic power by ~1.3%. If a similar mass is added to the lower limbs (300 g on each foot) of runners without a TTA, prior work (Franz et al. 2012; Hoogkamer et al. 2016) suggests that metabolic power would increase by ~3%. However, our findings indicate that metabolic power would increase by 5.2% in runners with a TTA due to the 1.74% increase in

metabolic power per 100 g on the RSP and biological foot. Further, the mass location affects the time during a stride that the metabolic penalty occurs. For example, when mass is added to the waist, the additional metabolic cost occurs during stance phase due to the additional force that the legs must produce to support the weight of the body during running (Arellano and Kram 2014; Teunissen et al. 2007; Farley and McMahon 1992; Taylor et al. 1980). But when mass is added to the feet, the legs need support the increased body weight and raise the foot with the added mass off the ground, swing it forward, and decelerate it before contacting the ground again (Modica and Kram 2005; Myers and Steudel 1985; Frederick et al. 1984). Thus, added mass to the feet incurs an additional metabolic cost during stance and swing phase.

Adding mass to the feet affects the lower leg's moment of inertia, which influences the metabolic energy required to swing the leg during running (Myers and Steudel 1985; Modica and Kram 2005; Martin 1985). We found that runners with a TTA have a larger increase in metabolic power due to mass added to their RSP and biological foot compared to runners without a TTA (1.74% vs. ~ 1% increase per 100 g on each foot (Frederick et al. 1984; Franz et al. 2012; Hoogkamer et al. 2016; Divert et al. 2008). Individuals with a TTA have approximately half the mass below the knee on their affected leg compared to a biological leg (Brüggemann et al. 2008; De Leva 1996) and thus 100 g added to the RSP represents a larger relative increase in the lower leg's moment of inertia relative to the knee, and presumably requires more metabolic energy to swing the leg. Using previously published inertial properties for an RSP, socket, and residual limb of a sprinter with TTAs (Brüggemann et al. 2008), we estimate that adding 100 g to the distal end of the RSP would increase the affected leg's moment of inertia by approximately 9% compared to 4% in an individual without a TTA. While the effects of leg moment of inertia on metabolic cost and muscle activation have been examined during walking in individuals with and without a TTA

(Royer and Martin 2005; Smith and Martin 2013; Selles et al. 2004), to our knowledge no studies have quantified the relationship between lower leg moment of inertia and metabolic cost during running in individuals with a TTA. We suspect that the greater metabolic costs incurred by individuals with a TTA when mass is added to the RSP are due to these disproportionately larger inertial loads, but this requires further investigation.

We found that adding mass to the RSP alone or to the RSP and biological foot of runners with a TTA had no effect on peak vGRF, stance-average vGRF, and step time asymmetry. It is possible that the mass added to the RSP in the present study was simply not enough to elicit changes in kinetic or kinematic asymmetry. However, we do not suspect that adding larger amounts of mass to the RSP would decrease biomechanical asymmetries enough to offset the increased metabolic power associated with the added mass. Prior work found that a 10% decrease in peak vGRF SI correlated to a 1.9% decrease in net metabolic cost of transport (energy expenditure per unit distance instead of unit time) in runners with a TTA (Beck et al. 2017), but when we added 300 g to the RSP, there was no effect on peak vGRF SI and gross metabolic power increased by ~2.6%. Thus, it is likely that any decrease in asymmetry would be outweighed by the metabolic cost of running with an additional mass on the RSP. Affected and unaffected leg swing time did not change with mass added to the RSP and biological foot, but unaffected leg swing time was consistently longer than affected leg swing time regardless of whether mass was added or not. The swing time of both legs increased as mass was added to the RSP alone. Thus, adding mass to the RSP alone increases affected leg swing time but participants increased unaffected leg swing time and thereby maintained leg swing time asymmetry. Grabowski et al. (2009) found that swing time between the affected and unaffected leg did not differ when adding 100 and 300 g to the RSP compared to no added mass at running speeds of 3 m/s up to maximum speed (Grabowski et al.

2009). However, our findings do not corroborate those of Grabowski et al. (2009). It is possible that different results between studies are due to differences in statistical power, as Grabowski et al. (2009) state that they may have had limited statistical power due to including six participants in their study (Grabowski et al. 2009).

We chose to add 100 g and 300 g to the RSP and biological foot of our participants to make direct comparisons to prior work (Frederick et al. 1984; Franz et al. 2012; Hoogkamer et al. 2016). A future study investigating how metabolic power is affected by adding a proportional amount of mass to the legs of runners with and without a TTA could further elucidate the effect of added mass on runner's feet by effectively normalizing to lower leg mass. However, small amounts of mass may only be realistically added to the RSP before the socket fit is compromised and becomes unattached from the residual limb during running. We were unable to compare the effect of added mass on metabolic power between male and female runners with a TTA because only 2 females volunteered to participate in the present study. However, we normalized metabolic power to body mass so that we could quantify the effect of added lower limb mass across participants with different body masses. Previous work (Frederick et al. 1984; Franz et al. 2012; Hoogkamer et al. 2016; Divert et al. 2008) has determined how oxygen consumption and metabolic power are affected by adding mass to the shoes of individuals who ran at faster speeds (3.35–4.88 m/s) than the speed we tested (2.5 m/s), which may limit the generalizability of our findings. Additionally, Frederick et al. (1984) found that the effect of added mass on oxygen consumption may decrease with faster speeds (Frederick et al. 1984). While other previous studies have found that metabolic power and oxygen consumption increases ~1% for every 100 g added to each foot at speeds from 3.35 to 3.61 m/s (Franz et al. 2012; Hoogkamer et al. 2016; Divert et al. 2008), it is possible that runners with a TTA may experience a reduced effect of added mass at speeds faster than 2.5 m/s.

Further studies are required to better understand the effect of added mass on metabolic power across a wide range of running speeds.

1.5 Conclusions

Adding 100 and 300 g to the RSP alone increased metabolic power by 0.86% per 100 g and had no effect on stance-average vGRF, peak vGRF, or step time asymmetry. Adding 100 and 300 g to the RSP and biological foot of runners with a TTA increased metabolic power by 1.74% per 100 g on each leg. The swing time of the unaffected leg in runners with a TTA was greater than the swing time of the affected leg across all conditions and adding mass to the RSP alone increased the swing time of both legs proportionally. Adding mass to the RSP and biological foot had no effect on stance-average vGRF, peak vGRF, or step time asymmetry. Thus, adding mass to the RSP alone does not decrease asymmetry and would likely worsen distance running performance due to the associated increase in metabolic power. In contrast, reducing RSP mass may improve distance running performance in individuals with a transtibial amputation by reducing metabolic power while having no effect on biomechanical asymmetry.

1.6 References

Alcantara RS (2019) Dryft: A Python and MATLAB package to correct drifting ground reaction force signals during treadmill running. *Journal of Open Source Software* 4(44):1910

Arellano CJ, Kram R (2014) Partitioning the metabolic cost of human running: a task-by-task approach. *Integrative and Comparative Biol*ogy 54(6):1084–1098

Arellano CJ, McDermott WJ, Kram R, Grabowski AM (2015) Effect of running speed and leg prostheses on mediolateral foot placement and its variability. *PLoS One* 10(1):e0115637

Baum BS, Hobara H, Kim YH, Shim JK (2016) Amputee locomotion: Ground reaction forces during submaximal running with running-specific prostheses. *Journal of Applied Biomechanics* 32(3):287–294

Beck ON, Grabowski AM (2017) The biomechanics of the fastest sprinter with a unilateral transtibial amputation. *Journal of Applied Physiology* 124(3):641–645

Beck ON, Taboga P, Grabowski AM (2017) Prosthetic model, but not stiffness or height, affects the metabolic cost of running for athletes with unilateral transtibial amputations. *Journal of Applied Physiology* 123(1):38–48

Brockway J (1987) Derivation of formulae used to calculate energy expenditure in man. *Human Nutrition: Clinical Nutrition* 41(6):463–471

Brüggemann GP, Arampatzis A, Emrich F, Potthast W (2008) Biomechanics of double transtibial amputee sprinting using dedicated sprinting prostheses. *Sports Technology* 1(4–5):220–227

Claremont AD, Hall SJ (1988) Effects of extremity loading upon energy expenditure and running mechanics. *Medicine & Science in Sports Exercise* 20(2):167–171

Clark KP, Ryan LJ, Weyand PG (2017) A general relationship links gait mechanics and running ground reaction forces. *Journal of Experimental Biology* 220(2):247–258

Daly C, McCarthy Persson U, Twycross-Lewis R, Woledge R, Morrissey D (2016) The biomechanics of running in athletes with previous hamstring injury: a case–control study. *Scandinavian Journal of Medicine & Science in Sports* 26(4):413–420

De Leva P (1996) Adjustments to Zatsiorsky-Seluyanov's segment inertia parameters. *Journal of Biomechanics* 29(9):1223–1230

Divert C, Mornieux G, Freychat P, Baly L, Mayer F, Belli A (2008) Barefoot-shod running differences: shoe or mass effect? *International Journal of Sports Medicine* 29(06):512–518

Farley CT, McMahon TA (1992) Energetics of walking and running: insights from simulated reduced-gravity experiments. *Journal of Applied Physiology* 73(6):2709–2712

Faul F, Erdfelder E, Lang AG, Buchner A (2007) G* power 3: a flexible statistical power analysis program for the social, behavioral, and biomedical sciences. *Behavioral Research Methods* 39(2):175–191

Franz JR, Wierzbinski CM, Kram R (2012) Metabolic cost of running barefoot versus shod: is lighter better*? Medicine & Science in Sports & Exercise* 44(8):1519–1525

Frederick E, Daniels J, Hayes J (1984) The effect of shoe weight on the aerobic demands of running. Urban & Schwarzenberg, Vienna

Fuller JT, Bellenger CR, Thewlis D, Tsiros MD, Buckley JD (2015) The effect of footwear on running performance and running economy in distance runners. *Sports Medicine* 45(3):411–422

Grabowski AM, McGowan CP, McDermott WJ, Beale MT, Kram R, Herr HM (2009) Running-specific prostheses limit ground-force during sprinting. *Biology Letters* 6(2):201–204

Herzog W, Nigg BM, Read LJ, Olsson E (1989) Asymmetries in ground reaction force patterns in normal human gait. *Medicine & Science in Sports & Exercise* 21(1):110–114

Hoogkamer W, Kipp S, Spiering BA, Kram R (2016) Altered running economy directly translates to altered distance-running performance. *Medicine & Science in Sports & Exercise* 48(11):2175–80

Innovations F (2014) Catapult running foot instructions for use. Freedom Innovations, Irvine

Jones BH, Toner MM, Daniels WL, Knapik JJ (1984) The energy cost and heart-rate response of trained and untrained subjects walking and running in shoes and boots. *Ergonomics* 27(8):895–902

Lloyd CH, Stanhope SJ, Davis IS, Royer TD (2010) Strength asymmetry and osteoarthritis risk factors in unilateral trans-tibial, amputee gait. *Gait & Posture* 32(3):296–300

Martin PE (1985) Mechanical and physiological responses to lower extremity loading during running. *Medicine & Science in Sports & Exercise* 17(4):427–433

McGowan CP, Grabowski AM, McDermott WJ, Herr HM, Kram R (2012) Leg stiffness of sprinters using running-specific prostheses. *Journal of the Royal Society Interface* 9(73):1975–1982

Modica JR, Kram R (2005) Metabolic energy and muscular activity required for leg swing in running. *Journal of Applied Physiology* 98(6):2126–2131

Moed B, Kram R (2005) Metabolic costs of forward propulsion and leg swing at different running speeds. In: *ISB XXth congress ASB 29th annual meeting*, Cleveland, OH

Myers M, Steudel K (1985) Effect of limb mass and its distribution on the energetic cost of running. *Journal of Experimental Biology* 116(1):363–373

Pinheiro J, Bates D, DebRoy S, Sarkar D (2018) R core team (2018). nlme: Linear and nonlinear mixed effects models. r package version 3.1-137

R Core Team (2019) R: A language and environment for statistical computing. R Foundation for Statistical Computing, Vienna, Austria. https://www.R-proje ct.org/

Royer TD, Martin PE (2005) Manipulations of leg mass and moment of inertia: Effects on energy cost of walking. *Medicine & Science in Sports & Exercise* 37(4):649–656

Selles RW, Bussmann JB, Van Soest AK, Stam HJ (2004) The effect of prosthetic mass properties on the gait of transtibial amputees–a mathematical model. *Disability Rehabilitation* 26(12):694–704

Smith JD, Martin PE (2013) Effects of prosthetic mass distribution on metabolic costs and walking symmetry. *Journal of Applied Biomechanics* 29(3):317–328

Taylor CR, Heglund NC, McMahon TA, Looney TR (1980) Energetic cost of generating muscular force during running: A comparison of large and small animals. *Journal of Experimental Biology* 86(1):9–18

Teunissen LP, Grabowski A, Kram R (2007) Effects of independently altering body weight and body mass on the metabolic cost of running. *Journal of Experimental Biology* 210(24):4418–4427

Wickham H (2016) ggplot2: elegant graphics for data analysis. Springer, New York. https://ggplot2.tidyv erse.org

2 Biomechanics of maximum effort sprinting on flat curves

To sprint along a curve, an athlete must produce vertical and centripetal ground reaction forces (GRFs) to support their body weight and accelerate towards the inside of the curve. Competitive sprinters navigate different radius curves depending on lane assignment and track design. GRFs of the inside and outside leg relative to the curve may change with curve radius and be affected by leg joint kinematics and kinetics. We measured the maximum velocity and leg-specific GRFs, joint kinematics, and joint kinetics of 9 experienced sprinters (8 M, 1 F; 400 m personal best: 47.76 ± 1.49 s) as they ran at maximum effort on a straightaway, 36.5 m radius curve, and 17.2 m radius curve. Maximum velocity decreased 8% (0.65 m/s) from the 36.5 m radius curve to the 17.2 m radius curve ($p < 0.001$). On the 36.5 m radius curve, the inside leg produced 0.17 BW greater stance-average centripetal GRFs than the outside leg ($p < 0.001$) but there was no difference between inside and outside leg stance-average centripetal GRFs on the 17.2 m radius curve ($p = 0.357$). The outside leg produced 0.10 BW greater stance-average vertical GRFs than the inside leg on the 36.5 m radius curve ($p = 0.006$) and 0.21 greater stance-average vertical GRFs than the inside leg on the 17.2 m radius curve ($p < 0.001$). There were differences between ankle, knee, and hip peak joint angles and moments in the sagittal, frontal, and transverse planes between legs. We also found that the effect of curve radius on the joint kinematics and kinetics of the outside leg may differ from those of the inside leg. Our findings indicate that leg-specific kinematics and kinetics may limit maximum velocity on a curve, which can inform training programs for athletes seeking to improve curve sprinting performance.

2.1 Introduction

For outdoor track events such as the 200 m and 400 m sprint, more than half the race is completed on a flat curve (Meinel, 2008). Maximum sprinting velocity is slower on a curve relative to a straightaway (Chang & Kram, 2007; Churchill et al., 2015, 2016; Greene, 1985; Jain, 1980) with smaller curve radii resulting in slower maximum sprinting velocities than larger curve radii (Chang & Kram, 2007; Greene, 1985; Jain, 1980). Thus, the ability of a sprinter to navigate a track's curves likely limits performance in track events like the 200 m and 400 m sprint.

Track and field athletes must navigate a range of curve radii due to lane assignment or track design. Track curve radii can range from 17.2 m (innermost lane of a regulation 200 m indoor track) to 45.0 m (outermost lane of a regulation 400 m outdoor track). Previous studies measured maximum velocity on a curve with a radius equivalent to lane 2 of a 400 m track (37.72 m) and lane 1 of a 200 m track (17.2 m) and found that maximum velocity decreased 2.3% - 4.7% from the straightaway to the 37.72 m radius curve (Churchill et al., 2015, 2016) and 8.9% from the straightaway to the 17.2 m curve (Taboga et al., 2016). Greene (1985) developed a theoretical mathematical model of the changes in maximum velocity across a wide range of curve radii (approx. 3 – 30 m), and based the model on experimental data collected on grass and concrete surfaces (Greene, 1985). To better understand potential performance limitations during track and field sprints, we determined maximum velocity on curves with radii typical of track and field competitive conditions, and compared this to theoretical models describing the relationship between maximum velocity and curve radius.

Sprinting on a curved path requires an athlete to produce centripetal ground reaction forces (cGRF) to accelerate their body towards the inside of the curve, where maintaining a given velocity for a smaller curve radius requires an increase in cGRF. Moreover, experimental data show that

cGRF production of the inside and outside leg likely affects maximum curve velocity (Chang & Kram, 2007; Churchill et al., 2016; Judson et al., 2019; Luo & Stefanyshyn, 2012a). There is also evidence that leg-specific cGRF production may change with curve radius, as the inside leg produces greater cGRF than the outside leg on a 37.72 m radius curve (Churchill et al., 2016) but lower cGRF than the outside leg on 1 – 6 m radii curves (Chang & Kram, 2007; Smith et al., 2006). Additionally, vertical ground reaction force (vGRF) production is similar for the inside and outside leg on a 37.72 m radius curve (Churchill et al., 2016), but the inside leg produced lower vGRF than the outside leg on 1 – 6 m radii curves (Chang & Kram, 2007). Quantifying leg-specific cGRF and vGRF may potentially explain changes in maximum velocity when sprinting on curves with different radii.

The inward lean of the upper body relative to the lower body during curve sprinting places the inside and outside leg in distinct kinematic configurations in the frontal and transverse planes (Alt et al., 2015; Churchill et al., 2015; Judson, Churchill, Barnes, Stone, Brookes, et al., 2020). When sprinting on a curve, peak ankle joint angles in the frontal plane differ between the inside and outside leg, with the inside ankle everted (up to 35°) and the outside ankle more inverted (2.6 ± 5.1°) (Alt et al., 2015; Luo & Stefanyshyn, 2012a). Previous studies have also found that the knee of the outside leg had 4° greater peak internal rotation than the knee of the inside leg and that the hip of the inside leg had 8.3 – 9.8° greater peak adduction than the hip of the outside leg when sprinting on 36.5 m and 37.72 m radii curves. (Alt et al., 2015; Churchill et al., 2015). These leg-specific kinematics indicate that the inside and outside leg have distinct biomechanical functions during curve sprinting and may be responsible for leg-specific differences in force production (Chang & Kram, 2007, 2007; Churchill et al., 2015; Luo & Stefanyshyn, 2012a), but it is unknown how kinematic differences are affected by curve radii typical of track and field sprint events.

Considering the range of radii that track and field athletes navigate, a comparison of leg-specific kinematics changes between different curve radii may further contribute to our understanding of the biomechanical limitations to curve sprinting.

Ankle plantarflexor and knee extensor muscles are primarily responsible for vGRF production when sprinting on a straightaway (Dorn et al., 2012) and directly affect sprinting performance as greater velocities are primarily achieved via increased stance-average vGRF ($vGRF_{Avg}$) production (Weyand et al., 2000). The lower extremity moments generated by muscles surrounding the ankle, knee, and hip joints contribute to the production of vGRF during straightaway sprinting, but their contribution to cGRF and vGRF production during curve sprinting is unknown. Prior studies have determined joint moments when navigating a 2.5 m radius curve (Luo & Stefanyshyn, 2012a, 2012b) and during the start (0 – 12 m) of a sprint on a 37.72 m radius curve (Judson, Churchill, Barnes, Stone, & Wheat, 2020), but an investigation into joint moments during maximum velocity sprinting may provide insight into underlying differences in force production between the inside and outside leg during curve sprinting.

An analysis of maximum effort sprinting and the corresponding changes in velocity, force production, and lower body biomechanics on curves representative of those experienced by track and field athletes would identify curve sprinting limitations and provide potential opportunities to improve curve sprinting performance. We sought to investigate changes in maximum velocity, force production, joint kinematics, and joint moments of track and field athletes sprinting on a straightaway and two flat track curves (17.2 m and 36.5 m radii). Based on previous studies (Churchill et al., 2015, 2016; Taboga et al., 2016) and theoretical models (Greene, 1985), we hypothesized that: 1) maximum sprinting velocity would decrease on curves relative to a straightaway, 2) the 17.2 m radius curve would result in slower maximum velocities than the 36.5

m radius curve, and 3) sprinting in the clockwise (CW) direction on a curve would result in slower velocities than the counterclockwise (CCW) direction due to training. We also hypothesized that: 4) the inside leg would produce greater $cGRF_{Avg}$ than the outside leg on both curves, but 5) the outside leg would produce greater $vGRF_{Avg}$ than the inside leg on both curves. Based on a previous study of joint kinematics and kinetics during sprinting on a 36.5 m radius curve (Alt et al., 2015), we hypothesized that: 6) the inside ankle, knee, and hip would have similar sagittal plane peak joint angles but different frontal and transverse plane peak joint angles as the outside ankle, knee, and hip on both curves. Considering the relationship between sagittal plane joint moments and vGRF, we hypothesized that: 7) peak ankle, knee, and hip sagittal plane moments would be greater in the outside leg than the inside leg on both curves. In agreement with peak joint moments measured near the start of a sprint (12 m) on a 37.72 m radius curve (Judson, Churchill, Barnes, Stone, & Wheat, 2020), we hypothesized that: 8) the inside ankle, knee, and hip would have greater frontal and transverse plane peak moments than the outside ankle, knee and hip on both curves.

2.2 Methods

2.2.1 Study Population

Nine National Collegiate Athletic Association (NCAA) track and field athletes (8 Male, 1 Female; 200 m personal best: 22.60 ± 2.39 s; 400 m personal best: 47.76 ± 1.49 s; body mass: 74.6 ± 9.5 kg; height: 1.83 ± 0.10 m; age: 21 ± 1 years) with curve sprinting experience participated in this study. Participants reported no musculoskeletal injures at the time of data collection and provided written informed consent prior to participating in the study. The experimental protocol was approved by the University of Colorado Boulder Institutional Review Board (#18-0005).

2.2.2 Experimental Design

Athletes completed a randomized series of 40 m sprints on a flat indoor track. Athletes were instructed to perform maximal effort sprints on a straightaway and on clockwise (CW) and counterclockwise (CCW) curves with radii of 17.2 m and 36.5 m, marked with cones and representative of the innermost lane on a regulation 200 m and 400 m track (Meinel, 2008), respectively (**Figure 1**). During competition, the 200 m and 400 m sprint events are performed in the CCW direction, but we included the CW condition to quantify the effect of curve sprinting direction on maximum sprinting velocity. Kinematic and kinetic data collected on the CW and CCW curves were combined to analyze the biomechanics of the inside and outside leg with the assumption that the left and right legs are symmetric in sprinters without any apparent musculoskeletal injury. Athletes practiced sprinting on the curves and adjusted their starting position to allow them to reach maximum sprinting velocity halfway along the straightaway or curve. Sprints were repeated for each condition until athletes successfully landed on a force plate with each leg at least once. We considered a trial unsuccessful if an athlete's foot was not entirely on the force plate during stance phase or they failed to stay within the lane of the curve (approximately 1.2 m width) for the entire 40 meters. Data from all successful trials were used for data analysis. Athletes wore their own spiked sprinting footwear, compression shorts, and were provided ≥ 8 minutes of rest between trials.

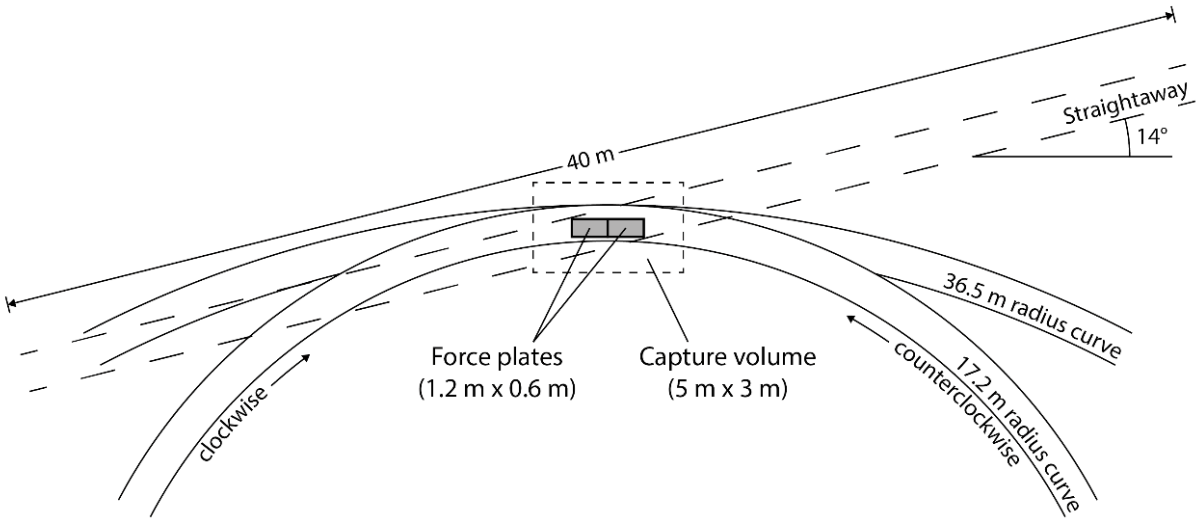

Figure 2.1 Illustration of the experimental setup (to scale). The force plates and capture volume were located halfway along the 40 m straightaway and curves. Athletes could adjust their starting position on the curves to attain maximum sprinting velocity within the capture volume. The straightaway was rotated 14° relative to the force plates due to the location of the force plates in the indoor track facility.

2.2.3 Materials

Two force plates (1000 Hz; 1.2 x 0.6 m; AMTI, Watertown, MA, USA) covered in Mondo (Mondo S.p.A., Alba, Italy) track surface were embedded in the ground so that the top surface was level with the track and located halfway along the straightaway or curve. Ten motion capture cameras (200 Hz; 3 x 5 m capture volume; Vicon, Centennial, CO, USA) surrounded the force plates (**Figure 2.1**). We adhered retroreflective markers to the pelvis and feet, on joint centers, and with rigid retroreflective marker clusters tightly strapped to both thighs and shanks to measure lower body kinematics. Athletes completed standing static trials with calibration markers located at the greater trochanter, medial femoral epicondyle, lateral femoral epicondyle, medial malleolus, and lateral malleolus. We used the standing trial to define a neutral pose and thus represented 0° for the ankle, knee, and hip joint angles.

2.2.4 Processing

Data processing was performed in MATLAB (R2020a; Mathworks, Natick, MA, USA) with custom scripts and packages (Alcantara, 2019). 3D GRFs and kinematic data were filtered with a 4th order zero-lag low-pass Butterworth filter with a 50 Hz cutoff. GRFs and kinematic data were filtered identically to avoid introducing artefacts into joint moment calculations due to different filter parameters (Bezodis et al., 2013; Bisseling & Hof, 2006).

To measure cGRF during the stance phase, we used a 5 N vGRF threshold and transformed the local coordinate system of the force plate so that the horizontal axes were aligned relative to the position of the athlete on the curve. On the curve conditions, this was accomplished by projecting the horizontal forces on new coordinate system vectors rotated by the angle formed by the 3rd metatarsal head marker at the time of peak vertical GRF, the center of the curve, and the origin of the global coordinate system (where the horizontal axes of the force plate are tangential and radial). The transformed horizontal axes were rotated < 3° from the force plate's original coordinate system. It was necessary to rotate the straightaway by 14° due to the location of the force plates in the indoor track facility (Figure 1). Thus, we projected the horizontal forces collected on the straightaway on new coordinate system vectors rotated by 14°.

Joint kinetics and kinematics were calculated using a rigid-segment model in Visual3D (C-Motion, Rockville, MD, USA). Internal joint moments were normalized to body weight (BW) and the duration of the stance phase. Joint angles were defined as the rotation of the distal segment relative to the proximal segment where 0° represents the orientation of the joint during the standing trial and were normalized to the duration of the stance phase. Left leg joint angles and moments in the frontal and transverse planes were multiplied by -1 to match the direction of the right leg's joint angles and moments.

For the curve conditions, we measured sprinting velocity using the average pelvis marker velocity, which was calculated using markers located bilaterally on the iliac crests, anterior superior iliac spines, and posterior superior iliac spines. Sprinting velocity was averaged over the length of the capture volume (~5m) for the curve conditions. Due to the location of the force plates in the indoor track facility, athletes were unable to adjust their starting position backwards on the straightaway to ensure that maximum velocity was attained within the capture volume. Thus, we used a radar gun (47 Hz; Stalker ATS II, Applied Concepts Inc, Plano TX) to measure the maximum sprinting velocity along the 40 m straightaway. We used the maximum value from a moving average of the radar gun velocity data (0.32 s window) to determine maximum sprinting velocity on the straightaway.

We calculated discrete variables individually for the inside and outside leg during the curve sprinting conditions and averaged between legs for the straightaway condition. We calculated peak 3D angles for the ankle, knee, and hip during the stance phase to allow for comparison with previous studies (Alt et al., 2015; Churchill et al., 2015; Judson, Churchill, Barnes, Stone, Brookes, et al., 2020; Luo & Stefanyshyn, 2012a). We also calculated peak joint moments for the ankle, knee, and hip to allow for comparison with previous studies (Judson, Churchill, Barnes, Stone, & Wheat, 2020; Luo & Stefanyshyn, 2012b).

2.2.5 Analysis

Data analysis was performed in R (version 3.6.3) using custom scripts and packages (Lenth, 2020; Pinheiro et al., 2020; R Core Team, 2020; Wickham, 2009; Wickham et al., 2020; Wickham & RStudio, 2020). We used a paired t-test ($\alpha = 0.05$) to compare maximum curve sprinting velocity to Greene's (Equation 11 in Greene, 1985) predictions. We constructed linear mixed-effects models to quantify changes in maximum velocity, force production, joint

kinematics, and joint kinetics across conditions. We considered curve running direction (CCW, CW), and condition (straightaway, 17.2 m radius curve, 36.5 m radius curve), and leg side (inside, outside) as categorical fixed effects and athlete as a random effect. Models were first constructed with interaction terms, but non-statistically significant model coefficients were removed from the model on the basis that the coefficient was not significantly different than zero. When statistically significant ($p < 0.05$) interactions were present, we performed *post-hoc* pairwise comparisons to analyze simple effects and applied the Bonferroni correction method to each family of comparisons. We report the numerical difference between each level of a fixed effect (e.g. inside vs. outside leg) or the unstandardized model coefficients (B) alongside the p value.

2.3 Results

2.3.1 Velocity

The linear mixed-effects model revealed that maximum sprinting velocity on the straightaway (9.12 m/s) was 11.7% faster than on the 17.2 m radius curve in the CW direction ($B = 1.07$ m/s; $p < 0.001$) and 10.2% faster than the CCW direction ($B = 0.93$ m/s; $p < 0.001$; **Figure 2.2**). Additionally, maximum sprinting velocity on the straightaway was 4.3% faster than on the 36.5 m radius curve in the CW direction ($B = 0.39$, $p < 0.001$) and 3.4% faster than the CCW direction ($B = 0.31$ m/s; $p < 0.001$).

We found no interaction effect of sprinting direction and curve radius on maximum sprinting velocity ($p = 0.479$), indicating that the effect of curve radii and sprinting direction on maximum sprinting velocity were not dependent upon each other. For a given sprinting direction, maximum sprinting velocity on the 36.5 m radius curve was 8.0% greater than on the 17.2 m radius curve ($B = 0.65$ m/s; $p < 0.001$). For a given curve radius, maximum sprinting velocity in the CCW

direction was 1.4% faster than the CW direction ($B = 0.11$ m/s; $p = 0.001$). Greene (1985) presented an equation (Eq. 11) that predicts that, regardless of sprinting direction, the maximum velocity of the athletes in the present study should decrease by 5.8 ± 0.9% from the 36.5 m to the 17.2 m radius curve (Greene, 1985). Combining data from both sprinting directions, maximum velocity decreased by 7.2 ± 2.4%, which was significantly greater than the change predicted by Greene (paired two-tailed t test, $p = 0.048$).

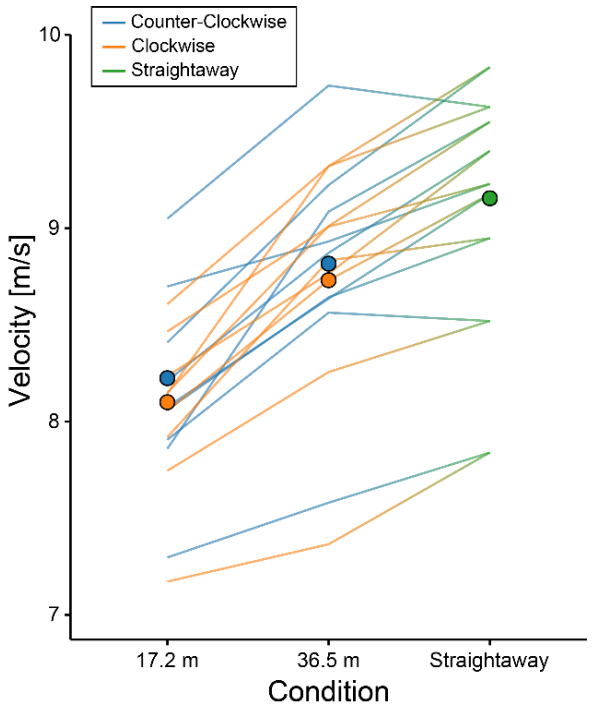

Figure 2.2 Maximum velocity on curves and the straightaway. Each point indicates the mean across all athletes (individual lines). Color denotes the straightaway and clockwise (CW) or counterclockwise (CCW) directions on the 17.2 m and 36.5 m radii curves.

2.3.3 Centripetal Forces

We found a significant interaction effect of curve radius and inside or outside leg on $cGRF_{Avg}$ ($p = 0.029$). On the 36.5 m radius curve, $cGRF_{Avg}$ for the inside leg was 0.48 BW, which was 0.10 BW greater than for the outside leg ($p < 0.001$), but there was no significant difference ($p = 0.357$) in $cGRF_{Avg}$ between the inside (0.68 BW) and outside leg (0.645 BW) on the 17.2 m radius curve (**Figure 3A**). $cGRF_{Avg}$ on the 17.2 m radius curve was 0.21 BW greater than on the 36.5 m radius

curve for the inside leg ($p < 0.001$) and 0.27 BW greater than the 36.5 m radius curve for the outside leg ($p < 0.001$).

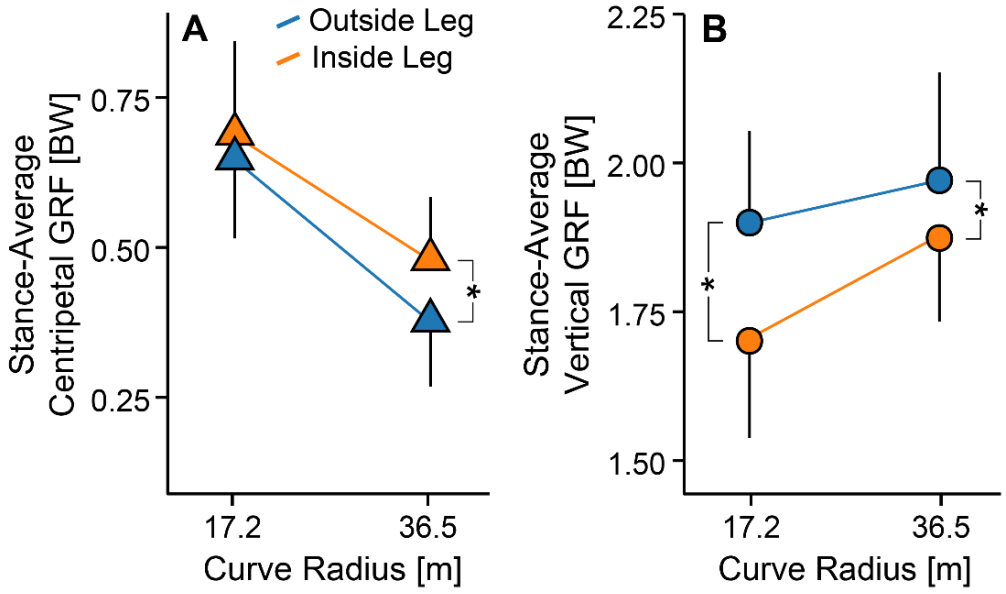

Figure 2.3 Stance-average centripetal and vertical ground reaction force (GRF) on the 17.2 m and 36.5 m radii curves. Error bars represent 1 standard deviation from the mean across athletes. A) Stance-average centripetal GRF for the inside leg was 0.17 BW greater than for the outside leg only on the 36.5 m radius curve ($p < 0.001$). B) Stance-average vertical GRF for the inside leg was 0.21 BW lower than for the outside leg on the 17.2 m radius curve ($p < 0.001$) and 0.10 BW lower than for the outside leg on the 36.5 m radius curve ($p = 0.006$).

2.3.3 Vertical Forces

Mean ± SD $vGRF_{Avg}$ on the straightaway was 1.91 ± 0.16 BW. There was no significant difference between $vGRF_{Avg}$ when sprinting on the straightaway compared to the inside leg ($p = 0.183$) or outside leg ($p = 0.070$) on the 36.5 m radius curve. On the 17.2 m radius curve, the inside leg $vGRF_{Avg}$ was 0.22 BW lower than on the straightaway ($p < 0.001$), but the outside leg $vGRF_{Avg}$ was not significantly different than on the straightaway ($p = 0.730$).

We found a significant interaction effect of curve radius and inside or outside leg on $vGRF_{Avg}$ ($p = 0.009$). $VGRF_{Avg}$ of the inside leg was 1.70 BW on the 17.2 m radius curve, which

was 0.17 BW lower than on the 36.5 m radius curve ($p < 0.001$). Stance average vGRF of the outside leg had was not significantly different ($p = 0.101$) between the 17.2 m (1.90 BW) or 36.5 m radius (1.97 BW) curves. $VGRF_{Avg}$ of the inside leg was 0.21 BW ($p < 0.001$) and 0.10 BW ($p = 0.006$) lower than the outside leg on the 17.2 m and 36.5 m radii curves, respectively (**Figure 2.3B**).

2.3.4 Joint Kinematics

Sagittal Plane

There was no interaction effect of curve radius and inside or outside leg on peak ankle dorsiflexion angle ($p = 0.378$). The peak ankle dorsiflexion angle was 18.3° on the 36.5 m radius curve and 16.9° on the 17.2 m radius curve for the outside leg, which was 5.0° greater than the peak ankle dorsiflexion angle for both curve radii for the inside leg ($p < 0.001$; **Figure 2.4A**). There was no significant effect of curve radius on the peak ankle dorsiflexion angle for the inside or outside leg ($p = 0.107$).

There was no interaction effect of curve radius and inside or outside leg on peak knee flexion angle ($p = 0.791$). The peak knee flexion angle was 44.4° on the 36.5 m radius curve and 46.1° on the 17.2 m radius curve for the outside leg, which was 3.3° greater than the peak knee flexion angle for the inside leg ($p < 0.001$; **Figure 2.4D**). Peak knee flexion was 1.7° lower when sprinting on the 36.5 m radius curve compared to the 17.2 m radius curve for both legs ($p = 0.044$).

There was no interaction effect of curve radius and inside or outside leg on peak hip flexion ($p = 0.119$) or hip extension ($p = 0.133$) angles. The peak hip flexion angle was 44.0° on the 36.5 m radius curve and 48.6° on the 17.2 m radius curve for the outside leg, which was 2.0° less than the peak hip flexion angle for the inside leg ($p < 0.0232$; **Figure 2.4G**). The peak hip extension

angle was 9.5° on the 36.5 m radius curve and 7.7° on the 17.2 m radius curve for the outside leg, which was 2.1° greater than the peak hip extension angle for the inside leg ($p = 0.019$). For both legs, peak hip flexion was 4.7° lower when sprinting on the 36.5 m radius curve compared to the 17.2 m radius curve ($p < 0.001$), but peak hip extension angle was 1.8° greater when sprinting on the 36.5 m radius curve compared to the 17.2 m radius curve ($p = 0.048$).

Frontal Plane

There was a significant interaction effect of curve radius and inside or outside leg on peak ankle eversion ($p < 0.001$). The peak ankle eversion angle was 28.0° on the 36.5 m radius curve for the inside leg, which was 29.9° more everted than the peak ankle eversion angle for the outside leg on the 36.5 m radius curve ($p < 0.001$). The peak ankle eversion angle was 36.5° on the 17.2 m radius curve for the inside leg, which was also 43.6° more everted than the outside ankle on the 17.2 m radius curve ($p < 0.001$). Peak ankle eversion increased 8.46° from the 36.5 m to 17.2 m radius curve for the inside leg ($p < 0.001$), while peak ankle inversion increased 5.21° from the 36.5 m to 17.2 m radius curve for the outside leg ($p < 0.001$; **Figure 2.4B**

There was no significant interaction effect of curve radius and inside or outside leg on peak knee frontal plane angle ($p = 0.137$). The peak knee adduction angle when sprinting on the 36.5 m radius curve was 2.2° greater than on the 17.2 m radius curve for both legs ($p < 0.001$; **Figure 2.4E**). For both curve radii, the peak knee adduction angle of the inside leg was 3.9° greater than the peak knee adduction angle of the outside leg ($p < 0.001$).

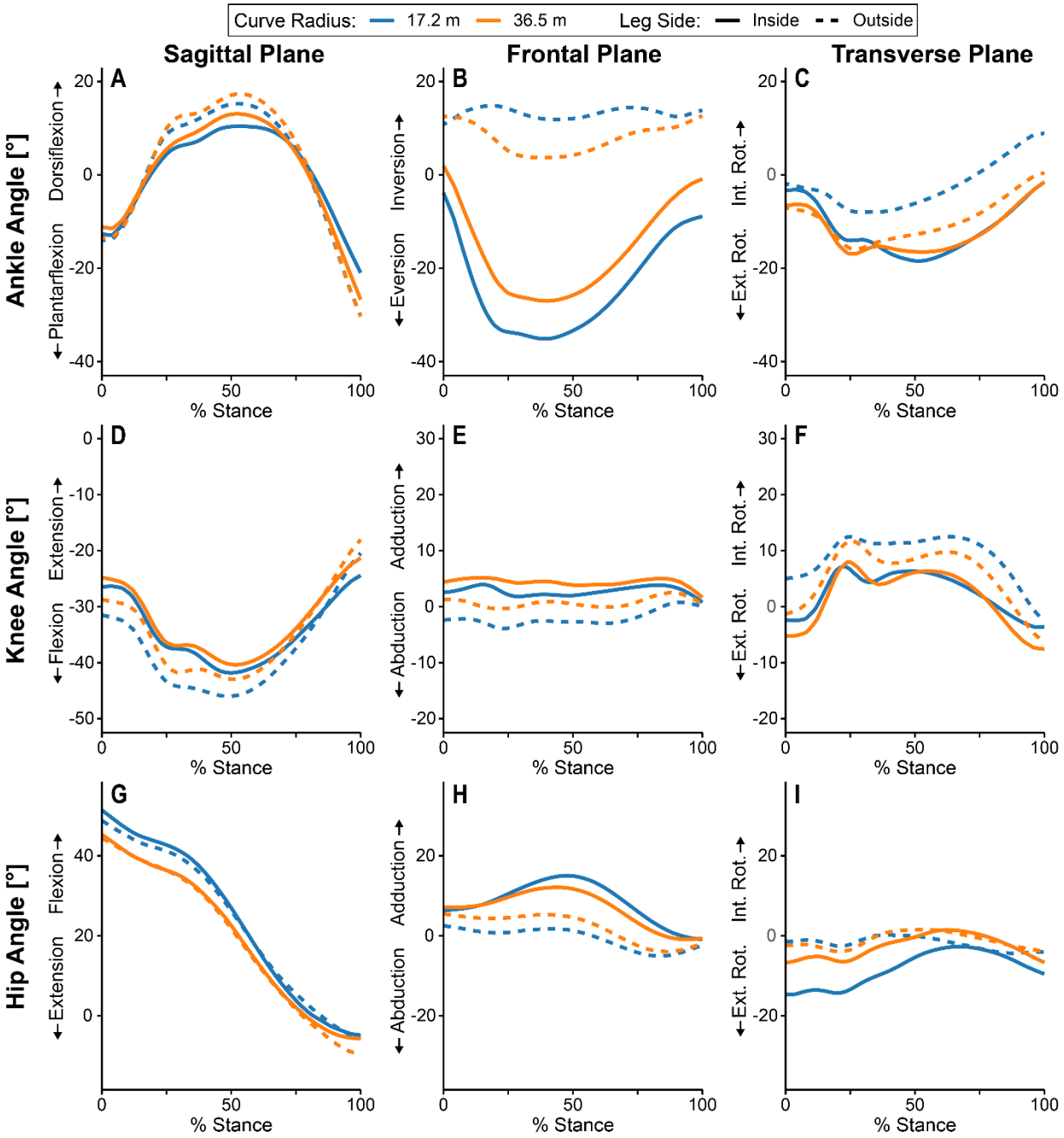

Figure 2.4 3D joint angles of the ankle, knee, and hip as a percentage of the stance phase averaged across athletes. The inside leg is represented by a solid line and the outside leg is represented by a dashed line. Colors denote the 17.2 m radius curve (blue) and 36.5 m radius curve (orange). Int. Rot. and Ext. Rot. are internal and external rotation, respectively.

There was a significant interaction effect of curve radius and inside or outside leg on peak hip frontal plane angle ($p < 0.001$). The peak hip adduction angle of the inside leg was 6.0° greater than the peak hip adduction angle of the outside leg on the 36.5 m radius curve ($p < 0.001$), but 11.7° greater than the peak hip adduction angle of the outside leg on the 17.2 m radius curve ($p < 0.001$; **Figure 2.4H**). The peak hip adduction angle of the inside leg increased by 2.7° from the 36.5 m to the 17.2 m radius curve ($p = 0.027$), but the peak hip adduction angle of the outside leg decreased by 3.1° from the 36.5 m to the 17.2 m radius curve ($p = 0.004$).

Transverse Plane

There was no interaction effect of curve radius and inside or outside leg on peak ankle internal rotation ($p = 0.968$). Additionally, there was no significant difference in peak ankle internal rotation angle between both curve radii ($p = 0.818$) or the inside and outside leg ($p = 0.336$; **Figure 2.4C**).

There was no interaction effect of curve radius and inside or outside leg on peak knee internal rotation ($p = 0.596$). For both legs, peak knee internal rotation when sprinting on the 36.5 m radius curve was not significantly different than when sprinting on the 17.2 m radius curve ($p = 0.638$), but the outside leg had a 5.2° greater peak knee internal rotation angle than the inside leg ($p = 0.034$) on both curve radii (**Figure 2.4F**).

There was a significant interaction effect of curve radius and inside or outside leg on peak hip internal rotation ($p = 0.033$). When sprinting on the 36.5 m radius curve, there was no significant difference between the peak hip internal rotation of the inside leg and the outside leg ($p = 0.457$; **Figure 2.4I**). However, the peak hip internal rotation angle of the outside leg was 5.3° greater than the peak hip internal rotation angle of the inside leg when sprinting on the 17.2 m radius curve (p

< 0.001). The peak hip internal rotation angle of the inside leg decreased by 4.1° from the 36.5 m to the 17.2 m radius curve ($p = 0.018$), but there was no significant difference in the peak internal rotation angle of the outside leg between the 36.5 m and 17.2 m radii curves ($p = 0.929$).

2.3.5 Joint Kinetics

Sagittal Plane

There was no interaction effect of curve radius and inside or outside leg on peak ankle plantarflexion moment ($p = 0.585$). For both legs, the peak ankle plantarflexion moment was 0.04 BW*m greater when sprinting on the 36.5 m radius curve than the 17.2 m radius curve ($p = 0.002$; **Figure 2.5A**). The peak ankle plantarflexion moment of the outside leg was 0.06 BW*m greater than the peak ankle plantarflexion moment of the inside leg when sprinting on both curve radii ($p < 0.001$).

There was no interaction effect of curve radius and inside or outside leg on peak knee extension moment ($p = 0.730$). Additionally, there was no significant difference in peak knee extension moment between both curve radii ($p = 0.391$) or the inside and outside leg ($p = 0.284$; **Figure 2.5D**).

There was no interaction effect of curve radius and inside or outside leg on peak hip flexion ($p = 0.607$) or extension ($p = 0.688$) moments (**Figure 2.5G**). The peak hip flexion moment was not significantly different between the inside and outside leg ($p = 0.502$) or when sprinting on the 36.5 m and 17.2 m radii curves ($p = 0.180$). The peak hip extension moment was not significantly

different between the inside and outside leg ($p = 0.525$) or when sprinting on the 36.5 m and 17.2 m radii curves ($p = 0.427$).

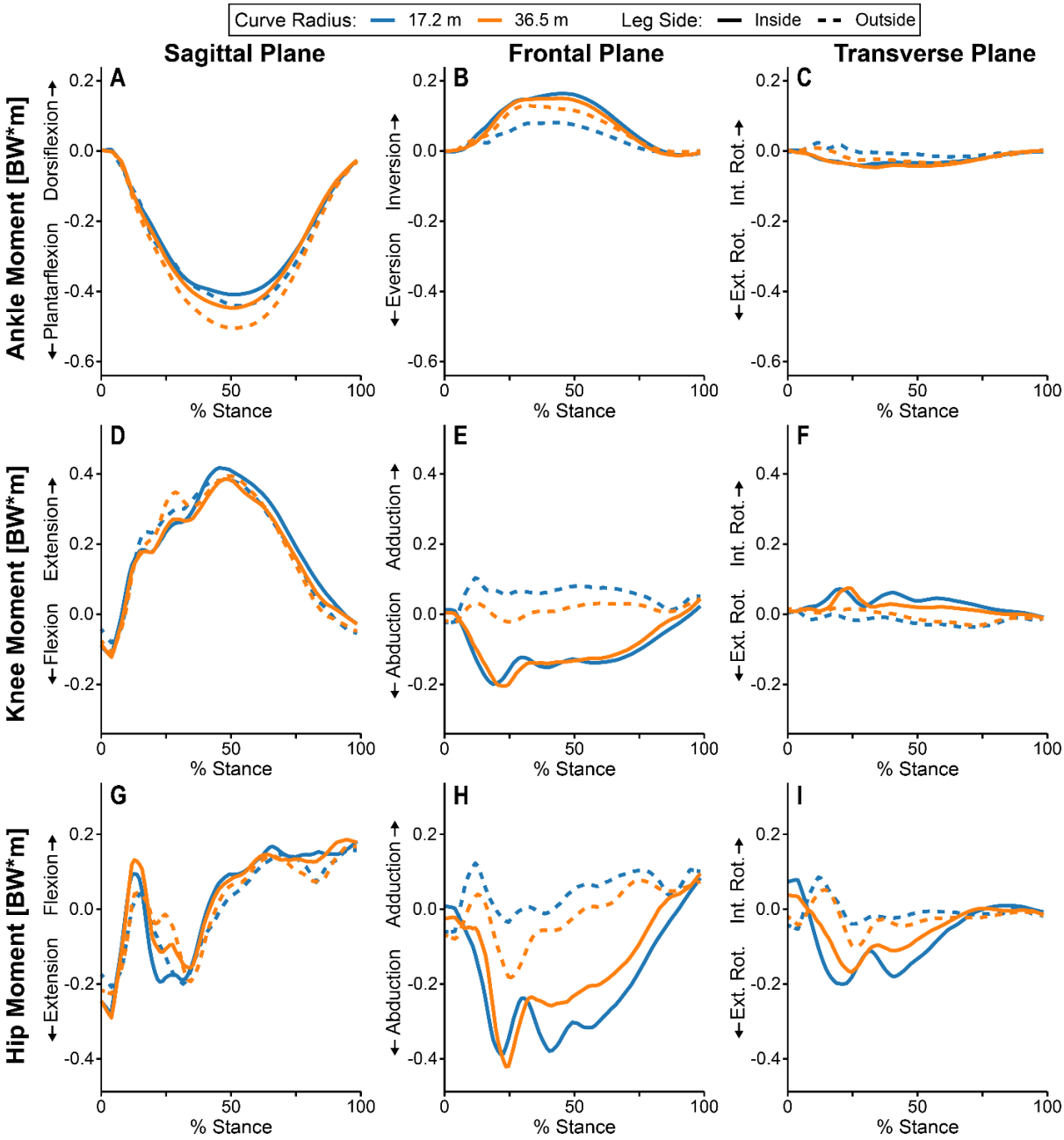

2.5 Internal 3D joint moments for the ankle, knee, and hip as a percentage of stance phase averaged across athletes. The inside leg is represented by solid lines and the outside leg is represented by dashed lines. Colors denote the 17.2 m radius curve (blue) and 36.5 m radius curve (orange). Int. Rot. and Ext. Rot. are internal and external rotation, respectively.

Frontal Plane

There was a significant interaction effect of curve radius and inside or outside leg on peak ankle inversion moment ($p = 0.005$). The peak ankle inversion moment of the inside leg was 0.06 BW*m greater than the peak ankle inversion moment of the outside leg on the 17.2 m radius curve ($p < 0.001$), but the peak ankle inversion moment for both legs were not significantly different on the 36.5 m radius curve ($p = 0.692$; **Figure 2.5B**). The peak ankle inversion moment of the inside leg did not change across both curve radii ($p = 0.466$), but the peak ankle inversion moment of the outside leg decreased 0.04 BW*m from the 36.5 m radius curve to the 17.2 m radius curve ($p = 0.004$).

There was no interaction effect of curve radius and inside or outside leg on peak knee abduction moment ($p = 0.160$). Across both curve radii, there was a knee adduction moment for the outside leg while there was a significantly different knee abduction moment for the inside leg ($p < 0.001$; **Figure 2.5E**). Both legs had a 0.04 BW*m greater peak knee abduction moment on the 36.5 m radius curve than the 17.2 m radius curve ($p < 0.001$).

There was a significant interaction effect of curve radius and inside or outside leg on peak hip abduction moment ($p = 0.015$). The peak hip abduction moment of the inside leg was 0.23 BW*m ($p < 0.001$) and 0.32 BW*m ($p < 0.001$) greater than the peak hip abduction moment of the outside leg on the 36.5 m radius curve and the 17.2 m radius curve, respectively. The peak hip abduction moment of the inside leg did not change from the 36.5 m radius curve to the 17.2 m radius curve ($p = 0.998$), but the peak hip abduction moment of the outside leg was 0.09 BW*m greater on the 36.5 m radius curve than on the 17.2 m radius curve ($p < 0.001$; **Figure 2.5H**).

Transverse Plane

There was no interaction effect of curve radius and inside or outside leg on peak ankle external rotation moment ($p = 0.582$). There was no effect of curve radius on peak ankle external rotation moment ($p = 0.502$), but the peak ankle external rotation moment of the inside leg was 0.02 BW*m greater than the peak ankle external rotation moment of the outside leg ($p = 0.043$; **Figure 2.5C**).

There was a significant interaction effect of curve radius and inside or outside leg on peak knee moment in the transverse plane ($p = 0.043$). There was a knee internal rotation moment for the inside leg while there was a significantly different knee external rotation moment for the outside leg on the 36.5 m ($p < 0.001$) and 17.2 m radii curves ($p < 0.001$; **Figure 2.5F**). The peak knee internal rotation moment of the inside leg did not change from the 36.5 m to the 17.2 m radius curve ($p = 0.495$), but the peak knee external rotation moment of the outside leg increased 0.02 BW*m from the 36.5 m to the 17.2 m radius curve ($p = 0.026$; **Figure 2.5F**).

There was a significant interaction effect of curve radius and inside or outside leg on peak hip external rotation moment ($p < 0.001$). The peak hip external rotation moment of the inside leg was 0.12 BW*m ($p < 0.001$) and 0.21 BW*m ($p < 0.001$) greater than the peak hip external rotation moment of the outside leg on the 36.5 m radius curve and 17.2 m radius curve, respectively (**Figure 2.5I**). The peak hip external rotation moment of the outside leg did not change from the 36.5 radius curve to the 17.2 m radius curve ($p = 0.640$), but the peak hip external rotation moment of the inside leg increased 0.07 BW*m from the 36.5 m radius to the 17.2 m radius curve ($p = 0.004$).

2.4 Discussion

We partially reject our first hypothesis that maximum sprinting velocity would decrease on flat curves compared to the straightaway. Contrary to previous studies (Chang & Kram, 2007; Churchill et al., 2015, 2016; Greene, 1985; Jain, 1980; Taboga et al., 2016), some athletes achieved faster velocities when sprinting CCW on the 36.5 m radius curve than when sprinting on the straightaway (**Figure 2.2**). We suspect that this result is due to the straightaway condition being randomly assigned to be the last condition for 4 out of 9 athletes. Three of these athletes ran faster on the 36.5 m radius curve than on the straightaway. It is possible that these athletes experienced fatigue after performing multiple sprinting trials even with unrestricted recovery time between trials and were unable to achieve their maximum velocity on the straightaway. This may also be responsible for the 2.2% discrepancy between our velocity data and the predictions from Greene's theoretical model (Greene, 1985), as the model's predictions depend on the sprinter's maximum velocity on a straightaway.

Our findings support our second and third hypotheses that maximum sprinting velocity would decrease with curve radius and that sprinting in the CW direction would elicit slower velocities than the CCW direction. We found that the 17.2 m radius curve elicited maximum sprinting velocities that were 8% slower than the 36.5 m radius condition, regardless of sprinting direction. Additionally, we found that athletes were 1.4% slower in the CW direction compared to the CCW direction regardless of the curve radius. This effect of sprinting direction is similar to the 1.9% decrease in maximum curve-running velocity on a 17.2 radius curve (Taboga et al., 2016) and may be attributed to familiarity of sprinting in the CCW direction for competitions. Our findings are in agreement with previous studies that show maximum velocity decreases as curve radius decreases (Chang & Kram, 2007; Greene, 1985; Jain, 1980).

We partially reject our fourth hypothesis that the inside leg would produce greater $cGRF_{Avg}$ than the outside leg on both curve radii. The greater $cGRF_{Avg}$ produced by the inside leg on the 36.5 m radius curve is consistent with previous studies investigating leg-specific cGRF on a curve radius of 37.72 m (Churchill et al., 2016; Judson et al., 2019), but contradict results from running on curve radii ≤ 6 m (Chang & Kram, 2007). At curve radii ≤ 6 m, the outside leg produces greater cGRF than the inside leg, similar to performing a "cutting" maneuver during running (Chang & Kram, 2007; Rand & Ohtsuki, 2000). We found that the inside leg produced greater $cGRF_{Avg}$ than the outside leg on the 36.5 m radius curve, but there was no significant difference between the inside and outside leg cGRF on the 17.2 m radius curve (**Figure 2.3B**). These findings highlight a potential transition in how the inside and outside leg produce the necessary cGRF to navigate smaller curve radii and may partially explain results from studies that collected data on small (1 – 6 m) and large (37.72 m) radii curves. Further research is necessary to confirm the interaction effect of curve radius and inside or outside leg on cGRF.

Our findings support our fifth hypothesis that the outside leg would produce greater $vGRF_{Avg}$ than the inside leg on the 36.5 m and 17.2 m radii curves. We found that $vGRF_{Avg}$ was 0.10 – 0.21 BW greater for the outside leg compared to the inside leg (**Figure 2.3B**). Considering the role of the ankle plantarflexor muscles in vGRF production and sprinting performance (Dorn et al., 2012; Weyand et al., 2000), the greater $vGRF_{Avg}$ produced by the outside leg may be due to the greater peak ankle plantarflexion moment of the outside leg compared to the inside leg (**Figure 2.3A**).

We reject our sixth hypothesis that ankle, knee, and hip kinematics would be similar in the sagittal plane but different in the frontal and transverse planes for inside and outside legs during curve sprinting. We found that peak ankle dorsiflexion angle was 5° smaller for the inside leg than

the outside leg and that the ankle was 29.9 – 43.6° more everted for the inside leg than the outside leg during curve sprinting (**Figure 2.4B**). Previous research has found that ankle plantarflexion moments decrease when the ankle experiences ~35° eversion (Luo & Stefanyshyn, 2012b), which may explain why peak ankle plantarflexion moment was lower for the inside than the outside leg on both curve radii (**Figure 2.5A**). Contrary to our sixth hypothesis, we also found that the peak knee flexion angle was greater for the outside leg and that the peak hip flexion angle was lower, but the peak hip extension angle was greater for the outside leg than the inside leg. Similar to previous data collected on a 36.5 m radius curve, we found that the peak hip adduction angle was greater for the inside leg than the outside leg on the 36.5 and 17.2 m radii curves (**Figure 2.4H**). Overall, these findings suggest that a smaller curve radius affects the kinematics of each joint differently and are in agreement with previous studies suggesting that the inside and outside legs have distinct kinematic configurations during curve sprinting.

We partially reject our seventh hypothesis that sagittal plane joint moments would be greater in the outside leg than the inside leg. Although we found that the peak ankle plantarflexion moment was greater for the outside leg than the inside leg, we also found no effect of inside or outside leg on knee and hip peak sagittal plane moments. Additionally, we found no effect of curve radius on knee and hip peak sagittal plane moments, suggesting that the function of knee extensor muscles during curve sprinting did not change despite changes in curve radius, velocity, and leg-specific force production.

Our findings support our eighth hypothesis that the ankle, knee, and hip would have greater frontal and transverse plane peak moments for the inside leg than the outside leg. We found that the peak ankle inversion moment (**Figure 2.5B**) and peak external rotation moment were greater for the inside leg (**Figure 2.5C**) than the outside leg during curve sprinting. We also found that

there was a knee abduction moment for the inside leg while there was a knee adduction moment for the outside leg during curve sprinting, similar to what has been observed during the start of a sprint on a 37.72 m radius curve (Judson, Churchill, Barnes, Stone, & Wheat, 2020). Peak hip moments also differed between the inside and outside leg, with greater hip peak abduction and external rotation moments for the inside leg than the outside leg (**Figure 2.5H**). These findings suggest that the changes in leg-specific force production as curve radius decreased from 36.5 m to 17.2 m may be accomplished via changes in sagittal plane plantarflexion moments and non-sagittal plane moments at the ankle, knee, and hip.

3.5 Conclusions

We identified distinct kinematic and kinetic functions of the inside and outside leg during maximum velocity curve sprinting. We also observed how leg-specific kinematics and kinetics can change as curve radius decreases from 36.5 m to 17.2 m. cGRF production is crucial to maintaining a given velocity with a smaller curve radius and our findings suggest that changes in leg-specific kinematics and kinetics occur in an effort to meet the increased cGRF requirements during maximum velocity curve sprinting. The underlying mechanics of maximal effort curve sprinting may also inform the training program of sprinters, who may benefit from strengthening ankle plantarflexors or knee and hip stabilizing muscles under kinematic configurations typical to curve sprinting to potentially improve performance.

3.6 References

Alcantara RS (2019) Dryft: A Python and MATLAB package to correct drifting ground reaction force signals during treadmill running. *Journal of Open Source Software*, *4*(44), 1910. https://doi.org/10.21105/joss.01910

Alt T, Heinrich K, Funken J, Potthast W (2015) Lower extremity kinematics of athletics curve sprinting. *Journal of Sports Sciences*, *33*(6), 552–560. https://doi.org/10.1080/02640414.2014.960881

Bezodis NE, Salo AIT, Trewartha G (2013) Excessive fluctuations in knee joint moments during early stance in sprinting are caused by digital filtering procedures. *Gait & Posture*, *38*(4), 653–657. https://doi.org/10.1016/j.gaitpost.2013.02.015

Bisseling RW, Hof AL (2006) Handling of impact forces in inverse dynamics. *Journal of Biomechanics*, *39*(13), 2438–2444. https://doi.org/10.1016/j.jbiomech.2005.07.021

Chang Y, Kram R (2007) Limitations to maximum running speed on flat curves. *Journal of Experimental Biology*, *210*(6), 971–982. https://doi.org/10.1242/jeb.02728

Churchill SM, Salo AIT, Trewartha G (2015) The effect of the bend on technique and performance during maximal effort sprinting. *Sports Biomechanics*, *14*(1), 106–121. https://doi.org/10.1080/14763141.2015.1024717

Churchill SM, Trewartha G, Bezodis IN, Salo AIT (2016) Force production during maximal effort bend sprinting: Theory vs reality. *Scandinavian Journal of Medicine & Science in Sports*, *26*(10), 1171–1179. https://doi.org/10.1111/sms.12559

Churchill SM, Trewartha G, Salo AIT (2019) Bend sprinting performance: New insights into the effect of running lane. *Sports Biomechanics*, *18*(4), 437–447. https://doi.org/10.1080/14763141.2018.1427279

Colyer SL, Evans M, Cosker DP, Salo AIT (2018) A review of the evolution of vision-based motion analysis and the integration of advanced computer vision methods towards developing a markerless system. *Sports Medicine - Open*, *4*(1), 24. https://doi.org/10.1186/s40798-018-0139-y

Dorn TW, Schache AG, Pandy MG (2012) Muscular strategy shift in human running: Dependence of running speed on hip and ankle muscle performance. *Journal of Experimental Biology*, *215*(11), 1944–1956. https://doi.org/10.1242/jeb.064527

Greene PR (1985) Running on flat turns: Experiments, theory, and applications. *Journal of Biomechanical Engineering*, *107*(2), 96–103. https://doi.org/10.1115/1.3138542

Jain PC (1980) On a discrepancy in track races. *Research Quarterly for Exercise and Sport*, *51*(2), 432–436. https://doi.org/10.1080/02701367.1980.10605212

Judson LJ, Churchill SM, Barnes A, Stone JA, Brookes IGA, Wheat J (2019) Horizontal force production and multi-segment foot kinematics during the acceleration phase of bend sprinting. *Scandinavian Journal of Medicine & Science in Sports*, *29*(10), 1563–1571. https://doi.org/10.1111/sms.13486

Judson LJ, Churchill SM, Barnes A, Stone JA, Brookes IGA, Wheat J (2020) Kinematic modifications of the lower limb during the acceleration phase of bend sprinting. *Journal of Sports Sciences*, *38*(3), 336–342. https://doi.org/10.1080/02640414.2019.1699006

Judson LJ, Churchill SM, Barnes A, Stone JA, Wheat J (2020) Joint moments and power in the acceleration phase of bend sprinting. *Journal of Biomechanics*, *101*. http://dx.doi.org/10.1016/j.jbiomech.2020.109632

Lenth R (2020) *emmeans: Estimated Marginal Means, aka Least-Squares Means* (1.4.5) [Computer software]. https://CRAN.R-project.org/package=emmeans

Luo G, Stefanyshyn D (2012a) Ankle moment generation and maximum-effort curved sprinting performance. *Journal of Biomechanics; Kidlington*, *45*(16), 2763–2768. http://dx.doi.org.colorado.idm.oclc.org/10.1016/j.jbiomech.2012.09.010

Luo G, Stefanyshyn D (2012b) Limb force and non-sagittal plane joint moments during maximum-effort curve sprint running in humans. *Journal of Experimental Biology*, *215*(24), 4314–4321. https://doi.org/10.1242/jeb.073833

Meinel K (2008) *IAAF track and field facilities manual IAAF requirements for planning, constructing, equipping and maintaining* (D. Wilson, R. Bryborn, A. Guy, D. Katz, K. Meinel, J. Salcedo, & K. Wauhkonen, Eds.; 2008th ed.). Editions EGC.

Pinheiro J, Bates D, DebRoy S, Sarkar D, R Core Team (2020) *nlme: Linear and Nonlinear Mixed Effects Models* (3.1-152) [Computer software]. https://CRAN.R-project.org/package=nlme

R Core Team (2020) *R: A Language and Environment for Statistical Computing* (3.6.3) [Computer software]. R Foundataion for Statistical Computing.

Rand MK, Ohtsuki T (2000) EMG analysis of lower limb muscles in humans during quick change in running directions. *Gait & Posture*, *12*(2), 169–183. https://doi.org/10.1016/S0966-6362(00)00073-4

Smith N, Dyson R, Hale T, Janaway L (2006) Contributions of the inside and outside leg to maintenance of curvilinear motion on a natural turf surface. *Gait & Posture*, *24*(4), 453–458. https://doi.org/10.1016/j.gaitpost.2005.11.007

Taboga P, Kram R, Grabowski AM (2016) Maximum-speed curve-running biomechanics of sprinters with and without unilateral leg amputations. *Journal of Experimental Biology*, *219*(6), 851–858. https://doi.org/10.1242/jeb.133488

Weyand PG, Sternlight DB, Bellizzi MJ, Wright S (2000) Faster top running speeds are achieved with greater ground forces not more rapid leg movements. *Journal of Applied Physiology*, *89*(5), 1991–1999. https://doi.org/10.1152/jappl.2000.89.5.1991

Wickham H (2009) *ggplot2: Elegant Graphics for Data Analysis*. Springer-Verlag. https://doi.org/10.1007/978-0-387-98141-3

Wickham H, François R, Henry L, Müller K (2020) *dplyr: A Grammar of Data Manipulation* (0.8.5) [Computer software]. https://CRAN.R-project.org/package=dplyr

Wickham H, RStudio (2020) *tidyr: Tidy Messy Data* (1.1.2) [Computer software]. https://CRAN.R-project.org/package=tidyr

3 Sacral acceleration can predict whole-body kinetics and stride kinematics across running speeds

Stress fractures are injuries caused by repetitive loading during activities such as running. The application of advanced analytical methods such as machine learning to data from multiple wearable sensors has allowed for predictions of biomechanical variables associated with running-related injuries like stress fractures. However, it is unclear if data from a single wearable sensor can accurately estimate variables that characterize external loading during running such as peak vertical ground reaction force (vGRF), vertical impulse, and ground contact time. Predicting these biomechanical variables with a single wearable sensor could allow researchers, clinicians, and coaches to longitudinally monitor biomechanical running-related injury risk factors without expensive force-measuring equipment. We quantified the accuracy of applying quantile regression forest (QRF) and linear regression (LR) models to sacral-mounted accelerometer data to predict peak vGRF, vertical impulse, and ground contact time across a range of running speeds. Thirty-seven collegiate cross country runners (24 females, 13 males) ran on a force-measuring treadmill at 3.8 – 5.4 m/s while wearing an accelerometer clipped posteriorly to the waistband of their running shorts. We cross-validated QRF and LR models by training them on acceleration data, running speed, step frequency, and body mass as predictor variables. Trained models were then used to predict peak vGRF, vertical impulse, and contact time. We compared predicted values to those calculated from a force-measuring treadmill on a subset of data (n = 9) withheld during model training. We quantified prediction accuracy by calculating the root mean square error (RMSE) and mean absolute percentage error (MAPE). The QRF model predicted peak vGRF with a RMSE of 0.150 body weights (BW) and MAPE ± SD of 4.27 ± 2.85%, predicted vertical impulse with a RMSE of 0.004 BW*s and MAPE of 0.80 ± 0.91%, and predicted contact time with a RMSE

of 0.011 s and MAPE of 4.68 ± 3.00%. The LR model predicted peak vGRF with a RMSE of 0.139 BW and MAPE of 4.04 ± 2.57%, predicted vertical impulse with a RMSE of 0.002 BW*s and MAPE of 0.50 ± 0.42%, and predicted contact time with a RMSE of 0.008 s and MAPE of 3.50 ± 2.27%. There were no statistically significant differences between QRF and LR model prediction MAPE for peak vGRF ($p = 0.549$) or vertical impulse ($p = 0.073$), but the LR model's MAPE for contact time was significantly lower than the QRF model's MAPE ($p = 0.0497$). Our findings indicate that the QRF and LR models can accurately predict peak vGRF, vertical impulse, and contact time (MAPE < 5%) from a single sacral-mounted accelerometer across a range of running speeds. These findings may be beneficial for researchers, clinicians, or coaches seeking to monitor running-related injury risk factors without force-measuring equipment.

3.1 Introduction

Stress fractures are a common running-related injury associated with the mechanical fatigue of bones in the pelvis, legs, and feet (Bennell et al., 1999) and affect 8 - 27% of runners worldwide (Brukner & Bennell, 1997; Brunet et al., 1990). Mechanical fatigue of bone tissue refers to the accumulation of damage and gradual decrease in strength resulting from repetitive loading (Edwards, 2018). Mechanical failure (stress fracture) will occur if repetitive loading continues without sufficient time for bone remodeling, and can require several months of decreased physical activity to fully recover (Matheson et al., 1987; Rizzone et al., 2017). Increases in bone loading peak magnitude and duration (total amount of time a bone is loaded) result in a decreased number of loading cycles until mechanical failure and influence the risk of stress fracture development (Edwards, 2018; Loundagin et al., 2018). Although bone loading magnitude and duration have been measured *in vivo*, the invasiveness of this measurement limits the ability to monitor bone loading over weeks or months of running (Milgrom et al., 2007).

Instead of measuring bone loading directly, previous studies have estimated bone strains with finite element models (Edwards et al., 2009) and used external ground reaction forces to develop surrogate measures of internal bone loading (Kiernan et al., 2018; Matijevich et al., 2019). Although the vertical ground reaction force (vGRF) does not directly quantify the total force applied to the bones of the leg during running, research suggests that peak tibial bone loading (a combination of external reaction forces and internal muscle forces) occurs during midstance when the vGRF is greatest (Sasimontonkul et al., 2007; Scott & Winter, 1990). Additionally, there is a moderate correlation between peak axial tibial compressive force (calculated as the sum of the 3-D GRF projected on the tibia and ankle torque divided by the Achilles tendon moment arm) and peak vGRF during running across a range of speeds and on uphill/downhill slopes (Matijevich et

al., 2019). During running, peak vGRF is representative of the magnitude of external bone loading during stance phase and contact time is representative of external bone loading duration (Scott & Winter, 1990). Vertical impulse (integral of the vGRF with respect to contact time) considers both loading magnitude and duration and is representative of the total external loading with respect to time. For example, knee joint impulse has been investigated as a measure of total joint loading during running (Miller et al., 2014). However, peak vGRF, vertical impulse, and contact time are typically quantified using expensive and immobile force plates or force-measuring treadmills. Wearable devices provide a method for monitoring external loading variables longitudinally outside of a laboratory (Paquette et al., 2020), but the ability to simultaneously predict peak vGRF, vertical impulse, and contact time during running using a single wearable device and the accuracy of these predictions is not known. Predicting these biomechanical variables with a single wearable device could allow researchers, clinicians, and coaches to monitor external loading variables associated with bone loading magnitude and duration without the need of force-measuring equipment.

Inertial measurement units (IMUs) are wearable devices that contain an accelerometer, gyroscope, and magnetometer. These wearable devices can measure biomechanical variables in a variety of environments and have been used to measure limb segment accelerations during trail running (Giandolini et al., 2016), temporal variables (e.g. stride length, stride frequency) during marathons (Reenalda et al., 2016), and limb segment kinematics during an outdoor obstacle course (Vitali et al., 2019). Additionally, IMUs can be used to longitudinally monitor biomechanical variables that have been associated with running-related injuries. For example, IMUs have been used to measure peak tibial acceleration over the course of a marathon (Ruder et al., 2019) or estimate peak vGRF over several months of running (Kiernan et al., 2018); thus IMUs can be used

to directly measure biomechanical variables (e.g. limb segment acceleration) and estimate biomechanical variables (e.g. whole-body kinetics). Although IMUs have been used to monitor runners and identify variables associated with prospective injuries (Davis et al., 2016), using IMUs to estimate whole-body kinetic variables depends on sensor position (Tan et al., 2019), signal filtering (Day et al., 2021), number of sensors used (Karatsidis et al., 2016), and features included in predictive models (Neugebauer et al., 2012).

Placing an IMU near the center of mass may allow for accurate estimations of the vGRF during running via acceleration data because the vGRF is the product of body mass and the vertical acceleration of the center of mass (accounting for gravity), assuming air resistance is neglected (Cavagna et al., 1971). This estimate could then be used to calculate discrete variables such as peak vGRF, vertical impulse, and contact time. Such a physics-based approach would only require the use of one accelerometer. Using pelvis accelerations in this manner to estimate peak vGRF during treadmill running revealed moderate correlations with measures from gold standard force-measuring equipment across speeds (3.8 – 5.4 m/s; r = 0.64; Day et al., 2021) and moderate correlations when predicting the vGRF waveform during the stance phase of overground running (r = 0.50 ± 0.30; Gurchiek et al., 2017). Additionally, pelvis accelerations have been found to consistently overestimate (by ~2.5 times) peak resultant COM acceleration (calculated by dividing the 3-D ground reaction force by body mass and subtracting gravitational acceleration) in runners across a range of speeds (2 – 5 m/s) (Nedergaard et al., 2017). However, applying more advanced analysis methods may provide more accurate predictions of whole-body kinetics and stride kinematics during running with a single sacral-mounted accelerometer.

Advanced data analysis techniques like machine learning have been used to estimate biomechanical variables based on IMU measurements during running (Derie et al., 2020; Johnson

et al., 2021; Pogson et al., 2020; Wouda et al., 2018). However, training complex machine learning algorithms to predict vGRF data from wearable devices can result in limited model interpretability (the degree to which one can understand the cause of a machine learning model's decision) (Miller, 2019) despite high model accuracy (mean error ~0.10 body weight (BW)) (Komaris et al., 2019). Similarly, the number of IMUs required to estimate a given biomechanical variable affects the financial cost of data collection and usability for coaches or clinicians interested in simultaneously collecting data on multiple individuals. One benefit of using IMUs instead of a force-measuring treadmill to measure whole-body kinetics and stride kinematics is the reduced financial cost of using IMUs (<$1000 vs. $100,000), but the financial benefit diminishes if multiple IMUs are needed to estimate biomechanical variables. Minimizing the number of IMUs required to estimate vGRF characteristics while balancing model interpretability and accuracy would ultimately improve the applicability of IMU-based research for researchers, clinicians, coaches, and athletes.

Supervised machine learning models like linear regressions and random forests have been used to model complex relationships between biomechanical measures and clinical outcomes (Backes et al., 2020; Halilaj et al., 2018). Linear regression (LR) models are often used to predict biomechanical outcomes because regression coefficients allow for interpretable predictions but LR models are generally limited to linear relationships between independent and dependent variables (Chambers, 1992). Conversely, quantile regression forests (QRF) are a type of ensemble random forest machine learning algorithm that can model linear or non-linear relationships between independent and dependent variables, but a limitation of QRF algorithms is that they lack traditional regression coefficients that are present in LR models (Breiman, 2001; Meinshausen, 2006). Thus, QRF models can be more difficult to interpret despite potentially improved prediction accuracy (Marchese Robinson et al., 2017). Reporting the accuracy of multiple models applied to

a dataset may illustrate this interpretability-accuracy tradeoff and present options that prioritize either interpretability or accuracy. Developing predictive models of biomechanical variables such as peak vGRF, vertical impulse, and contact time may improve the ability to quantify running-related injury risk such as stress fracture risk by allowing coaches, clinicians, and researchers to use wearable devices to longitudinally monitor characteristics of loading outside of a laboratory setting.

The purpose of this study was to apply a QRF and LR model to data from a sacral-mounted accelerometer and determine the accuracy for predicting peak vGRF, vertical impulse, and ground contact time during running. Specifically, we used cross validation to train QRF and LR models to predict these biomechanical variables and compared them to gold standard measurements from a force-measuring treadmill. We hypothesized that the QRF model would have a lower mean absolute percent error (MAPE) than the LR model when predicting peak vGRF, vertical impulse, and contact time due to the model's complexity and ability to account for potential non-linear changes across running speeds (Marchese Robinson et al., 2017; Nilsson & Thorstensson, 1989).

3.2 Methods

3.2.1 Participants

Thirty-seven National Collegiate Athletic Association (NCAA) Division I Cross Country runners (24 Female, 13 Male, 55.8 ± 9.7 kg, 170 ± 8 cm, 20 ± 2 years) from the University of Colorado Boulder and University of Oregon participated. Participants were actively training and reported no musculoskeletal injuries at the time of data collection. The protocol was approved by the University of Colorado Boulder (protocol #: 17-0392) and University of Oregon (protocol #:

05162017.019) Institutional Review Boards and all participants provided written informed consent prior to data collection.

3.2.2 Experimental Design

Each participant ran on a level force-measuring treadmill (1000 Hz; Treadmetrix, Park City, UT or Bertec, Columbus, OH) for a series of consecutive 30-sec trials following a 5-minute self-paced warm up. Male participants ran at 3.8, 4.1, and 5.4 m/s while female participants ran at 3.8 and 4.9 m/s. We selected these speeds because they represent typical training run and race speeds for NCAA Division I Cross Country runners while maintaining a common speed between male and female participants. During all conditions, participants wore an accelerometer (500 Hz, 3 -axis ±16 g; IMeasureU, Centennial, CO) clipped posteriorly to the waistband of their running shorts near the sacrum as described in prior research (**Figure 3.1**; Day et al., 2021). The accelerometer was positioned near the sacrum as vertical displacement of the sacrum is strongly correlated (r = 0.95) with vertical displacement of the center of mass during running (Napier et al., 2020).

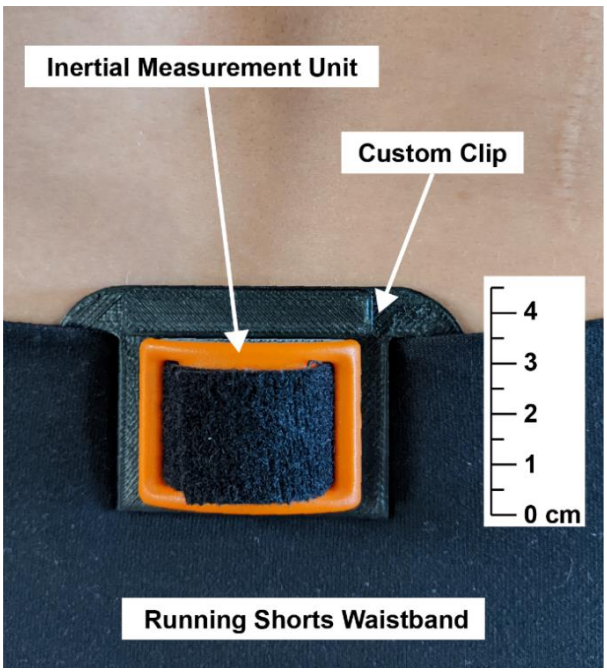

Figure 3.1 Inertial measurement unit located near the sacrum, attached posteriorly on the waistband of a participant's running shorts via a custom clip.

3.3.3 Processing

Acceleration and vGRF data were collected during the final 10 seconds of each condition using separate data collection software and required temporal synchronization prior to data analysis. First, we down-sampled the vGRF data to match the sampling frequency of the accelerometer data (500 Hz). Then, we synchronized acceleration and vGRF data by having participants perform a countermovement jump on the stationary force-measuring treadmill at the beginning and end of the data collection session while simultaneously measuring acceleration and force. For each jump, we temporally aligned the estimated vGRF signal calculated from the acceleration data to the vGRF measured by the treadmill based on the cross correlation of their frequency content using a custom MATLAB (Mathworks, Natick, MA) script based on the work by Savorani et al. (2013) (Savorani et al., 2013).

After time-synchronizing the data, we used a custom MATLAB (Mathworks, Natick, MA) script to filter and process the vGRF data measured by the instrumented treadmill and acceleration data measured by the accelerometer (Alcantara, 2019). We filtered vGRF data using a zero-lag 4^{th} order low pass Butterworth filter with a 30 Hz cut-off. All stance phases during the final 10 seconds of each condition (approximately 30 steps) were used to calculate the mean peak vGRF, vertical impulse, contact time, and step frequency (number of initial ground contacts per second), discrete variables that were compared to each model's predictions. Ground contact time was defined as the duration when the participant's vGRF exceeded a threshold of 5% body weight (BW) (Day & Hahn, 2019).

The vertical acceleration data relative to the accelerometer's local coordinate system were used for this analysis. We filtered acceleration data using a zero-lag 8^{th} order low pass Butterworth filter with a 10 Hz cut-off, which isolates the frequency content corresponding to the vertical

oscillation of the pelvis during running and the transient impact peak during early stance phase (Day et al., 2021). Ground contact time for accelerometer data was defined as the duration when the participant's sacral acceleration exceeded a threshold of 0 m/s^2 because the center of mass acceleration crosses 0 m/s^2 at the start and end of the stance phase during running (Brabandere et al., 2018; Cavagna & Legramandi, 2015; Gaudino et al., 2013). We multiplied sacral acceleration by participant body mass to obtain an estimate of vGRF over the entire stance phase and normalized vGRF to BW. Using this acceleration-based estimate of vGRF, we calculated peak vGRF, vertical impulse, and contact time for each condition. These discrete variables were used as inputs for the QRF and LR models.

3.3.4 Analysis

We compared the predictive accuracy of QRF and LR models using a train/test method. We chose to compare these models because LR models are generally interpretable due to the presence of regression coefficients but can be inaccurate when modeling nonlinear relationships and conversely, QRF models lack coefficients but can model nonlinear relationships. We partitioned the dataset into two subsets, with 28 runners (76% of enrolled participants: 9 Male, 19 Female; 65 total samples) used to train all models and 9 runners (24% of enrolled participants; 4 Male, 5 Female; 22 total samples) reserved to test model accuracy. Similar distributions of male and female runners were maintained in both subsets while ensuring that a runner's data were not present in both subsets. This precaution was taken to provide conservative measures of model accuracy as model predictions were based on data from runners who were unknown to the model during training.

A QRF and LR model were constructed for predicting peak vGRF, vertical impulse, and contact time. In addition to the discrete variables calculated from the acceleration-based estimate,

we included the runner's body mass, step frequency, and running speed as predictor variables in both models, as these variables have been associated with changes in running biomechanics (Nagahara et al., 2018; Nilsson & Thorstensson, 1989). QRF models are a type of ensemble regression tree machine learning algorithm that can be used to predict a continuous numerical output instead of a classification label (Breiman, 2001; Meinshausen, 2006) and prior research suggests ensemble regression tree algorithms can be used to estimate vGRF characteristics using data from wearable devices (Derie et al., 2020). We used k-fold cross validation (5 folds) to train the models on the 76% subset and optimize the QRF parameters, minimizing for root mean squared error (RMSE) between model predictions and observed values. The QRF model predictions represent an ensemble of 500 regression tree predictions (Meinshausen, 2006). Then we used the trained models to make predictions based on the testing subset and quantified the error between model predictions and observed values from the force-measuring treadmill. RMSE, MAPE, and correlation coefficient (r) were calculated across the entire testing subset (22 predictions) and reported as prediction accuracy metrics. Paired t-tests (two-tailed, $\alpha = 0.05$) were used to compare MAPE between models. Data analysis was performed in R (version 3.6.3) using custom scripts and packages (Arnold et al., 2019; Kuhn, 2020; Meinshausen, 2006; R Core Team, 2020; Wickham, 2009; Wickham & RStudio, 2020). For the LR models, the statistical significance level was set at $\alpha = 0.05$ to determine coefficients that significantly contributed to model predictions during training.

3.3 Results

Across all participants and conditions, mean ± SD peak vGRF, vertical impulse, and contact time calculated from the force-measuring treadmill data were 2.94 ± 0.23 BW, 0.33 ± 0.02 BW*s, and 0.189 ± 0.017 s, respectively (**Table 3.1**). Mean ± SD QRF model predictions of peak vGRF,

vertical impulse, and contact time were 2.95 ± 0.18 BW, 0.33 ± 0.02 BW*s, and 0.188 ± 0.017 s, respectively (**Table 3.2**). Mean ± SD LR model predictions of peak vGRF, vertical impulse, and contact time were 2.93 ± 0.18 BW, 0.33 ± 0.02 BW*s, and 0.189 ± 0.015 s (**Table 3.2**).

Table 3.1 Mean ± SD peak vertical ground reaction force (vGRF), vertical impulse, and contact time calculated from the ground reaction forces measured by the treadmill for all participants.

	Speed [m/s]	Peak vGRF [BW]	Vertical Impulse [BW*s]	Contact Time [s]
Females	3.8	2.79 ± 0.19	0.34 ± 0.02	0.201 ± 0.012
(n = 24)	4.8	2.94 ± 0.21	0.32 ± 0.02	0.175 ± 0.011
Males	3.8	2.94 ± 0.20	0.35 ± 0.01	0.204 ± 0.009
(n = 13)	4.1	3.00 ± 0.21	0.35 ± 0.01	0.196 ± 0.008
	5.4	3.14 ± 0.24	0.32 ± 0.01	0.168 ± 0.007

Cross validation of the QRF model revealed that the optimal number of variables randomly sampled as candidates for each split in each regression tree was 2 when predicting peak vGRF and 3 when predicting vertical impulse or contact time. When applying the QRF model to the testing subset, model predictions of peak vGRF had a RMSE of 0.150 BW and MAPE ± SD of 4.27 ± 2.85%, predictions of vertical impulse had a RMSE of 0.004 BW*s and MAPE of 0.80 ± 0.91%, and predictions of contact time had a RMSE of 0.011 s and MAPE of 4.68 ± 3.00% (**Figure 3.2**).

Table 3.2 Discrete variables calculated from the treadmill and predicted by the Quantile Regression Forest (QRF) or Linear Regression (LR) models for the testing subset of data. Mean ± SD peak vertical ground reaction force (vGRF), vertical impulse, and contact time for the nine participants in the testing subset of data.

Peak vGRF [BW]	Speed [m/s]	Observed	QRF Prediction	LR Prediction
Females	3.8	2.66 ± 0.18	2.78 ± 0.13	2.75 ± 0.05
(n = 5)	4.8	2.86 ± 0.15	2.88 ± 0.09	2.86 ± 0.05
Males	3.8	2.98 ± 0.08	2.98 ± 0.20	2.94 ± 0.13
(n = 4)	4.1	3.07 ± 0.10	3.02 ± 0.16	3.00 ± 0.15
	5.4	3.30 ± 0.20	3.14 ± 0.10	3.18 ± 0.16
Vertical Impulse [BW*s]				
Females	3.8	0.33 ± 0.02	0.33 ± 0.02	0.33 ± 0.02
(n = 5)	4.8	0.31 ± 0.02	0.31 ± 0.01	0.31 ± 0.02
Males	3.8	0.35 ± 0.01	0.35 ± 0.01	0.35 ± 0.01
(n = 4)	4.1	0.35 ± 0.01	0.35 ± 0.01	0.35 ± 0.01
	5.4	0.33 ± 0.01	0.33 ± 0.01	0.33 ± 0.01
Contact Time [s]				
Females	3.8	0.204 ± 0.014	0.198 ± 0.004	0.198 ± 0.008
(n = 5)	4.8	0.177 ± 0.012	0.167 ± 0.005	0.174 ± 0.008
Males	3.8	0.204 ± 0.009	0.203 ± 0.006	0.204 ± 0.005
(n = 4)	4.1	0.195 ± 0.007	0.201 ± 0.005	0.198 ± 0.005
	5.4	0.165 ± 0.007	0.173 ± 0.010	0.172 ± 0.002

Table 3.3 Linear regression (LR) coefficients following cross validation on the training subset. Unstandardized coefficients (*B*), coefficient standard errors (*SE*), t values (*t*), and p values (*p*) are listed for independent variables used to predict peak vertical ground reaction force (vGRF), vertical impulse, and contact time, where AE is the Acceleration-based estimate and Freq. is step frequency. Equations with statistically significant predictor variables are included. Bold *p* values indicate $p < 0.05$.

Peak vGRF [BW]	y = 2.23 + 0.15*Speed + 0.33*AE – 0.34*Step Freq.			
	B	*SE*	*t*	*p*
Intercept	2.23	0.46	4.87	**0.000**
Speed [m/s]	0.15	0.03	4.42	**0.000**
Acceleration-based Estimate [BW]	0.33	0.05	6.54	**0.000**
Step Frequency [Hz]	-0.34	0.12	-2.84	**0.006**
Body Mass [kg]	0.001	0.003	0.50	0.621
Vertical Impulse [BW*s]			y = 0.69 – 0.10*Step Freq.	
	B	*SE*	*t*	*p*
Intercept	0.69	0.02	31.13	**0.000**
Speed [m/s]	-0.002	0.001	-1.73	0.089
Acceleration-based Estimate [BW*s]	-0.05	0.03	-1.79	0.079
Step Frequency [Hz]	-0.10	0.004	-25.95	**0.000**
Body Mass [kg]	0.00003	0.00009	0.32	0.752
Contact Time [s]	y = 0.230 – 0.019*Speed + 0.151*AE. + 0.0007*Body Mass			
	B	*SE*	*t*	*p*
Intercept	0.230	0.033	6.88	**0.000**
Speed [m/s]	-0.019	0.002	-8.62	**0.000**
Acceleration-based Estimate [s]	0.151	0.063	2.42	**0.019**
Step Frequency [Hz]	-0.011	0.007	-1.51	0.135
Body Mass [kg]	0.0007	0.0002	4.05	**0.000**

Cross validation of the LR model revealed that running speed, acceleration-based estimations, and step frequency contributed significantly to model predictions of peak vGRF ($p = 0.000$, $p = 0.000$, and $p = 0.006$ respectively; **Table 3.3**). Step frequency was the only predictor variable that significantly contributed to predictions of vertical impulse ($p = 0.000$; **Table 3.3**). Lastly, running speed, acceleration-based estimations, and body mass contributed significantly to predictions of contact time ($p = 0.000$, $p = 0.019$, and $p = 0.000$ respectively; **Table 3.3**). When applying the LR model to the testing subset, we found that model predictions of peak vGRF had a RMSE of 0.139 BW and MAPE ± SD of 4.04 ± 2.57%, predictions of vertical impulse had a RMSE of 0.002 BW*s

and MAPE of 0.50 ± 0.42%, and predictions of contact time had a RMSE of 0.008 s and MAPE of 3.50 ± 2.27% (**Figure 3.2**).

There were no statistically significant differences between the QRF and LR model MAPE when predicting peak vGRF (p = 0.549), or vertical impulse (p = 0.073). However, the LR model predicted contact time with significantly less error based on MAPE (p = 0. 0497), compared to the QRF model.

3.4 Discussion

We developed QRF and LR models and quantified their accuracy when predicting peak vGRF, vertical impulse, and contact time from a sacral mounted IMU on data withheld during model training. We found that QRF predictions had a MAPE of 0.80 – 4.68% and the LR predictions had a MAPE of 0.50 – 4.04% for these biomechanical variables. Both models had the lowest MAPE when predicting vertical impulse, which may be due to the inclusion of step frequency in our models. For example, step frequency strongly contributed to the LR model prediction of vertical impulse (B = -0.10; p = 0.000; **Table 3.3**). This finding corroborates prior research that observed a strong negative correlation (r = -0.871 – -0.968) between step frequency and vertical impulse during overground sprinting (Nagahara et al., 2018). The QRF and LR models theoretically provide two levels of model accuracy and interpretability when predicting biomechanical variables with an accelerometer, but our data did not entirely support our hypothesis as both model types performed similarly when predicting peak vGRF and vertical impulse. Average differences in MAPE between the QRF and LR model predictions of peak vGRF and vertical impulse were ≤ 0.30% but when predicting contact time, the LR model had a significantly lower MAPE (3.50 ± 2.27%) than the QRF model (4.68 ± 3.00%; p = 0.0497). Additionally, the LR model predictions were more strongly correlated with the observed values from the treadmill data compared to the

QRF model predictions (**Figure 3.2**). These findings suggest that the LR model may more accurately describe the relationship between the predictor variables and contact time across the range of speeds tested (3.8 – 5.4 m/s; **Table 3.2**).

Prior research that has predicted biomechanical variables using wearable devices has utilized multiple IMUs or machine learning algorithms like artificial neural networks, which can be difficult to interpret despite low prediction errors (Johnson et al., 2021; Pogson et al., 2020; Wouda et al., 2018). This may ultimately limit the applicability of these prior findings because of the financial cost of using multiple IMUs or the computational requirements of applying the model. In the present study, we implemented a physics-based methodology of measuring acceleration at the sacrum from a single accelerometer clipped to a runner's waistband. Our predictive models also required the runner's body mass, speed, and step frequency, which can be measured using a scale, treadmill or GPS watch, and a stopwatch, respectively. We predicted biomechanical variables with a MAPE < 5% by using a single IMU, which reduces the financial cost of measuring biomechanical variables yet maintains prediction accuracy comparable to that achieved using multiple wearable devices, kinematic data from 3-D motion capture, and artificial neural networks. For example, Wouda et al. (2018) predicted peak vGRF during running using three IMUs and an artificial neural network with an average RMSE of 0.38 BW and Komaris et al. (2019) achieved a mean error ~ 0.10 BW when predicting peak vGRF using 3-D motion capture data and an artificial neural network. In contrast, our LR model predictions based on a single accelerometer achieved an RMSE of 0.139 BW for peak vGRF. Additionally, the RMSE of LR model predictions was smaller than the standard deviation of the peak vGRF, vertical impulse, and contact time values measured by the force-measuring treadmill (**Table 3.1**). We provided regression coefficients for the LR model (**Table 3.3**), which can be used to predict peak vGRF, vertical impulse, and contact

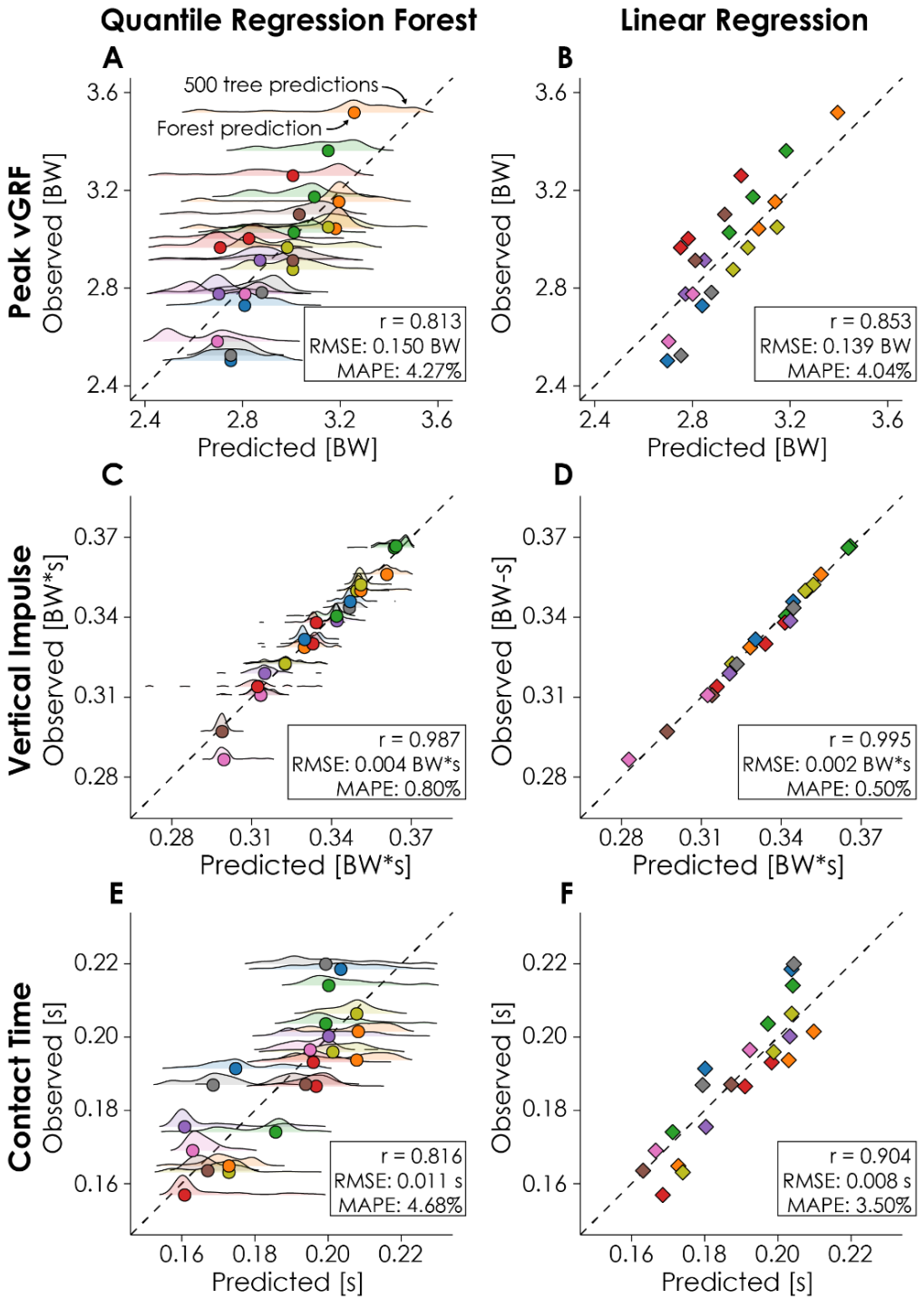

Figure 3.2 Quantile regression forest (QRF) and Linear regression (LR) model predictions. Model predictions (horizontal axes; QRF: circles, LR: diamonds) of peak vertical ground reaction force (vGRF), vertical impulse, and contact time are compared to the observed values (vertical axes) from the force-measuring treadmill. Dashed lines represent the line of identity, each point represents the value for a given condition-participant combination, and colors represent different participants in the testing subset (n = 9). Male participants completed three conditions and female participants completed two conditions. QRF model predictions are based on the predictions of 500 regression trees, with the distribution of tree predictions represented by the ridge plots.

time when provided with a runner's speed, sacral acceleration, step frequency, and body mass. The LR model coefficients may be useful for coaches or clinicians interested in monitoring peak vGRF, vertical impulse, or contact time in runners over the course of a season or during injury rehabilitation without needing to apply a complex machine learning algorithm or use a force-measuring treadmill.

We predicted variables that characterize the magnitude and duration of external loading using wearable device data, and these data could be used to predict more complex surrogates of internal bone loading or identify stress fracture risk in runners via more accurate estimations of variables that affect cumulative external loading. For example, prior research has proposed surrogates of internal bone loading, such as peak axial tibial compression, that have a weak-moderate correlation with vertical impulse ($r = -0.46 \pm 0.40$) and peak vGRF ($r = 0.72 \pm 0.42$) across a range of speeds and slopes (Matijevich et al., 2019). We have shown that these external loading variables can be predicted with wearable devices. It may be possible to map wearable device data to peak axial tibial compression during running using similar techniques. However, it is unknown if peak axial tibial compression can be used to prospectively identify stress fracture risk despite the association between a bone's load and risk of mechanical failure. If bone loading metrics can be identified as biomechanical risk factors, data collected by wearable devices could improve our understanding of stress fracture development in long distance runners as these data could be collected over the course of a run, competitive season, or several years in the environment experienced by runners daily and not only within a laboratory (Backes et al., 2020; Edwards, 2018; Ryan et al., 2020). Biomechanical risk factors could then be considered alongside other metrics such as bone mineral density or nutritional deficiencies when determining an individual's stress fracture risk (Wright et al., 2015).

There are potential limitations of the present study that may limit the generalizability of our findings. There may be a tendency for the QRF and LR models to overestimate lower peak vGRF and contact times and underestimate higher peak vGRF and contact times (**Figure 3.2E & F**). Variations in peak vGRF and contact time within a participant were due in part to changes in speed, so these biomechanical predictions may not generalize outside of the range of speeds tested (3.8 – 5.4 m/s). QRF model predictions may have benefitted from additional predictor variables as ensemble forests algorithms can be used to make predictions from hundreds or thousands of predictor variables (Breiman, 2001). However, we intentionally limited the number of predictor variables to increase model interpretability, likely at the cost of prediction accuracy. We collected data from level running and the prediction accuracy of the models may be affected by changes in slope, as uphill and downhill running affects kinematics and kinetics (Vernillo et al., 2020). The method we used to attach the accelerometer to the body may have introduced error in the acceleration data (Gurchiek et al., 2017). Specifically, the application of Newton's second law of motion assumes acceleration is measured at the center of mass and not the sacrum. Additionally, we did not rotate the acceleration signal to be vertical in the global coordinate system, but instead used the vertical axis in the local coordinate system of the accelerometer, which may have rotated with changes in waistband position or pelvic orientation during running and influenced prediction accuracy (Tan et al., 2019). However, our decision to attach the accelerometer to the runner's waistband and not rotate the vertical acceleration signal were in an effort to maintain the generalizability of results. Thus, our methodology presents conservative measures of model accuracy as using the global vertical acceleration from a device adhered directly to the skin would have likely improved signal quality. However, we observed predictions within 5% of peak vGRF, vertical impulse, and contact time across a range of speeds. The entirety of our participant

population consisted of NCAA Division I Cross Country runners who may not be representative of the general recreational running population. Differences in running biomechanics have been observed when comparing runners of different skill levels or weekly running mileage (Boyer et al., 2014; Cavanagh et al., 1977; García-Pinillos et al., 2019; Mo et al., 2020) and these differences may affect model prediction accuracy when applied to other running subpopulations. However, by testing the QRF and LR models on data withheld during model training, we provided a measure of model accuracy when applied to the data of runners who were unknown to the model.

3.5 Conclusions

We investigated the ability of quantile regression forest (QRF) and linear regression (LR) models to predict peak vertical ground reaction force, vertical impulse, and ground contact time in NCAA Division I Cross Country runners using sacral acceleration across a range of running speeds (3.8 – 5.4 m/s). Both models predicted these biomechanical variables on data withheld during model training with a mean absolute percent error (MAPE) < 5%. Our data indicate that a sacral-mounted accelerometer can be used to predict peak vGRF (RMSE: ≤ 0.150 BW), vertical impulse (RMSE: ≤ 0.003 BW*s), and contact time (RMSE: ≤ 0.011 s) during running. We also provide LR model coefficients (**Table 3.3**), used to predict peak vGRF, vertical impulse, and contact time from sacral-mounted accelerometer data. Accurate longitudinal monitoring of these biomechanical variables may aid in the quantification of stress fracture risk in runners.

3.6 References

Alcantara RS (2019) Dryft: A Python and MATLAB package to correct drifting ground reaction force signals during treadmill running. *Journal of Open Source Software*, 4(44), 1910. https://doi.org/10.21105/joss.01910

Arnold JB, Daroczi G, Werth B, Weitzner B, Kunst J, Auguie B, Rudis B, HW (Code from the ggplot2, package), JT (Code from the labeling, & London, J) (2019) ggthemes: Extra

Themes, Scales and Geoms for "ggplot2" (4.2.0). https://CRAN.R-project.org/package=ggthemes

Backes A, Skejø SD, Gette P, Nielsen RØ, Sørensen H, Morio C, Malisoux L (2020) Predicting cumulative load during running using field-based measures. *Scandinavian Journal of Medicine & Science in Sports*, 00, 1–9. https://doi.org/10.1111/sms.13796

Bennell K, Matheson G, Meeuwisse W, Brukner P (1999) Risk factors for stress fractures. *Sports Med*, 32.

Boyer KA, Silvernail JF, Hamill J (2014) The role of running mileage on coordination patterns in running. *Journal of Applied Biomechanics*, 30(5), 649–654. https://doi.org/10.1123/jab.2013-0261

Brabandere AD, Beéck TOD, Schütte KH, Meert W, Vanwanseele B, Davis J (2018) Data fusion of body-worn accelerometers and heart rate to predict VO2max during submaximal running. *PLoS ONE*, 13(6), e0199509. https://doi.org/10.1371/journal.pone.0199509

Breiman L (2001) Random Forests. *Machine Learning*, 45(1), 5–32. https://doi.org/10.1023/A:1010933404324

Brukner P, Bennell K (1997) Stress fractures in female athletes: Diagnosis, management and rehabilitation. *Sports Medicine*, 24(6), 419–429. https://doi.org/10.2165/00007256-199724060-00006

Brunet ME, Cook SD, Brinker MR, Dickinson JA (1990) A survey of running injuries in 1505 competitive and recreational runners. *Journal of Sports Medicine and Physical Fitness*, 30(3), 307–315.

Cavagna GA, Komarek L, Mazzoleni S (1971) The mechanics of sprint running. *Journal of Physiology*, 217(3), 709–721. https://doi.org/10.1113/jphysiol.1971.sp009595

Cavagna GA, Legramandi MA (2015) Running, hopping and trotting: Tuning step frequency to the resonant frequency of the bouncing system favors larger animals. *Journal of Experimental Biology*, 218(20), 3276–3283. https://doi.org/10.1242/jeb.127142

Cavanagh PR, Pollock ML, Landa J (1977) A biomechanical comparison of elite and good distance runners. *Annals of the New York Academy of Sciences*, 301(1), 328–345. https://doi.org/10.1111/j.1749-6632.1977.tb38211.x

Chambers J (1992) Chapter 4: Linear models. In: J. Chambers & T. Hastie (Eds.), *Statistical Models in S*. Wadsworth & Brooks/Cole, California.

Davis IS, Bowser BJ, Mullineaux DR (2016) Greater vertical impact loading in female runners with medically diagnosed injuries: A prospective investigation. *British Journal of Sports Medicine*, 50(14), 887–892.

Day EM, Alcantara RS, McGeehan MA, Grabowski AM, Hahn ME (2021) Low-pass filter cutoff frequency affects sacral-mounted inertial measurement unit estimations of peak vertical ground reaction force and contact time during treadmill running. *Journal of Biomechanics*, 119, 110323. https://doi.org/10.1016/j.jbiomech.2021.110323

Day EM, Hahn ME (2019) Dynamic angular stiffness about the metatarsophalangeal joint increases with running speed. *Human Movement Science*, 67, 102501. https://doi.org/10.1016/j.humov.2019.102501

Derie R, Robberechts P, Van den Berghe P, Gerlo J, De Clercq D, Segers V, Davis J (2020) Tibial acceleration-based prediction of maximal vertical loading rate during overground running: A machine learning approach. *Frontiers in Bioengineering and Biotechnology*, 8. https://doi.org/10.3389/fbioe.2020.00033

Edwards WB (2018) Modeling overuse injuries in sport as a mechanical fatigue phenomenon. *Exercise and Sport Sciences Reviews*, 46(4), 224–231. https://doi.org/10.1249/JES.0000000000000163

Edwards WB, Taylor D, Rudolphi TJ, Gillette JC, Derrick TR (2009) Effects of stride length and running mileage on a probabilistic stress fracture model. *Medicine & Science in Sports & Exercise*, 41(12), 2177–2184. https://doi.org/10.1249/MSS.0b013e3181a984c4

García-Pinillos F, García-Ramos A, Ramírez-Campillo R, Latorre-Román PÁ, Roche-Seruendo, LE (2019) How do spatiotemporal parameters and lower-body stiffness change with increased running velocity? A comparison between novice and elite level runners. *Journal of Human Kinetics*, 70(1), 25–38. https://doi.org/10.2478/hukin-2019-0036

Gaudino P, Gaudino C, Alberti G, Minetti AE (2013) Biomechanics and predicted energetics of sprinting on sand: Hints for soccer training. *Journal of Science and Medicine in Sport*, 16(3), 271–275. https://doi.org/10.1016/j.jsams.2012.07.003

Giandolini M, Horvais N, Rossi J, Millet GY, Samozino P, Morin J-B (2016) Foot strike pattern differently affects the axial and transverse components of shock acceleration and attenuation in downhill trail running. *Journal of Biomechanics*, 49(9), 1765–1771. https://doi.org/10.1016/j.jbiomech.2016.04.001

Gurchiek RD, McGinnis RS, Needle AR, McBride JM, van Werkhoven H (2017) The use of a single inertial sensor to estimate 3-dimensional ground reaction force during accelerative running tasks. *Journal of Biomechanics*, 61, 263–268. https://doi.org/10.1016/j.jbiomech.2017.07.035

Halilaj E, Rajagopal A, Fiterau M, Hicks JL, Hastie TJ, Delp SL (2018) Machine learning in human movement biomechanics: Best practices, common pitfalls, and new opportunities. *Journal of Biomechanics*, 81, 1–11. https://doi.org/10.1016/j.jbiomech.2018.09.009

Johnson WR, Mian A, Robinson MA, Verheul J, Lloyd DG, Alderson J (2021) Multidimensional ground reaction forces and moments from wearable sensor accelerations via deep learning. *IEEE Transactions on Biomedical Engineering*, 68(1), 289–297. https://doi.org/10.1109/TBME.2020.3006158

Karatsidis A, Bellusci G, Schepers HM, de Zee M, Andersen MS, Veltink PH (2016). Estimation of ground reaction forces and moments during gait using only inertial motion capture. *Sensors (Basel, Switzerland)*, 17(1). https://doi.org/10.3390/s17010075

Kiernan D, Hawkins DA, Manoukian MAC, McKallip M, Oelsner L, Caskey CF, Coolbaugh CL (2018) Accelerometer-based prediction of running injury in National Collegiate Athletic

Association track athletes. *Journal of Biomechanics*, 73, 201–209. https://doi.org/10.1016/j.jbiomech.2018.04.001

Komaris D-S, Pérez-Valero E, Jordan L, Barton J, Hennessy L, O'Flynn B, Tedesco S (2019) Predicting three-dimensional ground reaction forces in running by using artificial neural networks and lower body kinematics. *IEEE Access*, 7, 156779–156786. https://doi.org/10.1109/ACCESS.2019.2949699

Kuhn M (2020) caret: Classification and regression training. https://CRAN.R-project.org/package=caret

Loundagin LL, Schmidt TA, Edwards WB (2018) Mechanical fatigue of bovine cortical bone using ground reaction force waveforms in running. *Journal of Biomechanical Engineering*, 140(3), 031003. https://doi.org/10.1115/1.4038288

Marchese RL, Palczewska A, Palczewski J, Kidley N (2017) Comparison of the predictive performance and interpretability of random forest and linear models on benchmark data sets. *Journal of Chemical Information and Modeling*, 57(8), 1773–1792. https://doi.org/10.1021/acs.jcim.6b00753

Matheson GO, Clement DB, McKenzie DC, Taunton JE, Lloyd-Smith DR, MacIntyre JG (1987) Stress fractures in athletes. A study of 320 cases. *American Journal of Sports Medicine*, 15(1), 46–58. https://doi.org/10.1177/036354658701500107

Matijevich ES, Branscombe LM, Scott LR, Zelik KE (2019) Ground reaction force metrics are not strongly correlated with tibial bone load when running across speeds and slopes: Implications for science, sport and wearable tech. *PLoS ONE*, 14(1).

Meinshausen N (2006) Quantile regression forests. *Journal of Machine Learning Research*, 7, 983–999.

Milgrom C, Radeva-Petrova DR, Finestone A, Nyska M, Mendelson S, Benjuya N, Simkin A, Burr D (2007) The effect of muscle fatigue on in vivo tibial strains. *Journal of Biomechanics*, 40(4), 845–850. https://doi.org/10.1016/j.jbiomech.2006.03.006

Miller RH, Edwards WB, Brandon SCE, Morton AM, Deluzio KJ (2014) Why don't most runners get knee osteoarthritis? A case for per-unit-distance loads. *Medicine & Science in Sports & Exercise*, 46(3), 572–579. https://doi.org/10.1249/MSS.0000000000000135

Miller T (2019) Explanation in artificial intelligence: Insights from the social sciences. *Artificial Intelligence*, 267, 1–38. https://doi.org/10.1016/j.artint.2018.07.007

Mo S, Lau FOY, Lok AKY, Chan ZYS, Zhang JH, Shum G, Cheung RTH (2020) Bilateral asymmetry of running gait in competitive, recreational and novice runners at different speeds. *Human Movement Science*, 71, 102600. https://doi.org/10.1016/j.humov.2020.102600

Nagahara R, Takai Y, Kanehisa H, Fukunaga T (2018) Vertical impulse as a determinant of combination of step length and frequency during sprinting. *International Journal of Sports Medicine*. https://doi.org/10.1055/s-0043-122739

Napier C, Jiang X, MacLean CL, Menon C, Hunt MA (2020) The use of a single sacral marker method to approximate the centre of mass trajectory during treadmill running. *Journal of Biomechanics*, 108, 109886. https://doi.org/10.1016/j.jbiomech.2020.109886

Nedergaard N, Robinson M, Eusterwiemann E, Drust B, Lisboa P, Vanrenterghem J (2017) The relationship between whole-body external loading and body-worn accelerometry during team-sport movements. *International Journal of Sports Physiology and Performance,* 12, 18–26. https://doi.org/10.1123/ijspp.2015-0712

Neugebauer JM, Hawkins DA, Beckett L (2012) Estimating youth locomotion ground reaction forces using an accelerometer-based activity monitor. *PLoS ONE*, 7(10), e48182. https://doi.org/10.1371/journal.pone.0048182

Nilsson J, Thorstensson A (1989) Ground reaction forces at different speeds of human walking and running. *Acta Physiologica Scandinavica*, 136(2), 217–227. https://doi.org/10.1111/j.1748-1716.1989.tb08655.x

Paquette MR, Napier C, Willy RW, Stellingwerff T (2020) Moving beyond weekly 'distance': Optimizing quantification of training load in runners. *Journal of Orthopaedic & Sports Physical Therapy*, 1–20. https://doi.org/10.2519/jospt.2020.9533

Pogson M, Verheul J, Robinson MA, Vanrenterghem J, Lisboa P (2020) A neural network method to predict task- and step-specific ground reaction force magnitudes from trunk accelerations during running activities. *Medical Engineering & Physics*, 78, 82–89. https://doi.org/10.1016/j.medengphy.2020.02.002

R Core Team (2020) R: A Language and Environment for Statistical Computing (3.6.3) [Computer software]. R Foundation for Statistical Computing.

Reenalda J, Maartens E, Homan L, Buurke JH (2016) Continuous three dimensional analysis of running mechanics during a marathon by means of inertial magnetic measurement units to objectify changes in running mechanics. *Journal of Biomechanics*, 49(14), 3362–3367. https://doi.org/10.1016/j.jbiomech.2016.08.032

Rizzone KH, Ackerman KE, Roos KG, Dompier TP, Kerr ZY (2017) The epidemiology of stress fractures in collegiate student-athletes, 2004-2005 through 2013-2014 academic years. *Journal of Athletic Training*, 52(10), 966–975. https://doi.org/10.4085/1062-6050-52.8.01

Ruder M, Jamison ST, Tenforde A, Mulloy F, Davis IS (2019) Relationship of foot strike pattern and landing impacts during a marathon. *Medicine and Science in Sports and Exercise*, 51(10), 2073–2079. https://doi.org/10.1249/MSS.0000000000002032

Ryan MR, Napier C, Greenwood D, Paquette MR (2020) Comparison of different measures to monitor week-to-week changes in training load in high school runners. *International Journal of Sports Science & Coaching*, 174795412097030. https://doi.org/10.1177/1747954120970305

Sasimontonkul S, Bay BK, Pavol MJ (2007) Bone contact forces on the distal tibia during the stance phase of running. *Journal of Biomechanics*, 40(15), 3503–3509. https://doi.org/10.1016/j.jbiomech.2007.05.024

Savorani F, Tomasi G, Engelsen SB (2013) Alignment of 1D NMR data using the iCoshift tool: A tutorial. *Magnetic Resonance in Food Science: Food for Thought* (pp. 14–24). https://doi.org/10.1039/9781849737531-00014

Scott SH, Winter DA (1990) Internal forces of chronic running injury sites. *Medicine and Science in Sports and Exercise*, 22(3), 357–369.

Tan T, Chiasson DP, Hu H, Shull PB (2019) Influence of IMU position and orientation placement errors on ground reaction force estimation. *Journal of Biomechanic*s, 97, 109416. https://doi.org/10.1016/j.jbiomech.2019.109416

Vernillo G, Martinez A, Baggaley M, Khassetarash A, Giandolini M, Horvais N, Edwards WB, Millet GY (2020). Biomechanics of Graded Running: Part I - Stride Parameters, External Forces, Muscle Activations. *Scandinavian Journal of Medicine & Science in Sports*. https://doi.org/10.1111/sms.13708

Vitali RV, Cain SM, Ojeda LV, Potter MV, Zaferiou AM, Davidson SP, Coyne ME, Hancock CL, Mendoza A, Stirling LA, Perkins NC (2019) Body-worn IMU array reveals effects of load on performance in an outdoor obstacle course. *PLoS ONE*, 14(3), e0214008. https://doi.org/10.1371/journal.pone.0214008

Wickham H (2009) ggplot2: Elegant graphics for data analysis. Springer-Verlag. https://doi.org/10.1007/978-0-387-98141-3

Wickham H, RStudio (2020) tidyr: Tidy messy data (1.1.2) . https://CRAN.R-project.org/package=tidyr

Wouda FJ, Giuberti M, Bellusci G, Maartens E, Reenalda J, van Beijnum B-JF, Veltink PH (2018) Estimation of vertical ground reaction forces and sagittal knee kinematics during running using three inertial sensors. *Frontiers in Physiology*, 9. https://doi.org/10.3389/fphys.2018.00218

Wright AA, Taylor JB, Ford KR, Siska L, Smoliga JM (2015) Risk factors associated with lower extremity stress fractures in runners: a systematic review with meta-analysis. *British Journal of Sports Medicine*, 49(23), 1517–1523. https://doi.org/10.1136/bjsports-2015-094828

4 Predicting continuous ground reaction forces from accelerometers during uphill and downhill running: A recurrent neural network solution

Ground reaction forces (GRFs) are important for understanding the biomechanics of human movement but the measurement of GRFs is generally limited to a laboratory environment. Wearable devices like accelerometers have been used to measure biomechanical variables outside the laboratory environment, but they cannot directly measure GRFs. Previous studies have used neural networks to predict the entire GRF waveform during the stance phase from wearable device data, but these networks require normalization of GRFs to the duration of a step or stance phase, resulting in a loss of the GRF waveform's temporal component. Additionally, previous studies have predicted GRF waveforms during level-ground, but not uphill or downhill running. A method of predicting the normal (perpendicular to running surface) GRF waveform using wearable devices across a range of running speeds and slopes, while maintaining the GRF waveform's temporal component, could allow researchers and clinicians to predict kinetic and kinematic variables outside the laboratory environment. We sought to develop a recurrent neural network capable of predicting normal GRF waveforms across a range of running speeds and slopes using data from accelerometers located on the sacrum and shoe.

19 subjects completed 30-s running trials on a force-measuring treadmill at five slopes (0°, ±5°, ±10°) and three speeds (2.5, 3.33, and 4.17 m/s) per slope. One biaxial accelerometer was adhered to the sacrum and two uniaxial accelerometers were adhered to the right shoe during all trials. Accelerometers on the shoe were used to classify foot strike patterns as rearfoot, midfoot, or forefoot, and sacral acceleration data were divided into overlapping 12-ms windows, allowing the neural network to iteratively predict the experimentally-measured normal GRF waveform frame-by-frame. The mean, SD, and range of accelerometer data for each 12-ms window were

included as neural network input features, along with the subject's body mass, height, running speed, slope, and percentage of a trial's steps classified as a rearfoot, midfoot, or forefoot strike. We assessed the accuracy and generalizability of the neural network using leave-one-subject-out cross validation, which provided an ensemble of Root Mean Square Error (RMSE) and relative RMSE (rRMSE) values comparing the normal GRF waveform predicted by the neural network to the normal GRF waveform measured by the force-measuring treadmill. Additionally, we calculated the mean absolute percent error (MAPE) of step frequency, contact time, normal impulse, normal GRF active peak, and loading rate between the predicted and measured GRF waveforms.

The average ± SD RMSE was 0.16 ± 0.04 BW and rRMSE was 6.4 ± 1.5% for neural network predictions of each subject's normal GRF waveform compared to measured GRF waveforms across all conditions. RMSE values were lower during slow uphill running (2.5 m/s, +10°; 0.13 ± 0.07 BW) compared to fast downhill running (4.17 m/s, -10°; 0.20 ± 0.05 BW). The MAPE ± SD for step frequency was 0.1 ± 0.1%, contact time was 4.9 ± 4.0%, normal impulse was 6.4 ± 6.9%, normal GRF active peak was 8.5 ± 8.2%, and loading rate was 27.6 ± 36.1%.

We developed a recurrent neural network that uses accelerometer data to predict the continuous normal GRF waveform across a range of running speeds and slopes. The neural network does not require preliminary identification of the stance phase, maintains the temporal component of the GRF waveform, can be applied to up- and downhill running, and facilitates the prediction of kinetic and kinematic variables outside the laboratory environment. This represents a substantial step towards accurately quantifying and monitoring the external loads experienced by the body when running outdoors.

4.1 Introduction

Ground reaction forces (GRFs) are applied to the body when the foot is in contact with the ground and their measurement has facilitated numerous insights into the etiology of running-related injuries (Ceyssens *et al.*, 2019). However, the measurement of GRFs is generally restricted to a laboratory environment. To determine the effects of sport-specific environments on running kinetics and kinematics, previous research studies have replicated aspects of an athlete's training or competitive environment within a laboratory environment. For example, Kipp et al. (Kipp, Taboga and Kram, 2017) measured GRFs during a steeplechase "water jump" by mounting the steeplechase barrier to a force platform and embedding another force platform below the landing surface, Voloshina and Ferris (Voloshina and Ferris, 2015) developed a custom force-measuring treadmill with an uneven running surface to mimic a trail surface, and Whiting et al. (Whiting *et al.*, 2020) measured stride kinematics during uphill running on a custom treadmill inclined to 30° to mimic slopes experienced during trail running. However, measuring GRFs within a laboratory environment may not adequately replicate the conditions (e.g. running surface, non-constant velocity) encountered during training or competition.

Inertial measurement units (IMUs; wireless wearable devices that measure magnetism, linear acceleration, and angular velocity) have been used to measure athletes' leg joint angles, stride kinematics, and segmental accelerations during competitive events (Reenalda *et al.*, 2016; Clermont *et al.*, 2019; Ruder *et al.*, 2019). However, IMUs cannot directly measure GRFs and require the use of algorithms to estimate discrete variables like peak vertical GRF, ground contact time, vertical impulse, and vertical loading rate (Neugebauer, Hawkins and Beckett, 2012; Ancillao *et al.*, 2018; Kiernan *et al.*, 2018; Derie *et al.*, 2020). Recently, neural networks have been used to predict GRF waveforms during running (Wouda *et al.*, 2018; Dorschky *et al.*, 2020;

Pogson *et al.*, 2020; Johnson *et al.*, 2021), from which a variety of discrete variables can be calculated. Although predictions of the entire GRF waveform represent a more versatile outcome compared to predicting a discrete variable, previous studies have used neural network architectures that required data to be time-normalized to the duration of a step (Dorschky *et al.*, 2020) or stance phase (Wouda *et al.*, 2018; Johnson *et al.*, 2021), preventing the calculation of biomechanical variables with a non-normalized temporal component (e.g. ground contact time, step frequency, vertical impulse, and loading rate). Pogson et al. (2020) zero-padded the end of accelerometer data to the length of the longest stance phase to preserve the temporal component, but observed decreased accuracy when predicting the vertical GRF waveform during the stance phase (Root Mean Square Error ≈ 200 N)(Pogson *et al.*, 2020). Additionally, previous studies have only predicted GRF waveforms during level-ground running (Wouda *et al.*, 2018; Dorschky *et al.*, 2020; Pogson *et al.*, 2020; Johnson *et al.*, 2021), limiting the application to environments where no uphill or downhill running occurs (i.e. a level treadmill or athletics track). Road and trail running are internationally popular forms of physical activity (Running USA, 2019; International Trail Running Association, 2020) and require runners to navigate a variety of running slopes and terrain. A method of predicting GRF waveforms from wearable devices across a range of running slopes, while maintaining the temporal component, could allow researchers, clinicians, and coaches to measure a variety of kinetic and kinematic variables in a range of outdoor environments.

Long Short-Term Memory (LSTM) networks (Hochreiter and Schmidhuber, 1997) are a type of recurrent neural network that overcome the requirement of the time-normalized inputs like that of the neural networks used in previous research (Wouda *et al.*, 2018; Johnson *et al.*, 2021). LSTM networks overcome this limitation by recurrently predicting small, uniform portions of a larger sequence of data that can be of variable length. As such, a sequence of continuous GRF data

can be predicted if it can be broken up into uniform portions. For the prediction of a given portion, LSTM networks use information from previous portions, effectively "remembering" the portion's context. LSTM networks have been used in this manner to analyze a variety of sequential data, ranging from natural language processing (Wang and Jiang, 2016) to stock market forecasting (Selvin *et al.*, 2017). In the field of biomechanics, LSTM networks have been used to make frame-by-frame predictions of GRF waveforms using motion capture data (Mundt *et al.*, 2020) and predictions of the center of mass position relative to center of pressure from IMU data during walking (Choi, Jung and Mun, 2019). To our knowledge, LSTM networks have not been used to predict GRF waveforms from wearable device data exclusively during running. Developing such a network would allow researchers to predict the GRF waveform not only during the stance phase, but continuously for the entire duration of a run. Considering that IMUs have already been used to longitudinally measure biomechanical variables related to running injury (Reenalda *et al.*, 2016; Kiernan *et al.*, 2018; Clermont *et al.*, 2019; Ruder *et al.*, 2019), applying an LSTM network to such data would effectively provide a way to indirectly collect continuous GRF waveforms in environments and quantities currently impossible to accomplish.

The purpose of this exploratory study was to develop an LSTM network that could predict the normal (perpendicular to running surface) GRF waveform across a range of running speeds and slopes using data from accelerometers. Given the novelty of this approach, we sought to develop a network that could predict the GRF waveform with accuracy better than state-of-the-art predictions of time-normalized vertical GRF data during level ground running using data from multiple IMUs: a Root Mean Square Error (RMSE) of 0.21 BW (Dorschky *et al.*, 2020) and relative RMSE (rRMSE; RMSE normalized to the average range of the compared waveforms; Eq. 4.1) of 13.92% (Johnson *et al.*, 2021).

4.2 Methods

4.2.1 Subjects

We analyzed a pre-existing dataset (Baggaley *et al.*, 2019; Khassetarash *et al.*, 2020; Vernillo *et al.*, 2020) where 21 subjects ran at a combination of running speeds and slopes. Two subjects were excluded from the current analysis due to equipment data acquisition errors, leaving 19 subjects remaining (10 Male, 9 Female; 29 ± 9 years, 173 ± 9 cm, 68.1 ± 9.9 kg). All subjects provided informed consent and the experimental protocol was approved by the University of Calgary Conjoint Health Research Ethics Board (#REB14-1117).

4.2.2 Experimental Protocol

Following a 5-min warm up at a self-selected speed, each subject completed thirty 30-s trials on a force-measuring treadmill (2000 Hz; Bertec, OH, USA), which included five slopes (0°, ±5°, ±10°) at three speeds (2.5, 3.33, and 4.17 m/s) per slope, and three step frequencies (preferred and ± 10%) at 3.33 m/s for each slope. Three custom biaxial accelerometers (2000 Hz) were adhered with tape to subjects during all conditions: one on the sacrum and two on the right shoe. The accelerometers on the shoe were used to determine the foot strike pattern for each condition using a previously validated method (Giandolini *et al.*, 2014), which provided the percentage of a trial's foot strikes classified as either a rearfoot, midfoot, or forefoot strike. Only the vertical and anteroposterior axes relative to the local coordinate system of the sacral accelerometer and the normal (perpendicular to the treadmill surface) GRFs were used in the current analysis. We chose to exclude the shoe accelerometer data for predictions of GRF waveforms because the data were not available for both feet.

4.2.3 Processing

We analyzed 5 seconds of data from each trial (approximately 13 foot-ground contacts) and downsampled the normal GRF, vertical sacral acceleration, and anteroposterior sacral acceleration to 500 Hz to reduce the computational cost and match the sampling frequency of prior studies (Day *et al.*, 2021). The GRFs were normalized to bodyweight (BW) and filtered using a 4th order low-pass Butterworth filter with a cut-off frequency of 30 Hz and the sacral acceleration data were filtered with a 4th order low-pass Butterworth filter with a cut-off frequency of 20 Hz. Pilot testing revealed that a 20 Hz cut-off frequency improved prediction accuracy and preserved approximately 89% and 82% of the vertical and anteroposterior signal power, respectively.

The vertical accelerometer data were further processed so that all negative values were replaced with zeros. Pilot testing revealed that negative vertical acceleration values primarily occur during the aerial phase and replacing them with zeros helped the LSTM network avoid predictions of negative normal GRFs during the aerial phase. For each condition, we used the 2500-frame (5-s @ 500 Hz) sequences of vertical and anteroposterior sacral accelerometer data to predict the simultaneously collected 2500-frame sequence of normal GRFs. The recurrent nature of the LSTM network requires long sequences to be divided into smaller sequences that are iteratively used to make predictions. To accomplish this, we divided the acceleration data for each trial into overlapping windows with a width of 6 frames (12 ms) and padded the beginning and end of the acceleration data with the nearest value to ensure that the number of windows was equal to the number of frames in the normal GRFs (2500) and that the windows were centered on the corresponding frame in the normal GRFs (**Figure 4.1**). Pilot testing revealed that a window width of 6 frames was the smallest window we could use without decreasing LSTM network prediction

accuracy. Thus, the LSTM network iteratively predicted a single frame of the normal GRF at time t using acceleration data from frames t_{-3} through t_{+2} (**Figure 4.1**).

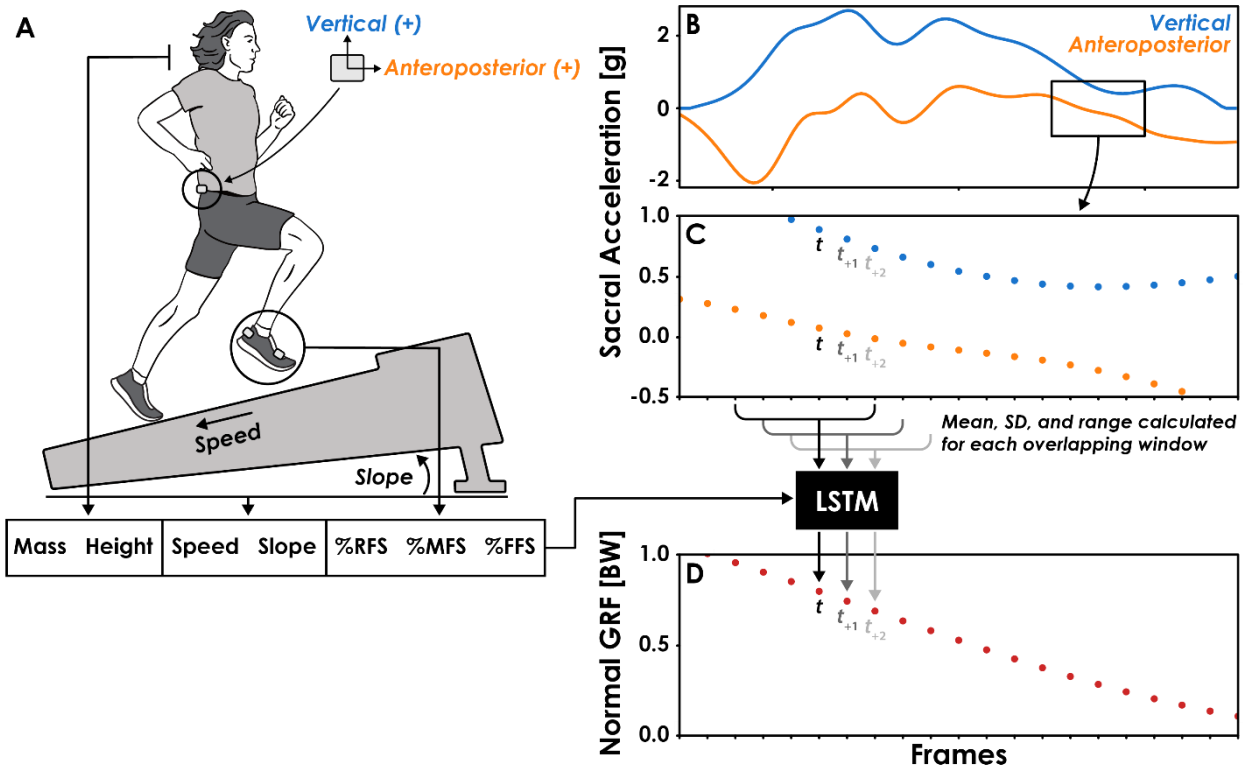

Figure 4.1 Overview of the Long Short-Term Memory (LSTM) network's input features. A) The LSTM network's input features included body mass, height, running speed, slope, and percentage of a trial's steps classified as a rearfoot (RFS), midfoot (MFS), or forefoot (FFS) strike. Foot strike percentages were calculated from data collected by accelerometers on the right foot. **B)** Filtered vertical and anteroposterior sacral acceleration data, relative to the device's local coordinate system. **C)** Accelerometer data were divided into overlapping 6-frame (12 ms) windows, one for each frame of the ground reaction force (GRF) data. The mean, standard deviation (SD), and range of vertical and anteroposterior sacral acceleration values were calculated for each window and were used as input features to the LSTM network. For the prediction of a normal GRF value at a given time (t), the respective window of acceleration data begins at t_{-3} and ends at t_{+2}. **D)** Normal GRFs were predicted frame-by-frame by the LSTM network using the 13 input features.

4.2.4 Feature Engineering

A total of 13 features were used as inputs to the LSTM network (**Figure 4.1**). We calculated the mean, standard deviation (SD), and range of vertical and anteroposterior acceleration data for each 12-ms window and used them as input features. The use of summary statistics as input

features has been shown to maintain neural network accuracy while benefiting from a reduced computational cost (Figo *et al.*, 2010). These three summary statistics were normalized to a range of 0 – 1 and represent 6 (3 features x 2 acceleration axes) of the 13 input features. The remaining input features were selected due to their effect on running kinetics and kinematics: subject height, body mass, running speed, slope, and percentage of steps classified as either a rearfoot, midfoot, or forefoot strike (Almeida, Davis and Lopes, 2015; Khassetarash *et al.*, 2020; Vernillo *et al.*, 2020; Vincent *et al.*, 2020). We chose not to include step frequency as an input feature, despite the presence of the ±10% preferred step frequency conditions, to increase the variability in the accelerometer data used to predict the GRF waveforms. Doing so represents a greater challenge for the LSTM network as there is known variability between trials that is not being explicitly accounted for as an input variable.

4.2.5 Neural Network Architecture

The neural network consisted of a Bidirectional LSTM and multilayer perceptron (MLP) with three fully connected layers containing 128, 384, and 320 neurons, respectively (**Figure 4.2**). The Bidirectional LSTM consists of two LSTM layers where the order of the input sequence is reversed for the second layer. Reversing the sequence for the second LSTM layer allows the network to utilize information from future portions of the sequence just as the first LSTM layer utilizes information from prior portions. The outputs from each LSTM layers are then averaged before being passed along to the MLP. The number and size of the layers in this network were determined using the Hyperband hyperparameter optimization algorithm (Li *et al.*, 2018) on the data of two randomly selected subjects. The LSTM network was trained using a batch size of 32, learning rate of 0.001, and Mean Square Error loss function. Network weights and biases were updated using the adaptive moment estimation (Adam) optimization algorithm at the end of each

epoch (Kingma and Ba, 2017) and training lasted a maximum of 1000 epochs or until the Mean Square Error failed to decrease by 0.001 BW after 30 consecutive epochs. The neural network was developed using the Tensorflow (v2.2.0) python library (Abadi *et al.*, 2016).

4.2.6 Network Validation

We assessed the accuracy and generalizability of the network using a leave-one-subject-out (LOSO) cross validation method (Halilaj *et al.*, 2018). LOSO cross validation is a variation of K-fold cross validation that requires the dataset to be subset by subject, with one subject's data set aside for testing purposes and the rest of the subjects' data used to train the network. This process is repeated until the network has been tested on every subject's data, ultimately providing an ensemble of networks and their respective accuracy metrics. These metrics illustrate how accurate the network is when applied to data from many different individuals. Performing LOSO cross validation is computationally costly, as the network must be trained and tested a number of times equal to the number of subjects (n = 19), but the benefits of this method include the ensemble of accuracy metrics and assurance that a subject's data is not included in both the training and testing subsets, which can artificially increase the reported accuracy of a network since it was tested on data from a subject included during training (Saeb *et al.*, 2017; Chaibub Neto *et al.*, 2019).

In addition to the LOSO cross validation method, we performed a test-train split according to slope (±5° trials reserved for testing, 0° and ±10° slopes used for training) for one representative subject's data to test the accuracy of a model when predicting speed-slope combinations that were not present during training. We selected subject 14 as a representative subject because their RMSE

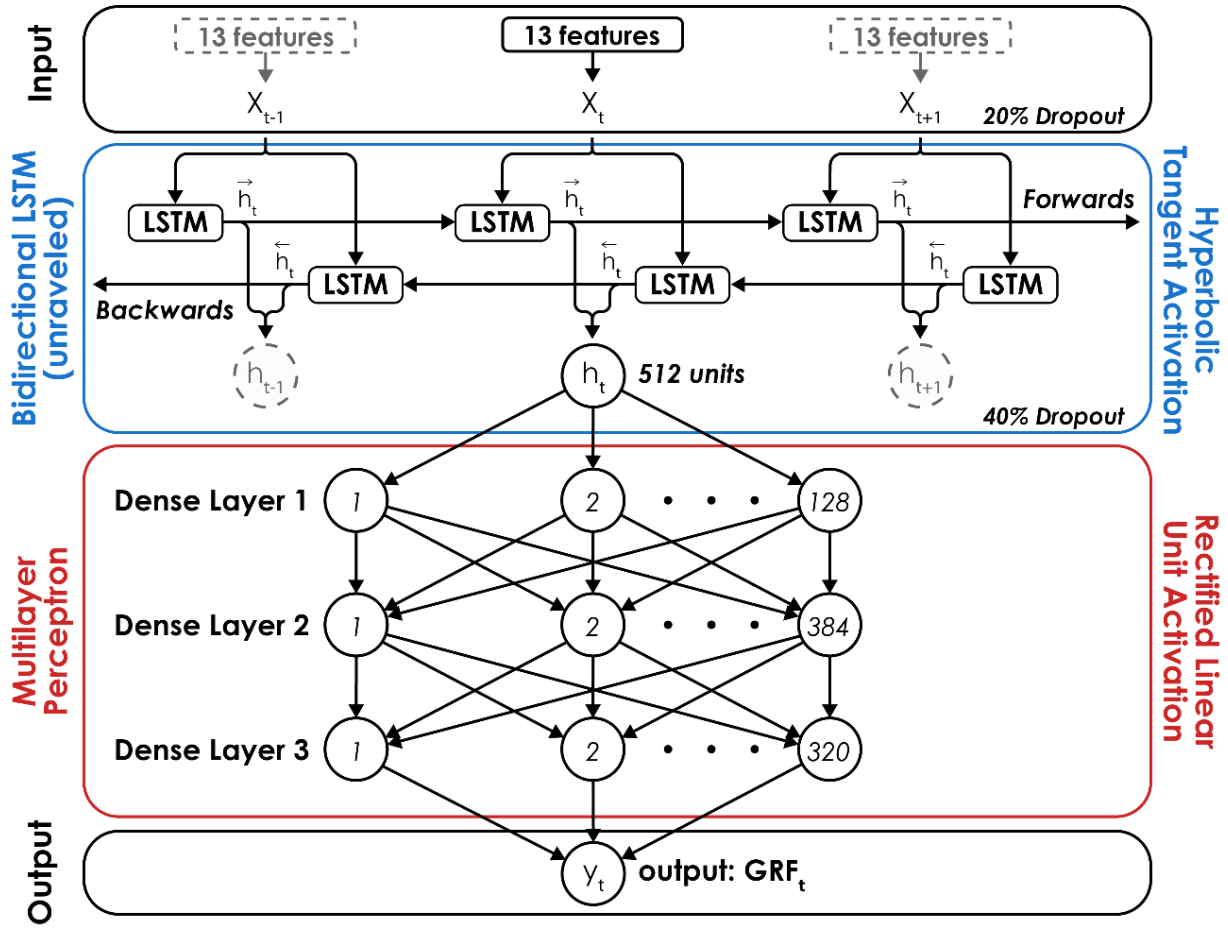

Figure 4.1 Neural Network Architecture. The Long Short-Term Memory (LSTM) network consisted of a Bidirectional LSTM layer with a hyperbolic tangent activation function followed by a multilayer perceptron (MLP) with rectified linear unit activation functions for three hidden layers with 128, 384, and 320 neurons, respectively. The Bidirectional LSTM layer is unraveled to illustrate its recurrent nature and dashed lines signify inputs (x) and outputs (h) at time t_{-1} and t_{+1}. A dropout rate of 20% was applied to the input layer of the network and a dropout rate of 40% was applied to the output of the Bidirectional LSTM layer to limit network overfitting. For each prediction of the normal GRF at a given time (t), the network received 13 features as inputs (x_t; **Figure 4.1**), passed the output from the Bidirectional LSTM layer (h_t) to the MLP, and predicted a single value (y_t) with a linear activation function in the output layer.

was similar to the average RMSE across all subjects (**Figure 4.3**) and their GRF waveforms illustrated the interaction between running slope and normal GRF impact peak magnitude (Gottschall and Kram, 2005). This single-subject validation method prioritizes accuracy over generalizability (the ability to make accurate predictions for a variety of athletes) and represents the potential circumstance of training the LSTM network on data collected from a single athlete

before the start of their competitive season and using it to predict the same athlete's GRF data during their competitive season.

Prediction error for each trial's GRF waveform was quantified as the Root Mean Square Error (RMSE) and relative RMSE (rRMSE), which is the RMSE normalized to the average range of the compared waveforms expressed as a percentage and defined as

$$rRMSE = \frac{RMSE}{0.5 * \sum_{i=1}^{2}(\max(x_i) - \min(x_i))} * 100\,, \tag{4.1}$$

where x_1 and x_2 are the GRF waveforms predicted by the LSTM network and measured by the force-measuring treadmill (Ren, Jones and Howard, 2008). Additionally, we used a threshold of 5% BW to identify the start and end of the stance phase and calculated the active peak of the normal GRF waveform, normal impulse, normal GRF loading rate, contact time, and step frequency from the predicted and measured GRF data. The normal GRF active peak was calculated as the maximum normal GRF value occurring between 40 – 60% of the stance phase because the magnitude of the impact peak can exceed the active peak during downhill running and occurs during early stance phase (0 - 30%) (Gottschall and Kram, 2005; Vernillo *et al.*, 2020). We calculated impulse as the integral of the normal GRF waveform during the stance phase with respect to time, loading rate as the average slope of the normal GRF waveform during the first 25 ms of the stance phase (Yong *et al.*, 2018), contact time as the duration when the normal GRF was greater than 5% BW, and step frequency as the number of initial foot-ground contacts per second. We report the mean absolute percent error (MAPE) of these discrete variables for each subject. Data analysis was performed in python and R using custom libraries (Wickham, 2009, 2019; Alcantara, 2019; Harris *et al.*, 2020; pandas development team, 2020; R Core Team, 2020; Virtanen *et al.*, 2020; Wickham *et al.*, 2020).

We applied two constraints to the predicted GRF waveform to ensure that the data fell within established biomechanical limits and could be used to calculate discrete biomechanical variables of interest. First, the predicted GRF waveform had to have an equal number of foot-ground contacts as the GRF waveform measured by the force-measuring treadmill, determined using a 5% BW threshold. Second, the step frequency over the duration of the predicted GRF waveform had to be ≤ 4 Hz. These criteria represent biomechanical constraints to the network predictions, as thresholds of 5% BW have been previously used to identify the stance phase for the calculation of kinetic or kinematic variables (Day *et al.*, 2021) and step frequency is ≤ 4 Hz during uphill and downhill running (Cavagna *et al.*, 1997; Snyder and Farley, 2011). Trials that failed to meet either of these criteria were used to calculate the LSTM network's prediction failure rate and removed from subsequent analyses.

4.3 Results

4.3.1 LSTM Network Prediction Failure Rate

We analyzed 529 trials for the present study. The predicted GRF waveforms for 32 trials (6%) failed to meet one or both criteria and were classified as failed predictions. Specifically, 22 trials (4%) required a threshold greater than 5% BW to identify an equal number of steps between the predicted and measured GRF waveforms and 10 trials (2%) had a step frequency greater than 4 Hz. Thus, 94% of the GRF waveforms predicted by the LSTM network fell within the imposed biomechanical boundaries.

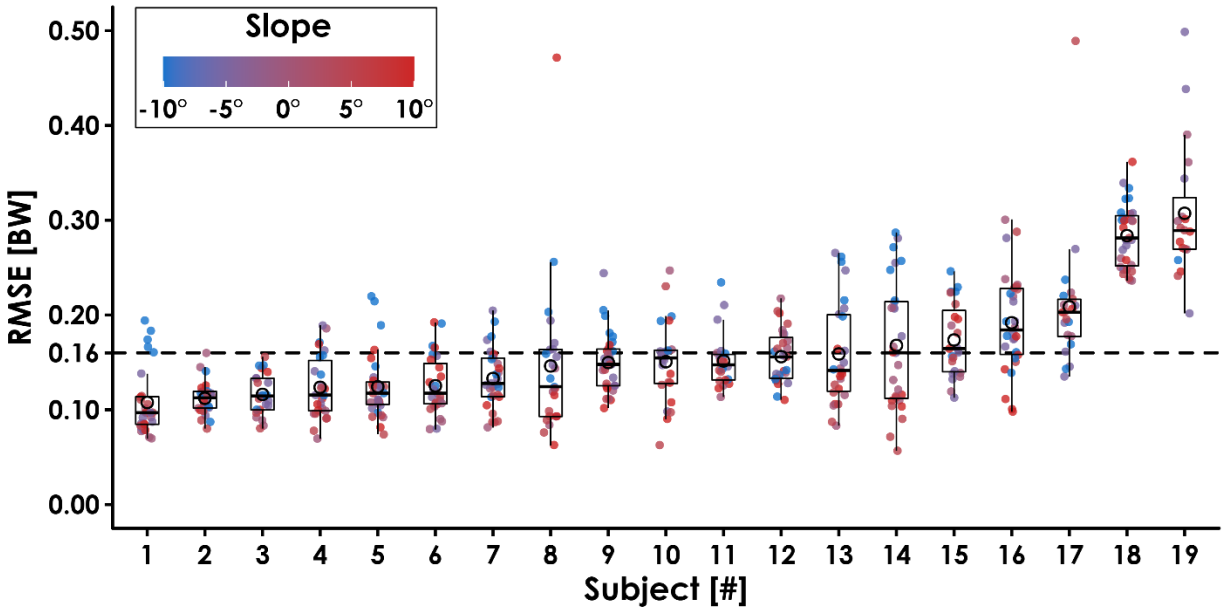

Figure 4.2 Ground reaction force waveform prediction error for each subject across all conditions. The average Root Mean Square Error (RMSE) across subjects was 0.16 BW (dashed horizontal line). Filled circles represent each trial, and the color indicates slope (0°, ±5°, ±10°) at three speeds (2.5, 3.33, and 4.17 m/s). Open circles represent each subject's average RMSE, horizontal bars are the median RMSE, box plot edges indicate the interquartile range (IQR; 25th and 75th percentile), and the whiskers encompass values that fall within 1.5*IQR. Subjects are sorted from lowest to highest RMSE.

4.3.2 LOSO Cross Validation

The average ± SD RMSE was 0.16 ± 0.04 BW (**Figure 4.3**) and rRMSE was 6.4 ± 1.5% for the LSTM network predictions of each subject's normal GRF waveforms compared to the GRF waveforms measured by the force-measuring treadmill across all conditions (**Table 4.1**). RMSE values were lower during slow uphill running (2.5 m/s, +10°; 0.13 BW) compared to fast downhill running (4.17 m/s, -10°; 0.20 BW) (**Figure 4.4** & **Figure 4.5**). The MAPE for step frequency was

0.1 ± 0.1%, contact time was 4.9 ± 4.0%, impulse was 6.4 ± 6.9%, normal GRF active peak was 8.5 ± 8.2%, and loading rate was 27.6 ± 36.1% (**Table 4.2**).

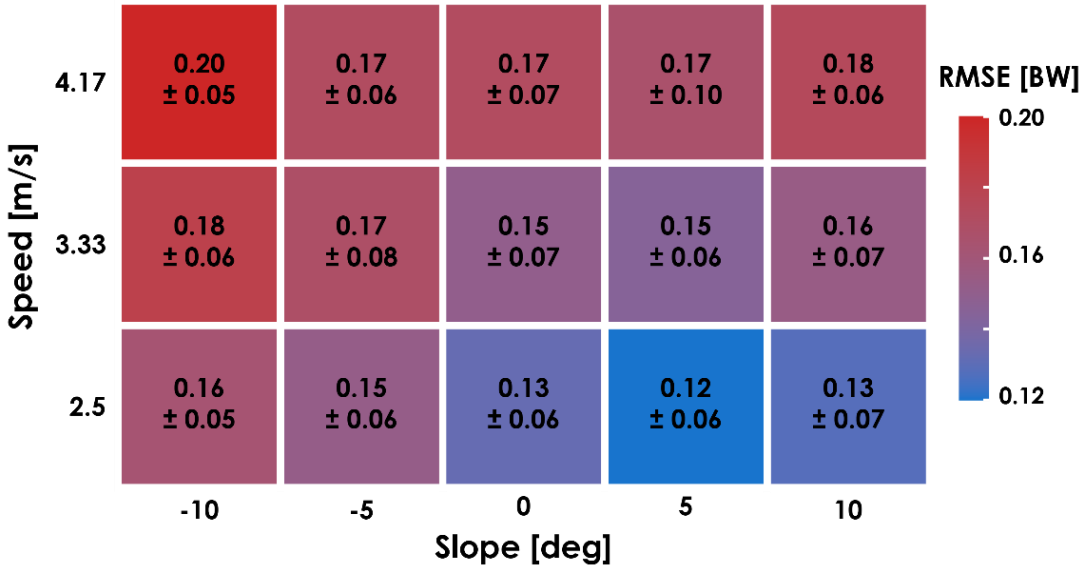

Figure 4.3 Ground reaction force waveform prediction error for each condition. The average ± SD Root Mean Square Error (RMSE) of the predicted ground reaction force (GRF) waveforms compared to the GRF waveform measured by the force-measuring treadmill for each condition during leave-one-subject-out cross validation.

4.3.3 Single-Subject Validation

The error metrics calculated during the single-subject validation reflect the accuracy of the LSTM network when tested on the data from a representative subject (Subject 14) during the ±5° slope trials and trained on their remaining trials. The prediction error for the representative subject's normal GRF waveforms at ±5° was lower than those resulting from the LOSO cross validation, with an average ± SD RMSE of 0.08 ± 0.02 BW and rRMSE of 3.3 ± 0.9%. The MAPE of step frequency (0.1 ± 0.1 %), contact time (3.0 ± 2.3%), impulse (2.5 ± 1.9%), normal GRF active peak (2.7 ± 2.0%), and loading rate (17.6 ± 16.9%) calculated from the GRF waveform predicted by the LSTM network were also generally lower than those resulting from the LOSO cross validation.

Table 4.1 Mean ± SD Root Mean Square Error (RMSE) and relative RMSE (rRMSE) for the normal GRF waveform predicted by the LSTM network compared to the measured normal GRF waveform for each subject.

Subject	RMSE [BW]	rRMSE [%]
1	0.11 ± 0.04	4.0 ± 1.1
2	0.11 ± 0.02	4.1 ± 0.7
3	0.12 ± 0.02	4.4 ± 0.9
4	0.12 ± 0.03	4.6 ± 1.2
5	0.12 ± 0.04	4.7 ± 0.9
6	0.12 ± 0.03	5.2 ± 1.4
7	0.13 ± 0.03	5.1 ± 1.2
8	0.15 ± 0.08	5.3 ± 3.3
9	0.15 ± 0.03	5.4 ± 1.0
10	0.15 ± 0.04	5.2 ± 1.3
11	0.15 ± 0.03	5.8 ± 0.8
12	0.16 ± 0.03	6.1 ± 1.1
13	0.16 ± 0.06	5.7 ± 1.5
14	0.17 ± 0.07	6.9 ± 2.5
15	0.17 ± 0.04	7.9 ± 2.0
16	0.19 ± 0.05	6.7 ± 1.7
17	0.21 ± 0.07	7.2 ± 2.5
18	0.29 ± 0.03	14.0 ± 1.7
19	0.31 ± 0.07	13.7 ± 2.7
Mean ± SD	0.16 ± 0.04	6.4 ± 1.5%

Table 4.2 Mean ± SD discrete variables calculated from the normal ground reaction force (GRF) waveform predicted by the LSTM network ("Predicted") and the normal GRF waveform measured by the force-measuring treadmill ("Measured") across all speeds and subjects for each slope.

	Step Frequency [Hz]		Contact Time [ms]		Impulse [BW*s]		Active Peak [BW]		Loading Rate [BW/s]	
Slope	Predicted	Measured	Predicted	Measured	Predicted	Measured	Predicted	Measured	Predicted	Measured
-10°	3.1 ± 0.3	3.1 ± 0.3	215 ± 26	214 ± 29	0.33 ± 0.03	0.33 ± 0.05	2.38 ± 0.24	2.36 ± 0.40	64.7 ± 19.9	68.4 ± 20.6
-5°	3.1 ± 0.3	3.1 ± 0.3	222 ± 23	223 ± 27	0.34 ± 0.04	0.34 ± 0.04	2.41 ± 0.25	2.45 ± 0.36	54.9 ± 16.7	60.6 ± 19.4
0°	3.1 ± 0.3	3.1 ± 0.3	228 ± 24	229 ± 27	0.33 ± 0.04	0.34 ± 0.04	2.42 ± 0.22	2.51 ± 0.36	42.0 ± 12.8	49.0 ± 17.2
+5°	3.2 ± 0.3	3.2 ± 0.3	228 ± 25	232 ± 26	0.32 ± 0.03	0.33 ± 0.04	2.36 ± 0.21	2.40 ± 0.33	34.8 ± 8.5	39.3 ± 13.3
+10°	3.4 ± 0.3	3.4 ± 0.3	223 ± 26	227 ± 26	0.30 ± 0.04	0.30 ± 0.04	2.24 ± 0.22	2.20 ± 0.29	30.1 ± 8.3	31.3 ± 12.7

4.4 Discussion

We developed a recurrent neural network capable of predicting the continuous normal GRF waveform across a range of running speeds (2.5 – 4.17 m/s), slopes (0°, ±5°, ±10°), and step frequencies (preferred, ±10%) from accelerometer data. Our findings indicate that an LSTM network given the runner's mass, height, running speed, slope, foot strike pattern, and sacral acceleration can predict the normal GRF waveform across a range of speeds and slopes with an RMSE of 0.12 – 0.20 BW and rRMSE of 5.4 – 7.3% (**Figure 4.4**). For comparison, recent studies report an RMSE of 0.39 ± 0.26 BW (Wouda *et al.*, 2018), an RMSE of 0.21 ± 0.03 BW (Dorschky *et al.*, 2020), and an rRMSE of 13.92% (Johnson *et al.*, 2021) when using neural networks to predict the stance phase vertical GRF waveform during level-ground running. Previous studies also quantified the accuracy of their networks using the Pearson correlation between the predicted and measured GRF waveforms, but we chose not to include correlation as a primary metric of accuracy. We refrained from calculating the Pearson correlation because it appears to lack the sensitivity of RMSE or rRMSE when comparing GRF waveforms (Ancillao *et al.*, 2018). Previous studies have achieved very strong correlations (≥ 0.90) when predicting the vertical GRF waveform but RMSE and rRMSE values were up to twice as large as the average values achieved in the present study.

In contrast to previous studies, the LSTM network does not require stance phase identification or time normalization, which preserves the temporal component of the predicted GRF waveform. This characteristic of the LSTM network allowed us to calculate stride kinematic variables like step frequency and contact time with a MAPE < 5%. Additionally, the recurrent nature of the LSTM network facilitates frame-by-frame predictions of the GRF waveform and can be used to make predictions over any duration of running if the length of the accelerometer signal

is divisible by the window width (12 ms). Thus, the LSTM network could be used to quantify changes in the normal GRF waveform over the course of prolonged runs (e.g. a marathon race).

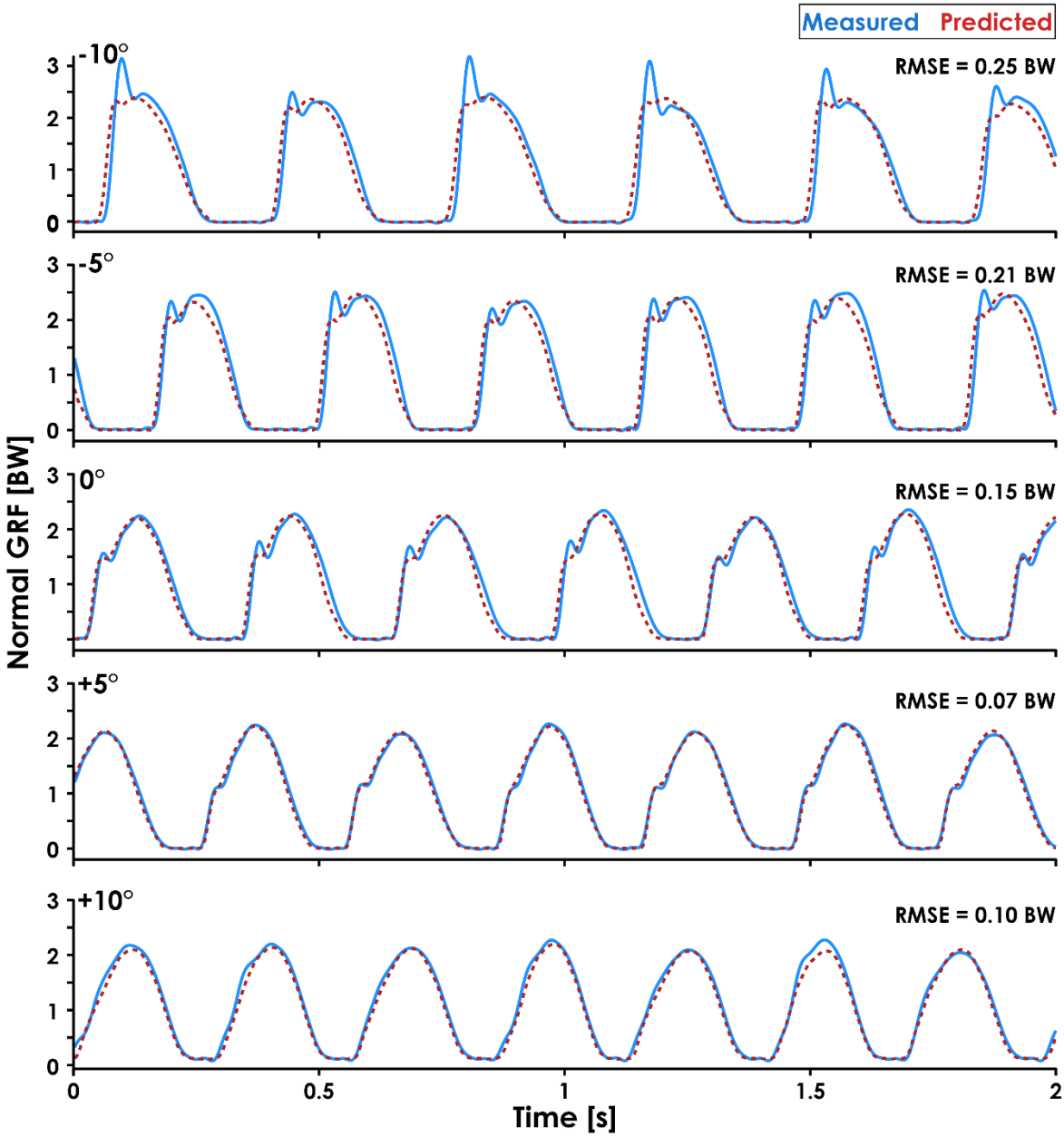

Figure 4.5 Predicted and measured normal GRF waveforms across slopes for a representative subject. The normal ground reaction force (GRF) waveforms predicted by the recurrent neural network (dashed red lines) and measured by the force-measuring treadmill (solid blue lines) at 3.33 m/s and all slopes (0°, ±5°, ±10°) are presented for Subject 14. Subject 14 was selected because they had similar RMSE values (0.17 ± 0.07 BW) as the average across all subjects (0.16 ± 0.04 BW) and their data illustrate the effect of slope on the presence of an impact peak in the normal GRF waveform.

The accuracy of the predicted GRF waveforms varied across speeds and slopes, with a combination of faster running speeds and negative slopes producing greater RMSE values than slower running speeds and positive slopes (**Figure 4.4**). We suspect that the greater RMSE values during downhill running may be due to the LSTM network's inability to account for changes in impact peak magnitude across slopes (**Figure 4.5**). Previous studies have found that the presence of an impact peak in the normal GRF waveform is subject-specific, affected by changes in running slope, and associated with the acceleration of the effective mass of the lower extremity during early stance phase (McMahon, Valiant and Frederick, 1987; Gottschall and Kram, 2005; Vernillo *et al.*, 2020). Thus, predictions of the normal GRF waveform across slopes may be further improved by incorporating accelerations measured at the feet or lower legs.

4.4.1 Single-Subject Validation

We quantified the accuracy of the LSTM network when trained and tested on data from the same subject. Although not a valid method of determining the generalizability of a machine learning algorithm, single-subject validation provides insight into how well a personalized neural network could predict an individual's GRF waveform for unknown combinations of speed and slope in the future. We found that predicted GRF waveforms during the ±5° slope conditions had an average ± SD RMSE of 0.08 ± 0.02 BW, indicating that a subject-specific LSTM network was approximately twice as accurate as the LOSO cross validated LSTM network. A single-subject approach may be particularly beneficial for researchers, coaches, or clinicians who have the resources to train personalized LSTM networks and wish to monitor a specific athlete's biomechanics over the course of a competitive season. For example, an athlete could run at a variety of speeds and slopes while wearing accelerometers during baseline testing on a force-measuring treadmill at the start of their competitive season and a personalized LSTM network

could be trained on their data. Then, if accelerometer data were collected from an athlete during training runs, their normal GRF waveforms and a variety of discrete values could be predicted and monitored longitudinally. Although this approach benefits from improved prediction accuracy, it requires computational resources necessary to train personalized LSTM networks for each athlete.

4.4.2 Discrete Variable Accuracy

The MAPE values for step frequency, contact time, impulse, and normal GRF active peak were ≤ 8.5%, but the loading rate MAPE was 27.6 ± 36.1%. The lower MAPE values for step frequency, contact time, impulse, and normal GRF active peak indicate that the LSTM network consistently identified the general shape of the GRF waveform and the boundaries of the stance phase despite changes in speed, slope, and step frequency. However, the network did not consistently predict the presence of an impact peak during early stance phase (**Figure 4.5**, -10° trial), which affects the slope of the GRF waveform during early stance phase and thus the accuracy of the loading rate values. Although the prominence of an impact peak in the normal GRF waveform is affected by foot strike pattern and slope (Gottschall and Kram, 2005), which are two variables that we included as input features for the LSTM network, the decreased accuracy when estimating loading rate may be because we did not include accelerometer data from the lower legs or feet. The impact peak of the GRF waveform is associated with the acceleration of the effective mass of the lower extremity during early stance phase (McMahon, Valiant and Frederick, 1987; Gottschall and Kram, 2005) and a previous study found moderate-strong correlations between axial tibial acceleration and vertical GRF impact peak magnitude ($r = 0.76$) and timing ($r = 0.94$) during running (Hennig and Lafortune, 1991). We did not include the accelerometer data from the shoes as inputs for the LSTM network because the data were not available for both feet but

including data from an accelerometer located on the lower legs or feet as inputs to a neural network may further improve the prediction accuracy of loading rate.

External cumulative loading is generally calculated as the product of a given external load's magnitude (e.g. peak GRF) and the number of steps taken over a given duration of running (Firminger and Edwards, 2016; Kiernan *et al.*, 2018; Backes *et al.*, 2020; Ryan *et al.*, 2020) and has been associated with running-related overuse injuries (Colby *et al.*, 2014; Bertelsen *et al.*, 2017; Kiernan *et al.*, 2018). Previous studies have predicted the peak vertical GRF from pelvis accelerometer data with a MAPE of 4.0 – 8.3% during level-ground running (Neugebauer, Hawkins and Beckett, 2012), but a personalized LSTM network could be used to measure an athlete's external cumulative load with improved accuracy (MAPE = 2.7 ± 2.0%) across a range of running speeds and slopes. Thus, an LSTM network could be used to monitor an athlete's risk of sustaining a running-related overuse injury over the course of a competitive season.

4.4.3 Considerations for LSTM Network Implementation

The LSTM network represents a promising strategy for predicting continuous normal GRFs from wearable devices in outdoor environments. The LSTM network required three accelerometers (one on the sacrum and two on the right shoe to determine foot strike pattern), but we performed a *post-hoc* analysis of the prediction accuracy without the foot strike pattern data to quantify the network's accuracy when only using data from one sacral accelerometer. The *post-hoc* analysis revealed that excluding foot strike pattern data slightly increased the average ± SD RMSE from 0.16 ± 0.04 BW to 0.17 ± 0.05 BW and rRMSE from 6.4 ± 1.5% to 6.7 ± 1.7%. Excluding foot strike pattern data affected the MAPE of discrete variables by < 3% (**Table 4.3**). These findings indicate that the LSTM network can predict normal GRF waveforms from a single accelerometer on the sacrum more accurately than neural networks implemented in previous

studies (RMSE = 0.21 – 0.39 BW, rRMSE = 13.92%), which require data from 3 – 7 wearable devices (Wouda *et al.*, 2018; Dorschky *et al.*, 2020; Johnson *et al.*, 2021).

Table 4.3 Error metrics for the predicted waveform and discrete variables when training the Long Short-Term Memory (LSTM) network with and without foot strike pattern as input features. Root Mean Square Error (RMSE) and relative RMSE (rRMSE) are presented for the normal ground reaction force (GRF) waveforms predicted by an LSTM network trained with and without foot strike pattern data from the two accelerometers on the right foot. Mean absolute percent error (MAPE) values are presented for the discrete variables calculated from the normal GRF waveforms predicted by both LSTM networks.

	LSTM With Foot Strike (Sacrum + Right Foot Accelerometers)	**LSTM Without Foot Strike (Only Sacrum Accelerometer)**
GRF Waveform		
RMSE [BW]	0.16 ± 0.04	0.17 ± 0.05
rRMSE	6.4 ± 1.5%	6.7 ± 1.7%
Discrete Variables MAPE		
Step Frequency	0.1 ± 0.1%	0.1 ± 0.1%
Contact Time	4.9 ± 4.0%	5.6 ± 4.5%
Impulse	6.4 ± 6.9%	6.0 ± 7.1%
Active Peak	8.5 ± 8.2%	7.7 ± 6.3%
Loading Rate	27.6 ± 36.1%	30.3 ± 41.6%

Using a recurrent neural network in combination with accelerometers and a global positioning system (GPS) device to obtain speed and slope data could potentially allow runners to receive accurate biomechanical feedback during an outdoor run. GPS devices are commonly used by runners (Janssen *et al.*, 2020), have been used to provide real-time feedback of step frequency (Willy *et al.*, 2016), and could provide the LSTM network with the running speed and slope data necessary to predict the GRF waveform (Scott, Scott and Kelly, 2016). This could facilitate near real-time predictions of the normal GRF waveform if the accelerometer data can be synchronized with the GPS data and split into portions with near constant speeds and slopes. Discrete biomechanical variables could then be calculated from the predicted normal GRF waveform and sent to a clinician, coach, researcher, or the runner themselves. A similar approach has been

implemented during outdoor walking and running using an integrated IMU-GPS device placed in a backpack, but it is unclear how generalizable or accurate this approach is as the network was trained and tested on data from the same three subjects and the reported accuracy metrics are combined for walking and running (Vitali *et al.*, 2019). To facilitate the calculation of GRF-based variables during outdoor running using accelerometers, we have made the LSTM networks, which were trained on all subjects, with and without the need for foot strike data, publicly available.

4.4.4 Limitations

There are potential limitations to consider alongside our findings. The accelerometers used in the present study were adhered to subjects using tape, and a less secure attachment method may introduce movement artefact into the accelerometer signal. Securing an IMU to the lower leg using a commercial strap resulted in peak accelerations that were 1.2 g greater than when securing the IMU with athletic tape (Johnson *et al.*, 2020), but the lower leg experiences larger accelerations than the sacrum during running (Baggaley *et al.*, 2019) and may be more sensitive to different attachment methods. Using the LSTM network to predict normal GRF waveforms from accelerometers adhered differently than in the present study may decrease prediction accuracy, but the 20 Hz low-pass filter we applied to the accelerometer data can potentially mitigate this effect. Additionally, predictions made with the LSTM network may not be generalizable for speeds or slopes that fall outside the range of the training data (2.5 – 4.17 m/s and ±10°) as biomechanics change when running on steep slopes (e.g. 20 – 40°) (Giovanelli *et al.*, 2016; Whiting *et al.*, 2020). Lastly, the LSTM network was trained on data collected on a stiff force-measuring treadmill and thus accelerometer data collected during running on less stiff surfaces (e.g. grass) may result in greater prediction errors given the effects of surface stiffness on running biomechanics and thus energy absorption (Derrick, Hamill and Caldwell, 1998; Ferris, Louie and Farley, 1998).

4.5 Conclusions

We developed a Long Short-Term Memory (LSTM) neural network that used accelerometer data to predict the continuous normal GRF waveform across a range of running speeds (2.5 – 4.17 m/s) and slopes (0°, ±5°, ±10°) with an average ± SD RMSE of 0.16 ± 0.04 BW and rRMSE of 6.4 ± 1.5%. Unlike neural networks implemented in prior studies, the LSTM network does not require preliminary identification of the stance phase or temporal normalization and allows for near real-time predictions of the normal GRF waveform during running. Accurate predictions of the normal GRF waveform using wearable devices will improve our ability to longitudinally monitor biomechanical variables in non-laboratory environments.

4.6 References

Abadi M, Agarwal A, Barham P, Brevdo E, Chen Z, Citro C, Corrado GS, Davis A, Dean J, Devin M, Ghemawat S, Goodfellow I, Harp A, Irving G, Isard M, Jia Y, Jozefowicz R, Kaiser L, Kudlur M, … Zheng X (2016) TensorFlow: Large-scale machine learning on heterogeneous distributed systems. ArXiv:1603.04467. http://arxiv.org/abs/1603.04467

Alcantara RS, Day E, Hahn M, Grabowski A (2021) Sacral acceleration can predict whole-body kinetics and stride kinematics across running speeds. *PeerJ, In Press*.

Alcantara RS (2019) Dryft: A Python and MATLAB package to correct drifting ground reaction force signals during treadmill running. *Journal of Open Source Software*, 4(44), 1910. https://doi.org/10.21105/joss.01910

Almeida MO, Davis IS, Lopes AD (2015) Biomechanical differences of foot-strike patterns during running: A systematic review with meta-analysis. *Journal of Orthopaedic & Sports Physical Therapy*, 45(10), 738–755. https://doi.org/10.2519/jospt.2015.6019

Ancillao A, Tedesco S, Barton J, O'Flynn B (2018) Indirect measurement of ground reaction forces and moments by means of wearable inertial sensors: A systematic review. *Sensors (Basel, Switzerland)*, 18(8). https://doi.org/10.3390/s18082564

Backes A, Skejø SD, Gette P, Nielsen RØ, Sørensen H, Morio C, Malisoux L (2020) Predicting cumulative load during running using field-based measures. *Scandinavian Journal of Medicine & Science in Sports*, 00, 1–9. https://doi.org/10.1111/sms.13796

Baggaley M, Vernillo G, Martinez A, Horvais N, Giandolini M, Millet GY, Edwards WB (2019) Step length and grade effects on energy absorption and impact attenuation in running. *European Journal of Sport Science*, 1–11. https://doi.org/10.1080/17461391.2019.1664639

Bertelsen ML, Hulme A, Petersen J, Brund RK, Sørensen H, Finch CF, Parner ET, Nielsen RO (2017) A framework for the etiology of running-related injuries. *Scandinavian Journal of Medicine & Science in Sports*, 27(11), 1170–1180. https://doi.org/10.1111/sms.12883

Cavagna GA, Mantovani M, Willems PA, Musch G (1997) The resonant step frequency in human running. *Pflügers Archiv*, 434(6), 678–684. https://doi.org/10.1007/s004240050451

Ceyssens L, Vanelderen R, Barton C, Malliaras P, Dingenen B (2019) Biomechanical risk factors associated with running-related injuries: A systematic review. *Sports Medicine*, 49(7), 1095–1115. https://doi.org/10.1007/s40279-019-01110-z

Chaibub NE, Pratap A, Perumal TM, Tummalacherla M, Snyder P, Bot BM, Trister AD, Friend SH, Mangravite L, Omberg L (2019) Detecting the impact of subject characteristics on machine learning-based diagnostic applications. *Digital Medicine*, 2(1), 1–6. https://doi.org/10.1038/s41746-019-0178-x

Choi A, Jung H, Mun JH (2019) Single inertial sensor-based neural networks to estimate COM-COP inclination angle during walking. *Sensors (Basel, Switzerland)*, 19(13). https://doi.org/10.3390/s19132974

Clermont CA, Benson LC, Edwards WB, Hettinga BA, Ferber R (2019) New considerations for wearable technology data: Changes in running biomechanics during a marathon. *Journal of Applied Biomechanics*, 35(6), 401–409. https://doi.org/10.1123/jab.2018-0453

Colby MJ, Dawson B, Heasman J, Rogalski B, Gabbett TJ (2014) Accelerometer and GPS-derived running loads and injury risk in elite Australian footballers. *The Journal of Strength & Conditioning Research*, 28(8), 2244–2252. https://doi.org/10.1519/JSC.0000000000000362

Day EM, Alcantara RS, McGeehan MA, Grabowski AM, Hahn ME (2021) Low-pass filter cutoff frequency affects sacral-mounted inertial measurement unit estimations of peak vertical ground reaction force and contact time during treadmill running. *Journal of Biomechanics*, 110323. https://doi.org/10.1016/j.jbiomech.2021.110323

Derie R, Robberechts P, Van den Berghe P, Gerlo J, De Clercq D, Segers V, Davis J (2020) Tibial Acceleration-Based Prediction of Maximal Vertical Loading Rate During Overground Running: A Machine Learning Approach. *Frontiers in Bioengineering and Biotechnology*, 8. https://doi.org/10.3389/fbioe.2020.00033

Derrick TR, Hamill J, Caldwell GE (1998) Energy absorption of impacts during running at various stride lengths. *Medicine and Science in Sports and Exercise*, 30(1), 128–135. https://doi.org/10.1097/00005768-199801000-00018

Dorschky E, Nitschke M, Martindale CF, van den Bogert AJ, Koelewijn AD, Eskofier BM (2020) CNN-Based Estimation of Sagittal Plane Walking and Running Biomechanics From Measured and Simulated Inertial Sensor Data. *Frontiers in Bioengineering and Biotechnology*, 8, 604. https://doi.org/10.3389/fbioe.2020.00604

Ferris DP, Louie M, Farley CT (1998) Running in the real world: adjusting leg stiffness for different surfaces. *Proceedings of the Royal Society of London*. Series B: Biological Sciences, 265(1400), 989–994. https://doi.org/10.1098/rspb.1998.0388

Figo D, Diniz P, Ferreira D, Cardoso J (2010) Preprocessing techniques for context recognition from accelerometer data. *Personal and Ubiquitous Computing*, 14, 645–662. https://doi.org/10.1007/s00779-010-0293-9

Firminger CR, Edwards WB (2016) The influence of minimalist footwear and stride length reduction on lower-extremity running mechanics and cumulative loading. *Journal of Science and Medicine in Sport*. https://doi.org/10.1016/j.jsams.2016.03.003

Giandolini M, Poupard T, Gimenez P, Horvais N, Millet GY, Morin J-B, Samozino P (2014) A simple field method to identify foot strike pattern during running. *Journal of Biomechanics*, 47(7), 1588–1593. https://doi.org/10.1016/j.jbiomech.2014.03.002

Giovanelli N, Ortiz ALR, Henninger K, Kram R (2016) Energetics of vertical kilometer foot races; is steeper cheaper? *Journal of Applied Physiology*, 120(3), 370–375. https://doi.org/10.1152/japplphysiol.00546.2015

Gottschall JS, Kram R (2005) Ground reaction forces during downhill and uphill running. *Journal of Biomechanics*, 38(3), 445–452. https://doi.org/10.1016/j.jbiomech.2004.04.023

Halilaj E, Rajagopal A, Fiterau M, Hicks JL, Hastie TJ, Delp SL (2018). Machine learning in human movement biomechanics: Best practices, common pitfalls, and new opportunities. *Journal of Biomechanics*, 81, 1–11. https://doi.org/10.1016/j.jbiomech.2018.09.009

Harris CR, Millman KJ, van der Walt SJ, Gommers R, Virtanen P, Cournapeau D, Wieser E, Taylor J, Berg S, Smith NJ, Kern R, Picus M, Hoyer S, van Kerkwijk MH, Brett M, Haldane A, del Río JF, Wiebe M, Peterson P, … Oliphant TE (2020) Array programming with NumPy. *Nature*, 585(7825), 357–362. https://doi.org/10.1038/s41586-020-2649-2

Hennig EM, Lafortune MA (1991) Relationships between ground reaction force and tibial bone acceleration parameters. *International Journal of Sport Biomechanics*, 7(3), 303–309.

Hochreiter S, Schmidhuber J (1997) Long Short-Term Memory. *Neural Computation*, 9(8), 1735–1789.

International Trail Running Association (2020) 2020 Trail Running Infographics. https://itra.run/documents/Infographics/EN-ITRA-Trail-Running-Infographics-2020.pdf

Janssen M, Walravens R, Thibaut E, Scheerder J, Brombacher A, Vos S (2020) Understanding different types of recreational runners and how they use running-related technology.

International Journal of Environmental Research and Public Health, 17(7). https://doi.org/10.3390/ijerph17072276

Johnson CD, Outerleys J, Tenforde AS, Davis IS (2020) A comparison of attachment methods of skin mounted inertial measurement units on tibial accelerations. *Journal of Biomechanics*, 113, 110118. https://doi.org/10.1016/j.jbiomech.2020.110118

Johnson WR, Mian A, Robinson MA, Verheul J, Lloyd DG, Alderson J (2021) Multidimensional ground reaction forces and moments from wearable sensor accelerations via deep learning. *IEEE Transactions on Biomedical Engineering*, 68(1), 289–297. https://doi.org/10.1109/TBME.2020.3006158

Khassetarash A, Vernillo G, Martinez A, Baggaley M, Giandolini M, Horvais N, Millet GY, Edwards WB (2020) Biomechanics of graded running: Part II—Joint kinematics and kinetics. *Scandinavian Journal of Medicine & Science in Sports*, 30(9), 1642–1654. https://doi.org/10.1111/sms.13735

Kiernan D, Hawkins DA, Manoukian MAC, McKallip M, Oelsner L, Caskey CF, Coolbaugh, CL (2018) Accelerometer-based prediction of running injury in National Collegiate Athletic Association track athletes. *Journal of Biomechanics*, 73, 201–209. https://doi.org/10.1016/j.jbiomech.2018.04.001

Kingma DP, Ba J (2017) Adam: A method for stochastic optimization. *ArXiv*:1412.6980 [Cs]. http://arxiv.org/abs/1412.6980

Kipp S, Taboga P, Kram R (2017) Ground reaction forces during steeplechase hurdling and waterjumps. *Sports Biomechanics*, 16(2), 152–165. https://doi.org/10.1080/14763141.2016.1212917

Li L, Jamieson K, DeSalvo G, Rostamizadeh A, Talwalkar A (2018) Hyperband: A novel bandit-based approach to hyperparameter optimization. *Journal of Machine Learning Research*, 18(185), 1–52.

McMahon TA, Valiant G, Frederick EC (1987) Groucho running. *Journal of Applied Physiology*, 62(6), 2326–2337. https://doi.org/10.1152/jappl.1987.62.6.2326

Mundt M, Koeppe A, David S, Bamer F, Potthast W, Markert B (2020) Prediction of ground reaction force and joint moments based on optical motion capture data during gait. *Medical Engineering & Physics*, 86, 29–34. https://doi.org/10.1016/j.medengphy.2020.10.001

Neugebauer JM, Hawkins DA, Beckett L (2012) Estimating youth locomotion ground reaction forces using an accelerometer-based activity monitor. *PLOS ONE*, 7(10), e48182. https://doi.org/10.1371/journal.pone.0048182

Pandas Development Team (2020) pandas-dev/pandas: Pandas. https://doi.org/10.5281/zenodo.3509134

Pogson M, Verheul J, Robinson MA, Vanrenterghem J, Lisboa P (2020) A neural network method to predict task- and step-specific ground reaction force magnitudes from trunk

accelerations during running activities. *Medical Engineering & Physics*, 78, 82–89. https://doi.org/10.1016/j.medengphy.2020.02.002

R Core Team (2020) R: A language and environment for statistical computing (3.6.3) [Computer software]. R Foundataion for Statistical Computing.

Reenalda J, Maartens E, Homan L, Buurke JH (2016) Continuous three dimensional analysis of running mechanics during a marathon by means of inertial magnetic measurement units to objectify changes in running mechanics. *Journal of Biomechanics*, 49(14), 3362–3367. https://doi.org/10.1016/j.jbiomech.2016.08.032

Ren L, Jones RK, Howard D (2008) Whole body inverse dynamics over a complete gait cycle based only on measured kinematics. *Journal of Biomechanics*, 41(12), 2750–2759. https://doi.org/10.1016/j.jbiomech.2008.06.001

Ruder M, Jamison ST, Tenforde A, Mulloy F, Davis IS (2019) Relationship of Foot Strike Pattern and Landing Impacts during a Marathon. *Medicine and Science in Sports and Exercise*, 51(10), 2073–2079. https://doi.org/10.1249/MSS.0000000000002032

Running USA (2019) 2019 U.S Running Trends Report.

Ryan MR, Napier C, Greenwood D, Paquette MR (2020) Comparison of different measures to monitor week-to-week changes in training load in high school runners. *International Journal of Sports Science & Coaching*, 174795412097030. https://doi.org/10.1177/1747954120970305

Saeb S, Lonini L, Jayaraman A, Mohr DC, Kording KP (2017) The need to approximate the use-case in clinical machine learning. *GigaScience*, 6(5). https://doi.org/10.1093/gigascience/gix019

Scott MTU, Scott TJ, Kelly VG (2016) The validity and reliability of global positioning systems in team sport: A brief review. *The Journal of Strength & Conditioning Research*, 30(5), 1470–1490. https://doi.org/10.1519/JSC.0000000000001221

Selvin S, Vinayakumar R, Gopalakrishnan EA, Menon VK, Soman KP (2017) Stock price prediction using LSTM, RNN and CNN-sliding window model. *2017 International Conference on Advances in Computing, Communications and Informatics (ICACCI)*, 1643–1647. https://doi.org/10.1109/ICACCI.2017.8126078

Snyder KL, Farley CT (2011) Energetically optimal stride frequency in running: The effects of incline and decline. *The Journal of Experimental Biology*, 214(Pt 12), 2089–2095. https://doi.org/10.1242/jeb.053157

Vernillo G, Martinez A, Baggaley M, Khassetarash A, Giandolini M, Horvais N, Edwards WB, Millet GY (2020) Biomechanics of graded running: Part I - Stride parameters, external forces, muscle activations. *Scandinavian Journal of Medicine & Science in Sports*, 30(9), 1632–1641. https://doi.org/10.1111/sms.13708

Vincent HK, Kilgore JE, Chen C, Bruner M, Horodyski M, Vincent KR (2020) Impact of body mass index on biomechanics of recreational runners. *PM&R*, 12(11), 1106–1112. https://doi.org/10.1002/pmrj.12335

Virtanen P, Gommers R, Oliphant TE, Haberland M, Reddy T, Cournapeau D, Burovski E, Peterson P, Weckesser W, Bright J, van der Walt SJ, Brett M, Wilson J, Millman KJ, Mayorov N, Nelson ARJ, Jones E, Kern R, Larson E, … van Mulbregt P (2020) SciPy 1.0: fundamental algorithms for scientific computing in Python. *Nature Methods*, 17(3), 261–272. https://doi.org/10.1038/s41592-019-0686-2

Vitali RV, Cain SM, Ojeda LV, Potter MV, Zaferiou AM, Davidson SP, Coyne ME, Hancock CL, Mendoza A, Stirling LA, Perkins NC (2019) Body-worn IMU array reveals effects of load on performance in an outdoor obstacle course. *PLOS ONE*, 14(3), e0214008. https://doi.org/10.1371/journal.pone.0214008

Voloshina AS, Ferris DP (2015) Biomechanics and energetics of running on uneven terrain. *Journal of Experimental Biology*, 218(5), 711–719. https://doi.org/10.1242/jeb.106518

Wang S, Jiang J (2016) Learning Natural Language Inference with LSTM. *ArXiv*:1512.08849 [Cs]. http://arxiv.org/abs/1512.08849

Whiting CS, Allen SP, Brill JW, Kram R (2020) Steep (30°) uphill walking vs. running: COM movements, stride kinematics, and leg muscle excitations. *European Journal of Applied Physiology*, 120(10), 2147–2157. https://doi.org/10.1007/s00421-020-04437-y

Wickham H (2009) ggplot2: Elegant graphics for data analysis. *Springer-Verlag*. https://doi.org/10.1007/978-0-387-98141-3

Wickham H (2019) stringr: Simple, consistent wrappers for common string operations (1.4.0) [Computer software]. https://CRAN.R-project.org/package=stringr

Wickham H, François R, Henry L, Müller K (2020) dplyr: A grammar of data manipulation (0.8.5) [Computer software]. https://CRAN.R-project.org/package=dplyr

Willy RW, Buchenic L, Rogacki K, Ackerman J, Schmidt A, Willson JD (2016). In-field gait retraining and mobile monitoring to address running biomechanics associated with tibial stress fracture. *Scandinavian Journal of Medicine & Science in Sports*, 26(2), 197–205. https://doi.org/10.1111/sms.12413

Wouda FJ, Giuberti M, Bellusci G, Maartens E, Reenalda J, van Beijnum B-JF, Veltink PH (2018) Estimation of vertical ground reaction forces and sagittal knee kinematics during running using three inertial sensors. *Frontiers in Physiology*, 9. https://doi.org/10.3389/fphys.2018.00218

Yong JR, Silder A, Montgomery KL, Fredericson M, Delp SL (2018). Acute changes in foot strike pattern and cadence affect running parameters associated with tibial stress fractures. *Journal of Biomechanics*, 76, 1–7. https://doi.org/10.1016/j.jbiomech.2018.05.017

5 Conclusion

My first study (Chapter 1) quantified the effects of RSP and lower limb mass on metabolic power and biomechanical asymmetry in individuals with a transtibial amputation running at 2.5 m/s. I found that added mass to the RSP and lower limb resulted in increased metabolic power but had no effect on measures of asymmetry. Additionally, when 100 g were added to each limb of runners with a transtibial amputation, they had greater increases in metabolic power than runners without an amputation. Considering the relationship between metabolic power and distance running performance, runners with a transtibial amputation might improve their performance by reducing the mass of their RSP.

My second study (Chapter 2) measured the leg-specific force production and lower body joint kinetics and kinematics during maximum velocity sprinting on a straightaway and two flat curve radii typical of track and field sprint events. My findings validate previous theoretical models, provide substantial evidence for leg-specific biomechanical functions during curve sprinting, and highlight opportunities to improve sprinting performance.

In my third study (Chapter 3), I developed a method of predicting running-related biomechanical variables with a single accelerometer clipped onto the back of running shorts. This approach was more accurate than previous attempts at predicting biomechanical variables from wearable devices. Accurate predictions with wearable devices in biomechanical research will improve our ability to measure an athlete's biomechanics and monitor injury risk.

In my fourth study (Chapter 4), I present a novel application of neural networks to accelerometer data that is capable of near-real time predictions of GRFs during running. Continuous predictions of the GRF waveform improves upon previous research predicting discrete

variables or only portions of the GRF waveform and could potentially allow runners to receive more accurate biomechanical feedback during an outdoor run. The application of machine learning and statistical models to wearable device data will potentially provide a way to collect accurate biomechanical data in environments and quantities previously impossible to accomplish.

In conclusion, my dissertation furthers our understanding of running physiology, sprinting biomechanics, and how wearable devices can be used to remotely monitor a runner's biomechanics and injury risk. These findings may provide information for long distance runners and sprinters to improve their performance as well as strategies for coaches, clinicians, and researchers to prevent overuse injuries in runners. Overall, my dissertation identifies current biomechanical and physiological limitations to human performance and provides strategies for overcoming these limitations.